Multiscale Methodology:
From Atoms to Continuum

by Peter W. Chung and Raju R. Namburu

20020118 226

Army Research Laboratory

Aberdeen Proving Ground, MD 21005-5067

Multiscale Methodology:
From Atoms to Continuum

Peter W. Chung and Raju R. Namburu
Computational and Information Sciences Directorate, ARL

Abstract

Research in multiscale methods has recently flourished with the help of ever-improving computer technology. These developments enable computational physics methods to challenge many of the fundamental limitations of continuum mechanics with larger atomistic simulations and sophisticated hybrid atomistic-continuum methods. The foundation of most hybrid methods presently lies in the judicious application of kinematic constraints between regions of atoms and regions of continuum finite elements. This juxtaposes atomic and continuum force fields and introduces an interface along which atoms and nodes are unnaturally constrained. The constraint is necessary to establish compatibility of displacements across the interface. This report is divided into three sections. Section 1 reports on an investigation of finding sources of numerical error due to this unphysical constraint. Bounding estimates on the numerical error are derived using summation rules of a classical interatomic potential and the geometry and periodicity of the molecular structure. A previously observed inverse relation between element size and interface error is demonstrated, and additional numerical experiments are presented. In section 2, a literature review of a technique that can potentially eliminate this error is presented. The review covers efforts in engineering for composite materials rooted in a firm mathematical basis for the so-called asymptotic expansion homogenization method (AEH). The homogenization method is used as a framework for developing a multiscale system of equations in elasticity, also in section 2. In section 3, AEH is used as a framework for developing analytical multiscale formulations for frozen atoms at the small scale and continuum mechanics at the large scale. The Tersoff-Brenner type II potential (Brenner, D. W. *Physical Review B*. Vol. 42, no. 15, pp. 9458–9471, 1990; Tersoff, J. *Physical Review Letters*. Vol. 61, no. 25, pp. 2879–2882, 1988) governs the atom interactions, and hyperelasticity governs the continuum. A quasi-static assumption is used together with the Cauchy-Born approximation to enforce the gross deformation of the continuum on the positions of the atoms. This makes the atomistic equations linear. The two-scale homogenization method establishes coupled self-consistent variational equations in which the information at the atomistic scale, formulated in terms of the Lagrangian stiffness tensor, feeds the material information to the continuum equations. Analytical results in one dimension are shown.

Acknowledgments

INTENTIONALLY LEFT BLANK.

Table of Contents

List of Figures

INTENTIONALLY LEFT BLANK.

List of Tables

INTENTIONALLY LEFT BLANK.

1. Estimating Numerical Error in Atomistic-Continuum Computational Methods in Graphene

1.1 Overview

The underlying premise of the finite element method (FEM), when applied to solving problems in computational mechanics, is that the material in question is a continuous medium infinitely divisible into smaller continuous components. Developments in the basic sciences such as chemistry and physics, however, have disputed this assumption long before the notion of FE was even first conceived. In most applications at macroscopic length scales, it is useful to think of materials as a system of continuously distributed mass. Yet today, with the development of advanced devices such as nano-/microelectromechanical systems (N/MEMS) whose features and characteristics challenge the most fundamental assumptions of continuum mechanics, it is clear that traditional FEM cannot be applied without additional considerations. Moreover, the numbers of atoms in these devices warrant the determination of properties that require computations on a scale unreachable by atomistic methods alone.

Methodologies for linking a continuum to an atomistic domain can be found in the literature as early 1971 [1] in which the treatment of the continuum is predominantly atomistic in nature. Finite element methods were later employed by Mullins and Dokainish [2] using a numerically decoupled domain approach with spatially overlapping atomistic and continuum regions in which the information from each region is fed into the other via boundary conditions. A review of these methods can be found in Cleri et al. [3]. Among these early analytic and computational studies, frequent issues regarding the treatment of the interface

arose which were primarily handled through creative use of kinematic constraints.

More recently Tadmor et al. [4] develop an entirely FE-based formulation, the so-called quasicontinuum method. Local and non-local formulations are used to discriminate between atoms in regions of low interest and high interest. The transition between the two regions is handled again through kinematic constraints and the mesh is adaptively refined in regions of large atom motion.

The so-called handshaking or coupling of length scales (CLS) method [5] adds an additional level of sophistication with a third region modeled using the tight-binding (TB) method which captures information about the electronic degrees of freedom. There are three regions of interest: (1) an FE region modeled using elasticity theory, (2) a molecular dynamics (MD) region using a classical potential, and (3) the TB region. The coupling at interfaces separating these regions is accomplished through kinematic constraints at the FE/MD interface and chemical constraints at the MD/TB interface.

A generalized scaling approach is developed in coarse-grained molecular dynamics (CGMD) [6] to better handle the propagation of waves through the atomistic-FE interface and the FE far field. A coarse graining procedure is used to "merge" the atomistic degrees of freedom from Hamilton's equations of motion to the smaller number of FE nodal degrees of freedom.

The common theme in the previously mentioned investigations is to directly connect a continuum region to an atomistic region either through kinematic or statistical constraints. The benefit of these types of approaches is the removal of complexity in regions of the domain where detailed atomic resolution is unnecessary by replacing a large number of atomic degrees of freedom with a smaller number of element/nodal degrees of freedom. This type of approach, however, does not ensure compatibility at the interface and, as a result, so-called "ghost forces" may occur [7].

Friesecke and James [8], as part of an investigation to derive a scheme that passes an atomistic energy to a continuum energy, showed that the sum of the energies of in the elements is greater than (less negative) the total energy of the original body before discretization. In fact, the difference between the sum and total energies is proportional to $O(1/h)$. This provides an indirect explanation for the ghost forces. The point of departure in this work is in the explicit calculation of the energy error based on geometry arguments of the molecular structure of the material.

There are two primary ways of classifying the forces: those due to the initial discretization or modeling error and those due to subsequent deformations of the mesh that stem from the discretization. The aim of this section of the report is to quantify the first type of error in terms of energy and to specify their origins from a classical potential. We will only briefly discuss the second.

In practice, creative constraints have been applied near the interface region using transition schemes to reduce the error [2, 7]. However, a systematic means of approximating this error is still unavailable. The objective of this section is, therefore, to make a first step in this direction by developing an approach where this error can be estimated directly from the classical potential and the structure of the molecular geometry. This has application to problems where the mechanical state of the system depends on the total energy. Examples may include problems of phase transition and local material instability. The present potential is specifically suited for semiconductor lattices with a two-atom basis, namely carbon, and accounts for two- and three-atom effects [9].

In section 1.2, some preliminary definitions are given; in section 1.3, a discussion of the sources of numerical error in atomistic-continuum computational schemes is presented. In section 1.4, a description of the actual classical potential used in the present calculations is described followed by estimates of the energy error and discussions of the results. Some additional considerations for more general studies will then be presented in section 1.5,

3

followed by final remarks in section 1.6.

1.2 Problem Definition

Consider a lattice of periodically spaced atoms in the n-dimensional space $\Omega \in \mathbb{R}^n$ with n_a atoms and n_b bonds connecting the nearest neighbor atoms. The atoms are initially undistorted and at zero temperature. The plane of atoms can be fully described by a set of primitive cell vectors $(\mathbf{e}_i)$ and additional translation vectors $(\mathbf{p}_j)$ if there is more than one atom in each basis cell. For carbon in the form of a single graphite sheet, graphene, there are two atoms in the basis $(j = 1)$ and therefore only one translation vector.

The sheet of atoms is permitted to deform. The deformation is measured by the deformation gradient $\mathbf{F}$. Let the deformation $\mathbf{u} : \Omega \to \mathbb{R}^n$ with gradient $\mathbf{F} = \frac{\partial \mathbf{u}}{\partial \mathbf{X}}$ have an energy density given in the general form

$$\mathcal{W} = \frac{1}{n_a} \sum_b^{n_b} \Phi_b (\mathbf{F}), \tag{1}$$

where b runs over all the bonds (n_b) in Ω, and the $\frac{1}{n_a}$ coefficient gives the energy density per atom. Assume that Φ is defined for all $\mathbf{F}$ that are real 2×2 matrices with det $\mathbf{F} > 0$ and that Φ exhibits the standard features of lattice invariant deformations in Ω.

The energy density expression can take any general form of a cluster potential. Therefore, the summation can involve bonds, bond angles, and higher bond-order effects. A specific case study is made in section 1.4 which requires a more exact description for the potential. However, the discussions here are generally applicable for any classical potential.

For the sake of discussion, assume that the energy in equation (1) can be decomposed into the sum of an energy due to a deformation and a non-zero reference equilibrium energy. The

4

reference equilibrium energy is based on the initial positions of the atom nuclei, $\mathbf{X}$, i.e.,

$$W = \frac{1}{n_a} \sum_b^{n_b} \phi_b(\mathbf{F}) + \frac{1}{n_a} \sum_b^{n_b} \phi_b^o(\mathbf{X}), \tag{2}$$

where

$$\phi_b(\mathbf{F} = \mathbf{I}) = 0. \tag{3}$$

Through a change of variables, equation (2) can be rewritten as a function of the atom displacements,

$$W = \frac{1}{n_a} \sum_b^{n_b} \phi_b(\mathbf{F}(\mathbf{u})) + \frac{1}{n_a} \sum_b^{n_b} \phi_b^o(\mathbf{X}). \tag{4}$$

The assumption that the energy is separable in equation (2) is nontrivial. In general classical potentials, the ansatz is highly nonlinear and behaves poorly in the traditional partial differential equation sense. It possesses at least one singularity, is nonconvex and noncoercive. The simplification introduced in equation (2) will be justified next through a bilinearization of the problem that removes this difficulty at the expense of generality.

In light of the small deformation assumption, we can take a bilinearization (harmonic approximation) about the equilibrium lattice configuration. This involves taking the Taylor series expansion of the energy as follows,

$$W = W|_{\mathbf{F}=\mathbf{I}} + \frac{\partial W}{\partial \mathbf{F}}\bigg|_{\mathbf{F}=\mathbf{I}} : (\mathbf{F} - \mathbf{I}) + \frac{1}{2}(\mathbf{F} - \mathbf{I})^T : \frac{\partial^2 W}{\partial \mathbf{F} \partial \mathbf{F}}\bigg|_{\mathbf{F}=\mathbf{I}} : (\mathbf{F} - \mathbf{I}) + \cdots . \tag{5}$$

When the system is in equilibrium, the first derivative is zero. Omitting higher order terms, this leaves

$$W = W|_{\mathbf{F}=\mathbf{I}} + \frac{1}{2}(\mathbf{F} - \mathbf{I})^T : \frac{\partial^2 W}{\partial \mathbf{F} \partial \mathbf{F}}\bigg|_{\mathbf{F}=\mathbf{I}} : (\mathbf{F} - \mathbf{I}). \tag{6}$$

By definition,

$$\mathbf{F} - \mathbf{I} = \nabla \mathbf{u}. \tag{7}$$

5

Substituting equation (7) into equation (6) gives

$$W = W|_{\mathbf{F}=\mathbf{I}} + \frac{1}{2}\left(\nabla\mathbf{u}\right)^T : \left.\frac{\partial^2 W}{\partial\mathbf{F}\partial\mathbf{F}}\right|_{\mathbf{F}=\mathbf{I}} : \left(\nabla\mathbf{u}\right). \tag{8}$$

Notice that the reference equilibrium energy occurs naturally in the expansion. This justifies the earlier assumption of decomposability.

As a consequence of the small deformation assumption and the resulting harmonicity in W, we can assume $\mathbf{u} \in H^1$. Or more conventionally, one can say $\mathbf{u} \in \mathcal{S}$ for a given set of conditions of $\mathbf{u}$ on $\Omega_\mathbf{u}$, where

$$\mathcal{S} = \{\mathbf{u}|\mathbf{u} \in H^1, \ \mathbf{u}|_{\Omega_\mathbf{u}} = \bar{\mathbf{u}}\}. \tag{9}$$

Furthermore, define $\mathcal{V} \subset \mathcal{S}$ such that

$$\mathcal{V} = \{\mathbf{w}|\mathbf{w} \in H^1, \ \mathbf{w}|_{\Omega_\mathbf{w}} = 0\}. \tag{10}$$

Then, for a given set of prescribed displacements $\bar{\mathbf{u}}$ on the boundary Ω_u, the stable configuration of the atoms is one which minimizes the total potential energy

$$\Pi(\mathbf{u}) = \inf_\mathbf{v}\left[\int_\Omega W d\Omega - \int_\Omega \mathbf{f}\cdot\mathbf{v}d\Omega - \int_{\Omega_g}\mathbf{t}\cdot\mathbf{v}d\Gamma\right], \tag{11}$$

where $\mathbf{v} \in \mathcal{S}$ are the trial functions, $\mathbf{f}$ is the body force per unit volume and $\mathbf{t}$ is the prescribed surface tractions per unit area on Ω_g. Substituting equation (8) into equation (11) gives,

$$\Pi(\mathbf{u}) - \Pi_o = \inf_\mathbf{v}\left[\int_\Omega \frac{1}{2}\left(\nabla\mathbf{v}\right)^T : \left.\frac{\partial W}{\partial\mathbf{F}\partial\mathbf{F}}\right|_{\mathbf{F}=\mathbf{I}} : \left(\nabla\mathbf{v}\right) - \int_\Omega \mathbf{f}\cdot\mathbf{v}d\Omega - \int_{\Omega_g}\mathbf{t}\cdot\mathbf{v}d\Gamma\right]. \tag{12}$$

Associated with equation (12) is a bilinear symmetric form $a(\cdot,\cdot)$ and inner products $(\cdot,\cdot)$ and $(\cdot,\cdot)_\Gamma$ where

$$a(\mathbf{w},\mathbf{u}) = \int_\Omega (\nabla\mathbf{w}) : \left.\frac{\partial^2 W}{\partial\mathbf{F}\partial\mathbf{F}}\right|_{\mathbf{F}=\mathbf{I}} : (\nabla\mathbf{u})d\Omega, \tag{13}$$

$$(\mathbf{f},\mathbf{u}) = \int_\Omega \mathbf{f}\cdot\mathbf{u}d\Omega, \tag{14}$$

$$(\mathbf{t},\mathbf{u})_\Gamma = \int_{\Omega_g} \mathbf{t}\cdot\mathbf{u}d\Gamma. \tag{15}$$

6

Then, the functional in equation (12) has the form,

$$\Pi(\mathbf{u}) - \Pi_o = \inf_{\mathbf{v}} \left[\frac{1}{2} a(\mathbf{v}, \mathbf{v}) - (\mathbf{f}, \mathbf{v}) - (\mathbf{t}, \mathbf{v})_\Gamma \right], \tag{16}$$

with the equivalent weak form of equation (16) given by: Find $\mathbf{u} \in \mathcal{S}$ for every $\mathbf{w} \in \mathcal{V}$ such that

$$a(\mathbf{w}, \mathbf{u}) = (\mathbf{w}, \mathbf{f}) + (\mathbf{w}, \mathbf{t})_\Gamma. \tag{17}$$

The finite element analogue of (17) is based on the conventional discretization of displacements and corresponding gradients,

$$\mathbf{u}^h \quad = \quad \sum_i^{n_e} w_i u_i, \tag{18}$$

$$\nabla \mathbf{u}^h \quad = \quad \sum_i^{n_e} \mathbf{B}_i u_i, \tag{19}$$

where $i = 1, ..., n_e$ are the nodes in the mesh, w_i are the weighting functions, and $\mathbf{B}_i$ are the gradients of the weighting functions. The finite dimensional approximations of $\mathcal{S}$ and $\mathcal{V}$ are denoted by $\mathcal{S}^h$ and $\mathcal{V}^h$, where $\mathcal{S}^h \subset \mathcal{S}$ and $\mathcal{V}^h \subset \mathcal{V}$.

1.3 Discretization Error

Classical potentials, such as empirical interatomic potentials, are phenomenological in nature and do not explicitly model the effects of the electron density. However, tests have shown that in studying strain energies, particularly in the context of mechanical deformation, classical potentials give equally reliable results compared to *ab initio* calculations (Figure 1) for homogeneous deformation under the present assumption of small strains (<10%). Despite the myriad sources of error that can stem ostensibly from the use of a classical potential, the aim of this work is to study the error that arises due to the introduction of the finite element discretization.

7
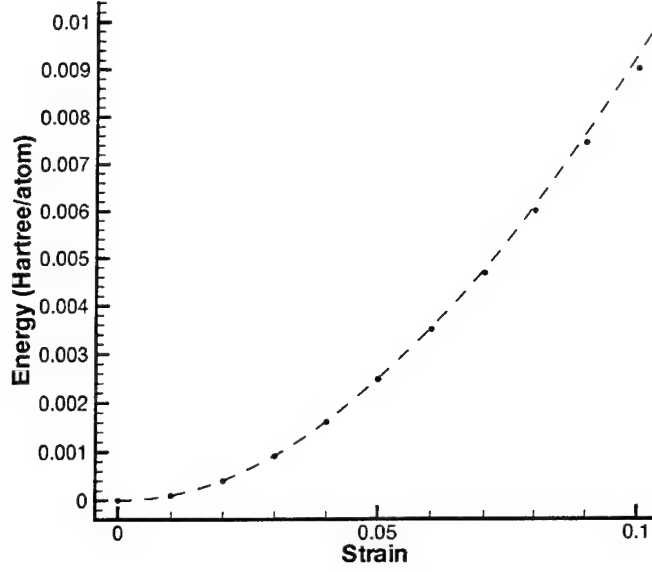
Figure 1. Deformation energy density comparisons for homogeneous stretching of graphene in the plane. Smooth line denotes the classical potential and dots denote computed *ab initio* values.

The internal energy must now be expressed in an approximate finite element form. Discretize Ω with a set of elements Ω_h^e such that

$$\Omega^h = \bigcup_e \Omega_h^e, \tag{20}$$

which has the associated minimization problem given by

$$\Pi^h(\mathbf{u}^h) - \Pi_o^h = \inf_{\mathbf{v}^h} \left[\frac{1}{2} a^h(\mathbf{v}^h, \mathbf{v}^h) - (\mathbf{f}, \mathbf{v}^h)^h - (\mathbf{t}, \mathbf{v}^h)_\Gamma^h \right], \tag{21}$$

where

$$a^h(\mathbf{w}^h, \mathbf{u}^h) = \int_{\Omega^h} (\nabla \mathbf{w}^h) : \left. \frac{\partial^2 \mathcal{W}^h}{\partial \mathbf{F} \partial \mathbf{F}} \right|_{\mathbf{F}=\mathbf{I}} : (\nabla \mathbf{u}^h) d\Omega^h, \tag{22}$$

$$(\mathbf{f}, \mathbf{u}^h)^h = \int_{\Omega^h} \mathbf{f} \cdot \mathbf{u}^h d\Omega^h, \tag{23}$$

$$(\mathbf{t}, \mathbf{u}^h)_\Gamma^h = \int_{\Omega_g^h} \mathbf{t} \cdot \mathbf{u}^h d\Gamma^h. \tag{24}$$

8

As in equation (17), the associated weak form is given as: Find $\mathbf{u}^h \in \mathcal{S}^h$ for every $\mathbf{w}^h \in \mathcal{V}^h$ such that

$$a^h(\mathbf{w}^h, \mathbf{u}^h) = (\mathbf{w}^h, \mathbf{f})^h + (\mathbf{w}^h, \mathbf{t})_\Gamma^h. \tag{25}$$

It remains to more carefully define the bilinear form $a^h(\cdot, \cdot)$. From equation (4), the internal energy is written, as a consequence of the discretization, as

$$\mathcal{W}^h = \frac{1}{n_a} \sum_i^{n_e} \sum_b^{n_b^e} \phi_b\left(\mathbf{F}(\mathbf{u})\right) + \frac{1}{n_a} \sum_i^{n_e} \sum_b^{n_b^e} \phi_b^o\left(\mathbf{X}\right), \tag{26}$$

where h runs over all the elements and b runs over all the bonds within the element, n_b^e. Then, define $\mathbf{u}^h \in \mathcal{S}^h$ as the solution that satisfies equation (25) for $\mathcal{W}^h$ given by

$$\mathcal{W}^h = \frac{1}{n_a} \sum_b^{n_b} \phi_b\left(\mathbf{F}(\mathbf{u^h})\right) + \frac{1}{n_a} \sum_i^{n_e} \sum_b^{n_b^e} \phi_b^o\left(\mathbf{X}\right), \tag{27}$$

subject to the prescribed loads and displacements on the boundary.

The driving motivation of atomistic-continuum problems is the reduction of the number of degrees of freedom. However, through the introduction of the finite element approximation, two sources of ghost forces arise. Notice that these can now be elucidated from equations (4), (16), (21), and (27). The first of these will be described briefly here. The second will be expounded in section 1.5. The first occurs at initial equilibrium, i.e., $\mathbf{u} = \mathbf{0}$, where the difference in total potential energies between exact and approximate is the difference in the reference lattice energies. Let the lattice of all bonds in Ω be denoted $\mathcal{L}_b$ and those in Ω^h be denoted $\mathcal{L}_b^h$. Then, the energy difference is given by

$$
\begin{aligned}
\Pi - \Pi^h &= \Pi_o - \Pi_o^h \\
&= \frac{1}{n_a} \sum_a^{n_a} \phi_a^o\left(\mathbf{X}\right) - \frac{1}{n_a} \sum_i^{n_e} \sum_a^{n_a^e} \phi_a^o\left(\mathbf{X}\right) \\
&= \frac{1}{n_a} \sum_{b \in \{\mathcal{L}_b \backslash \mathcal{L}_b^h\}} \phi_b^o(\mathbf{X}),
\end{aligned}
\tag{28}
$$

9

where b runs over all bonds that cut across element boundaries, i.e., all bonds that connect atoms in two different elements. The discretization of Ω leads to a set of disjoint sets of atoms that causes the two terms in equation (28) to be unequal generally. The only instance when they are equivalent is when $n_e = 1$ and $n_a = n_a^e$, or when $\mathcal{L}_b \backslash \mathcal{L}_b^h \in \emptyset$ and no discretization is performed.

Equation (28) is an equilibrium energy form of the ghost force error and is due to a more predominant assumption that stems from a discretization error as evidenced by the summation being over all bonds excluded in the meshing. Bond-counting arguments and summation rules can then be used to characterize and quantify this error near the interface.

There are two observations from the energy difference in equation (28). First, it is nonzero at equilibrium. Approximating Ω with Ω_h artificially introduces internal surfaces into the problem, effectively truncating the communication among the atoms (Figure 2).

Although this effect grows asymptotically smaller for very large elements (relative to atom spacings), the error is more pronounced as the element size becomes comparable to atom spacings. This situation occurs frequently in atomistic-continuum computational methods due to the kinematic constraints needed to enforce local compatibility between the atoms and the elements. Second, at small scales equation (28) is neither translation nor rotation invariant, a characteristic of isotropic continua, because of mesh-dependence at small scales. Figure 3 illustrates this by showing that the energy in element A is unequal to the energy in element B despite both elements having the same perimeter and areas. This is the nature of discretizing a problem that contains an already discrete set of atoms.

(a) Original graphene sheet with bonds denoted by straight lines and C-atoms denoted by black dots.

(b) Fragment of an unstructured finite element mesh used to approximate atomic degrees of freedom with nodes (open circles).
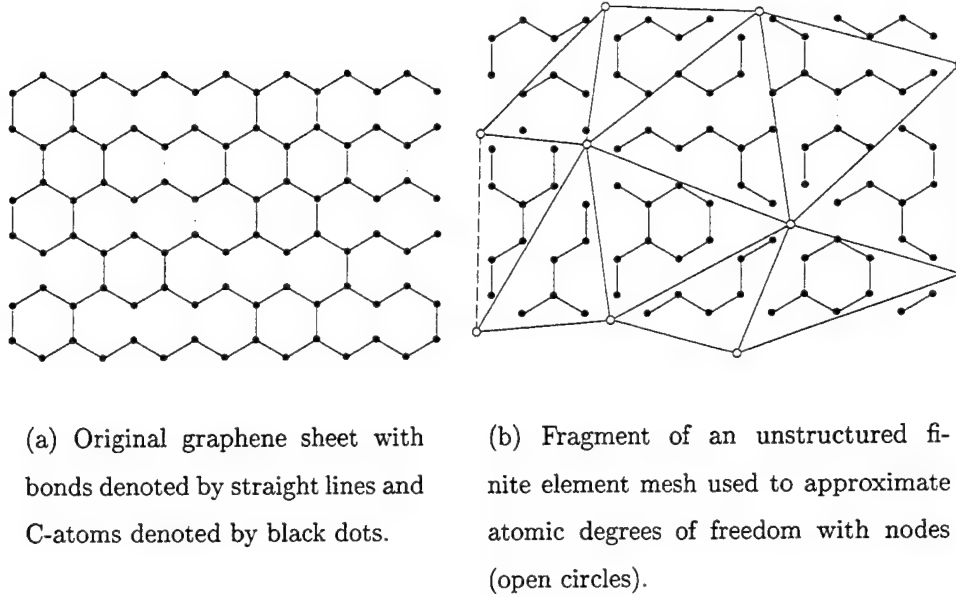
Figure 2. Element boundaries act as truncation lines that cut off the communication among atoms in different elements. The result is the artificial increase in the total energy.

1.4 Example: Graphene

We now attempt to quantify the error for the specific example of graphene using the Stillinger-Weber classical potential given by Stillinger and Weber [9] and Abraham and Batra [10]. It has been documented to give reliable lattice binding energy and atom spacing for graphite. The energy is given by

$$W = \sum_i \sum_{\substack{j \\ i<j}} \phi\left(r_{(ij)}\right) + \sum_i \sum_{\substack{j \\ i \neq j}} \sum_{\substack{k \\ i \neq j \neq k}} \psi\left(\mathbf{r}_{(ij)}, \mathbf{r}_{(ik)}\right) \chi\left(r_{(ij)}\right) \chi\left(r_{(ik)}\right), \tag{29}$$

where ϕ and ψ are the respective two- and three-atom terms, χ is the short-range cut-off function, (i, j, k) are atom indices, and the density is retrieved by dividing by the number of atoms $\mathcal{W} = W/n_a$. The two- and three-atom potentials and cut-off function are given

11
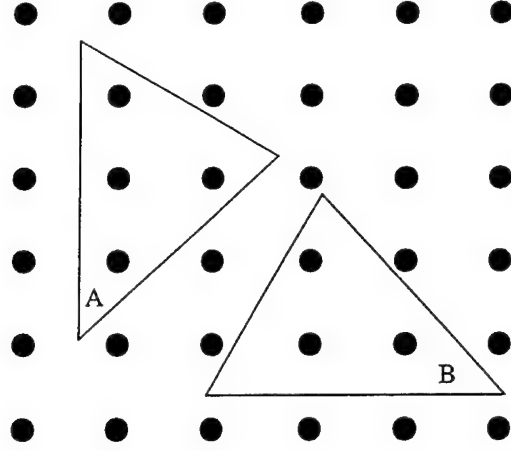
Figure 3. The total energies of elements A and B are not equivalent.

respectively by

$$\phi(r_{(ij)}) = \epsilon \begin{cases} A(Br_{(ij)}^{-4} - 1)\exp\left[(r_{(ij)} - a)^{-1}\right] & , \quad r < a \\ 0 & , \quad r \geq a \end{cases}, \tag{30}$$

$$\psi(\mathbf{r}_{(ij)}, \mathbf{r}_{(ik)}) = \epsilon\lambda \left[\frac{\mathbf{r}_{(ij)}}{r_{(ij)}} \cdot \frac{\mathbf{r}_{(ik)}}{r_{(ik)}} - \cos(\theta_*)\right]^2, \tag{31}$$

$$\chi(r_{(ij)}) = \begin{cases} \exp\left[\gamma(r_{(ij)} - a)^{-1}\right] & , \quad r < a \\ 0 & , \quad r \geq a \end{cases}, \tag{32}$$

where $A, B, a, \lambda, \theta_*, \gamma$ are material-specific constants, and the symbol $\mathbf{r}_{(ij)}$ denotes the vector originating from atom i and terminating at atom j. This material was chosen specifically because of its covalency as a semiconductor and the absence of significant long-range forces. For graphene, only short-range, nearest-neighbor forces need to be considered.

We introduce a local coordinate system centered on the graphene primitive cell. Any straight line that passes through the cell can be exactly defined by the set $(\mathbf{e}_e, \theta_e)$. Figure 4 depicts a straight line cutting through the primitive cell and the associated local coordinate system. The straight line is an idealization of an element boundary cutting through the atomistic region. It represents the line across which atoms are not permitted to "communicate." As a heuristic upper bound on the magnitude of the error, $(\mathbf{e}_e, \theta_e)$ can be permuted so that the
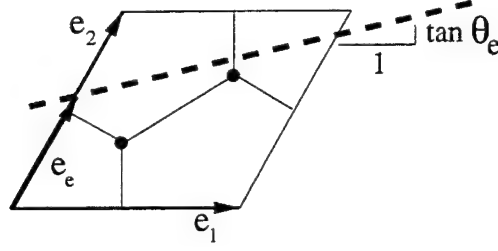
Figure 4. Local coordinate system and cutting line that represents fictitious element boundary.

line cuts through the largest number of bonds per unit length. This corresponds to the set $(\mathbf{e}_e, \theta_e) = (q\mathbf{e}_2, 0)$ for $\frac{1}{3} < q < \frac{2}{3}$. The symmetry of the hexagonal rings also implies there are six rotations that give equivalent results.

The interesting result here is the upper bound. Each bond has an energy equal to the pair potential value of ϕ for the undeformed nearest neighbor atom spacing of r_o. For the $(\mathbf{e}_e, \theta_e)$ upper bound parameters previously given on a periodic cell, two bonds are cut per $r_o\sqrt{3}$ distance. Therefore, the energy error density per unit area of the graphene sheet is

$$\Pi - \Pi^h = C\frac{1}{h}, \quad C \le \frac{2\phi}{r_o\sqrt{3}}. \tag{33}$$

Through numerical experiments, the efficacy of this upper bound can be tested for increasing element sizes. Figure 5 shows several example calculations for varying $\mathbf{e}_e$ and θ_e. The data sets marked $\theta_1, \theta_2, \theta_3, \theta_4, \theta_5$ respectively denote $(\mathbf{e}_e, \theta_e) = (\frac{1}{2}\mathbf{e}_2, 0)$, $(\frac{1}{4}\mathbf{e}_2, 0)$, $(\frac{1}{4}\mathbf{e}_2, \frac{\pi}{16})$, $(\frac{1}{2}\mathbf{e}_2, \frac{\pi}{16})$, $(\frac{1}{2}\mathbf{e}_2, \frac{\pi}{8})$, and $(\frac{1}{3}\mathbf{e}_2, 0)$. The scatter at smaller element sizes shows the breakdown of rotational and translational invariance near the atomistic region as previously discussed. The scatter is also attributed in part to the imprecise measure of bond density when only a few bonds are involved at very small element sizes. Notice that the magnitude of the error for small h is as high as 3 eV/Å with a mean value of approximately 2.2 eV/Å. The equilibrium interatomic distance in graphene is approximately 1.42 Å. The standard lattice binding energy is -7.44 eV per carbon atom. Then, in the extreme case where there is poor mesh selection, the energy error can exceed 4 eV/atom. For larger element sizes, the

13
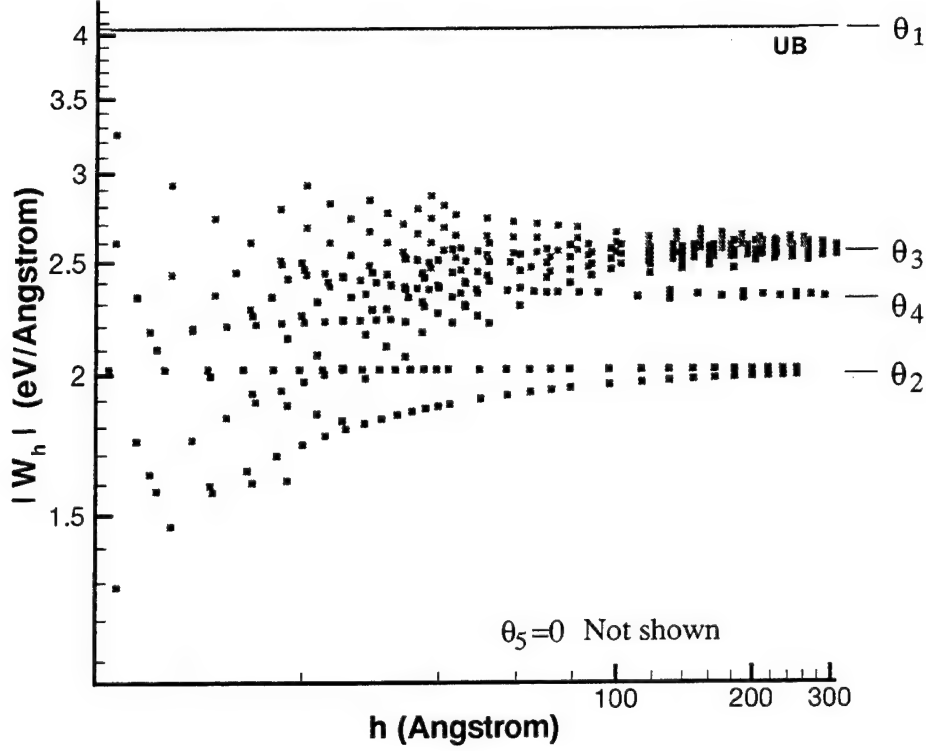
Figure 5. Numerical tests on the discretization error ($|\mathcal{W}^h| = C$).

coefficient of the error approaches a continuum limit where invariance sets in, and the error of the total energy density is even smaller due to the inverse dependence on h.

A lower bound can be generated likewise by choosing the best approximating scenario of the fictitious element boundary. If we assume that any line that cuts directly through an atom affects neither the atom nor the bonds emanating from it, then the lower bound is always zero since a line can always be oriented in a periodic graphite lattice to cut only through a line of atoms. An example of this is the set $(\mathbf{e}_e, \theta_e) = (q\mathbf{e}_2, 0)$ for $q = \frac{1}{3}$ or $\frac{2}{3}$. Specifically, the coefficient is found to be

$$C \geq \frac{2\psi\left(\mathbf{r}_{(ij)}, \mathbf{r}_{ik}\right)}{3r_o}. \tag{34}$$

14

This calculation suggests that refinement is not always desirable to atomic scales when employing finite element methods, an observation that is counterintuitive to conventional h-adaptive methods. A means of systematically correcting these effects is still currently unavailable.

1.5 Nontrivial Deformation

The second source of ghost forces comes from the first terms in equations (4) and (27), i.e.,

$$a(\mathbf{u}, \mathbf{u}) - a^h(\mathbf{u}^h, \mathbf{u}^h) = \frac{1}{n_a} \sum_a^{n_a} \phi_a(\mathbf{F}(\mathbf{u})) - \frac{1}{n_a} \sum_a^{n_a} \phi_a(\mathbf{F}(\mathbf{u}^h)) \tag{35}$$

$$= \int_\Omega (\nabla \mathbf{u}) : \left. \frac{\partial^2 \mathcal{W}}{\partial \mathbf{F} \partial \mathbf{F}} \right|_{\mathbf{F}=\mathbf{I}} : (\nabla \mathbf{u}) d\Omega$$

$$- \int_{\Omega^h} (\nabla \mathbf{u}^h) : \left. \frac{\partial^2 \mathcal{W}^h}{\partial \mathbf{F} \partial \mathbf{F}} \right|_{\mathbf{F}=\mathbf{I}} : (\nabla \mathbf{u}^h) d\Omega^h. \tag{36}$$

Despite the common expansions about $\mathbf{F} = \mathbf{I}$ in both integrals in equation (36), the Lagrangian stiffness terms are still unequal because of the differences in the implied summations over the requisite atoms (and/or bonds). More precisely, the number of bonds that are counted in $\mathcal{W}$ is unequal to the number in $\mathcal{W}^h$. Thus, standard numerical analysis techniques cannot be applied directly without significant modification.

In the limit as $h \to \infty$ and $r_o \to 0$, it has been shown that this atomistic error exhibits a boundedness proportional again to $\mathcal{O}\left(\frac{1}{h}\right)$ [8]. Furthermore, under these assumptions, one can show that the stiffness terms are equivalent in the limit, and the convergence rate of equation (36), the square of the energy norm, is bounded by some function of the element size h. Or in standard notation

$$||\mathbf{e}||_n \le ch^{k-n+1}||\mathbf{u}||_{k+1}, \tag{37}$$

where $\mathbf{e} = \mathbf{u}^h - \mathbf{u}$, c is some independent constant, k is the complete order of the piecewise smooth polynomial used in the interpolation and n is the order of the derivative in the

15

energy expression, i.e., the appropriate metric space. For continua, these types of rigorous estimates are well established [11]. However, for problems involving resolvable atomic details relative to finite element size, the precise magnitudes of error have not yet been ascertained in a generalized way as in continua. Such developments are potentially useful for error estimator/corrector schemes for implementation into existing computational methods.

Under limited distortions, however, simple estimates as in section 1.4 can again be obtained for deformed configurations. We presently consider the case where the in-plane shearing deformation of the atoms coheres to the Cauchy-Born rule [12]. Furthermore, the deformations are limited to the class of all uniform shears in which the coordination number of the atoms stays fixed. That is, the interatomic spacings do not change so that new bonds do not form and existing bonds do not break. The shear is characterized by the deformation gradient

$$
\mathbf{F} = \begin{pmatrix} 1 & \alpha & 0 \\ 0 & 1 & 0 \\ 0 & 0 & 1 \end{pmatrix},
\tag{38}
$$

where, based on the cut-off function in equations (29) and (32), and all relevant material parameters for carbon, we choose $0 < \alpha < 0.0617$. The deformed configuration of graphene is depicted in Figure 6. Under homogeneous deformation, the three vectors $\mathbf{a}$, $\mathbf{b}$, and $\mathbf{c}$ are the only vectors needed to describe the bond orientations and lengths in the entire sheet by appropriately tiling the plane. The Cartesian components of the deformed bonds are given by

$$
\mathbf{a} = \begin{pmatrix} \alpha r_o \\ r_o \\ 0 \end{pmatrix}, \quad
\mathbf{b} = \begin{pmatrix} \frac{r_o}{2}\left(\sqrt{3} - \alpha\right) \\ -\frac{r_o}{2} \\ 0 \end{pmatrix}, \quad
\mathbf{c} = \begin{pmatrix} -\frac{r_o}{2}\left(\sqrt{3} + \alpha\right) \\ -\frac{r_o}{2} \\ 0 \end{pmatrix}.
\tag{39}
$$

The restriction on α makes this a first order approximation. Pair interactions dominate over the higher order triple terms in equation (29). Using the earlier arguments for the

16
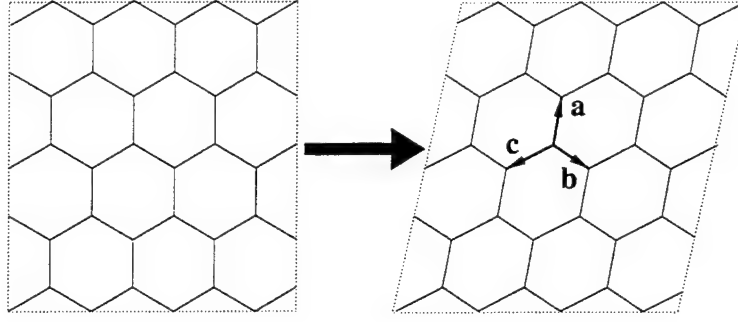
Figure 6. Homogeneous shear of graphene.

undeformed configuration, the UB and LB estimates for the error coefficients are

$$C^{\mathrm{UB}} = \frac{1}{r_U} \left[\phi(a) + \phi(b) + 2\psi(\mathbf{a}, \mathbf{b}) + 2\psi(\mathbf{a}, \mathbf{c}) + 2\psi(\mathbf{b}, \mathbf{c}) \right],$$

$$C^{\mathrm{LB}} = \frac{1}{r_L} \left[2\psi(\mathbf{a}, \mathbf{c}) + 2\psi(\mathbf{a}, \mathbf{b}) \right], \tag{40}$$

where

$$r_U = \frac{r_o}{2} \sqrt{12 - 6\sqrt{3}\alpha + 9\alpha^2}, \quad r_L = \sqrt{3} r_o, \tag{41}$$

and $a = |\mathbf{a}|$ and $b = |\mathbf{b}|$.

The change in the error estimates are shown vs. the extent of deformation in Figure 7. The variations are in the meV range. Further considerations must be undertaken to evaluate the error under larger deformations where changes in coordination and higher order atom interactions occur.

1.6 Closing Remarks

The area of computational multiscale method development remains a fertile area of research. It attempts to answer many of the most difficult questions of science at the nanoscale by leveraging the understanding of continua. In this report, we have proposed a first order
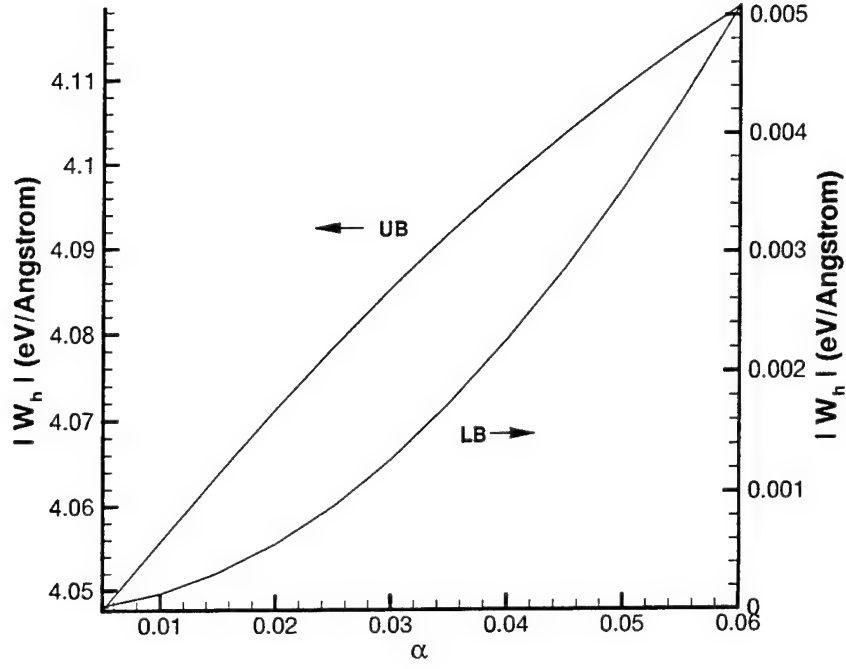
Figure 7. UB and LB estimates for the line density of the error as a function of deformation ($|\mathcal{W}_h| = C$).

characterization of the energy error in undeformed and limited deformed configurations of graphene using classical energy expressions. In the present carbon system where the force field is dominated by pairwise interactions of atoms, the findings show that the error introduced by discretization may lead to significant errors in the energy under certain mesh refinements.

2. A Literature Review of the Asymptotic Expansion Homogenization Method

The first part of section 2 briefly describes several key developments in homogenization. Their deficiencies in being unable to provide local information motivates the subsequent discussion of the so-called asymptotic expansion homogenization (AEH) approach. In section 2.2, various types of related and available homogenization methods are described that possess the homogenization/localization capability to handle complex linear/nonlinear behavior encountered in continuum and phenomenological engineering problems. Section 2.3 introduces the mathematical literature from which AEH finds its basis. Other names found in the literature for this approach include asymptotic homogenization, mathematical homogenization, and classical homogenization. All are based on the fundamental premise that the displacement, velocity, or temperature field is representable by an asymptotic series. To avoid confusion, the method will be referred to as AEH, whereas classical homogenization techniques will refer to homogenization methods based on classical mechanics principles. In section 2.4, application-oriented efforts for AEH for linear problems are summarized. Sections 2.5 and 2.6 describe inelastic and nonlinear problems in the AEH literature. The method is completely demonstrated for a linear elastic example in section 2.7. And final conclusions are drawn from the literature review in section 2.8.

2.1 Classical Homogenization Methods and the Introduction of AEH

Early efforts in finding the effective properties of composite materials frequently approached the problem from a mathematical point of view to predict bounds on properties [13–16]. The

19

simple geometries of spherical or cylindrical inclusions permitted the use of simplified analytical methods. Though these investigations reveal much about the mechanics of composite materials, assumptions on the geometry of the microstructure and ordering of constituent properties pose limitations on their applicability to advanced high performance composites with complex microstructures.

Recent composite technologies, such as sophisticated woven fabric composites, employ complex patterns in the weaving of reinforcement fibers. Thus, bounds or other approximations of the effective properties that were originally designed for simple microstructures such as regular arrays of uniform cylinders or uniformly distributed spheres, are inappropriate. The same difficulties exist in predicting other constitutive properties such as conductivity, permeability, diffusivity, thermal expansion, and the like. Furthermore, though a repeating cell may still be identifiable and assumed small, the assemblage of cells within the true global body may not exhibit homogeneity in the necessary statistical sense [17] making the direct application of analytical techniques difficult.

To incorporate the details of the weaving patterns of the bundled fibers and the dependence of microstructural parameters on the macro properties, some researchers have used laminated plate analytical continuum methods [18–23]. By varying the boundary conditions applied according to displacements or tractions consistent with the theorems of minimum potential and complementary energies, bounds for the effective plate stiffness and compliance were obtained. Unfortunately, these methods are either inherently one dimensional (1-D) or two dimensional (2-D) or are restricted to simple microstructures. They employ the so-called mosaic or crimp approximations for the woven fabric geometry that allows them to construct analytical expressions for the fiber shape and, consequently, the constitutive equations. As such, they do not provide insight into the three-dimensional (3-D) physics associated with advanced composites, particularly when the fibers are not in the shape of simple trigonometric functions or when complex boundary interactions dominate the internal behavior of the material.

20

Other efforts appear in the form of mechanics-of-materials approaches within the framework of numerical methods for determining the homogenized properties [24–28]. These approaches are useful for complex 3-D microstructures. They typically require some external boundary conditions to be applied to the unit cell from which an understanding of the response of the structure is obtained by comparisons with Hooke's Law or energy balance principles. Averaging operations of the phenomenological models over the unit cell, referred to as homogenization, yield the homogenized properties. Details of the unit cell are smeared away in favor of a single set of properties that characterizes the inhomogeneous material in an average sense. The mechanics-of-materials approaches perform homogenization for arbitrarily shaped microstructural features. The AEH approach, on the other hand, can handle arbitrary shapes but also enables one to return to the microlevel details in the unit cell (i.e., localization) based on the global solution. Whereas the mechanics-of-materials approaches provide homogenized properties, the AEH approach provides homogenized properties as well as localized information.

As composite manufacturing techniques grow in sophistication, so too does the demand for computational and analysis methods for predicting and modeling the manufacturing process. A step in this direction is computational approaches that handle the important multiscale issues typically associated with heterogeneous materials. Among the approaches discussed in this study, the AEH method appears viable and useful for determining the effective properties of composites and employing the computed properties in subsequent macrolevel analyses. The approach is predicated on two fundamental assumptions: that the displacements (or other primary variable such as temperature or flow velocity) can be characterized by an asymptotic series in ε and that the salient features of the microstructure are contained in a unit cell representative of the periodicity at the local scale. The first two terms of the series are assumed to be representative of the respective macro and micro responses (see Figure 8). These definitive macro and micro terms, then, subject to the periodicity constraints, provide tangible variables from which to extract local effective micromechanical properties, local gradients, and the overall global response. The approach can also be extended to ther-

21

(a) Physical schematic

ε-Space (Micro-Macro)   X-Space (Macro)   Y-Space (Micro)
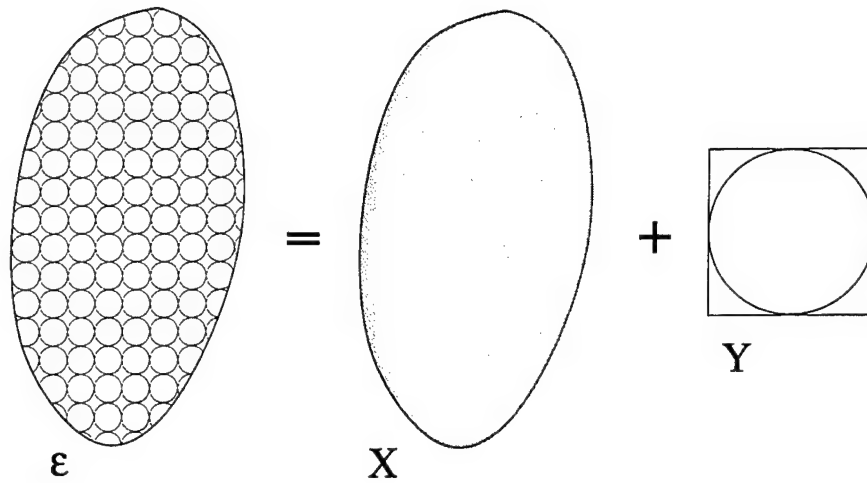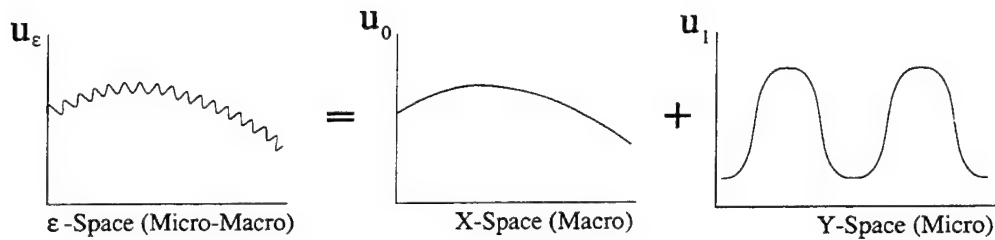
(b) Mathematical illustration

Figure 8. The body in ε-space is the realistic representation of the heteroge-
neous structure. The AEH approach isolates the micro from the
macro by approximating ε with an homogenized body in X and a
scaled representative unit cell in Y.

mal, flow or structural continuum problems. Its large range of computational applications
indicates its generality for a broad class of boundary value problems (BVP).

The AEH approach has also been studied in the context of problems involving three or
more scales [29] by using a reiterative scheme. By applying two-scale AEH successively
over multiple length scales, the AEH approach can be extended to problems involving three

or more length scales with little modification to existing formulations. The approach has been studied mathematically for linear heat conduction by Bensoussan et al. [29] and in engineering analysis for linear elasticity in Chang and Kikuchi [30].

The multiple scale abilities notwithstanding, the AEH approach can also be used as an approach only to estimate the homogenized properties. By deriving partial differential equations (PDEs) that govern the influence of inhomogeneities, no restrictions are placed on the size or complexity of shapes of the microstructure. The only limitation, therefore, is the significant preprocessing modeling effort needed to create the complex geometries associated with modern composites. Thus the same approach may be applied in a generalized manner to woven fabric composites, knit-fiber composites, metal matrix composites, and the like.

Researchers have also found AEH more apt for extension to the inelastic regime due to its ability to estimate microlevel information and continually update the homogenized macrolevel properties. With the localization capability inherently derivable through the formulations, microlevel information such as yield criteria or other nonlinear effects and state variables can be updated.

With the estimated information at the local level, global effects can then be estimated by re-homogenization based on the new local information. The new global information, then, influences the global homogenized problem in a circuitous manner [31–34]. Other popular homogenization approaches [13–28] do not permit the estimation of micro- and macrolevel information simultaneously. This key distinction is the redeeming quality of AEH that sets it apart from other homogenization approaches.

Conditions encountered in the analysis of composite materials are usually over a range of temperatures or structural behavior making them nonlinear. Traditional micromechanical techniques are suited best for conditions resembling linear or mildly nonlinear problems employing many simplifying assumptions on the geometric shapes or constitutive models

to make them tractable. Examples of restrictive assumptions may involve a simple microstructure geometry [13–17] or linear material models [18–22, 24–26]. Their ability to treat the micromechanical details of the material makes them useful for many applications. But the majority of the methods, without simplifying assumptions, are normally not applicable to nonlinear situations. Though other developments such as those in nonlinear continuum theories have been extensive, they are again inherently incapable of handling the complex micromechanical shapes and the aforementioned multiple-scale issues associated with advanced composites.

Though investigations in the literature for multiscale problems favor the AEH approach due to its fundamental developments in functional analysis, other homogenization/localization approaches are available. However, they suffer from several limitations. The approaches and the reasons for the choice of AEH are described in the next section.

2.2 Other Homogenization/Localization Methods

This study employs AEH, whose fundamental approximation is that the primary dependent variable can be composed by the superposition of a smooth global solution and a rapidly oscillating local solution. The sum of the two solutions is represented by the first two terms of an asymptotic series in ε. Based solely on this approximation, the underlying goal is to develop hierarchical continuum field equations for the coupled multiscale problem. The AEH method is not the only approach available which can handle the complex coupling in length scales for linear/nonlinear applications. Homogenization approaches for linear problems notwithstanding, methods of homogenizing material properties and subsequently localizing global solutions also appear elsewhere in the literature. The present state of progress in these areas appears to be in the early mathematical development stages or without sufficient generality that renders them useful only for the specific applications for which they are

derived. Few of these methods have yet to be used routinely in engineering applications for practical situations.

A detailed discussion and survey of four notable approaches: (1) the Fourier Series approach, (2) the Green's Function approach, (3) the Self Consistent approach, and (4) the Subvolume approach, are presented by Walker et al. [35] with emphasis in the analytical formulations. Despite the seemingly veritable merit in the approaches and the subsequent references therein, few researchers appear to employ these methods in computational mechanics elsewhere in the literature. This is in contrast to the sustained growth of AEH methods. The ease with which variational equations or PDEs can be formulated via AEH, unlike the methods described in Walker et al. [35], explains the popularity of the asymptotic approaches. Though the present study emphasizes mainly AEH, it is prudent in future investigations to scrutinize the methods of Walker et al. [35] closely in the framework of computational mechanics.

Moulinec and Suquet [36] employ Fast Fourier Transforms (FFT) to "pixelize" complex geometric microstructures and employ a superposition of displacements to develop an homogenization approach to study elastic and inelastic behavior of composites via FEM. The FFT circumvents meshing difficulties. The approach for nonlinear situations involves a step-by-step integration in time and incorporates the exact Green's function of the linear elastic and homogeneous analog of the material. Thus, the solution is expected to diverge from the true behavior of highly nonlinear materials where the Green's functions depart significantly from elastic and homogeneous conditions. In this way, the approach is restricted mainly to the linear regime. However, it shares the generality of the AEH approach in its ability to treat a large variety of microstructures.

Hou and Wu [37] integrate FEM with an AEH approach to formulate a method for homogenizing arbitrary heterogeneous structures not limited to periodic media but with rapidly oscillating microstructure. The developments presented are for elliptic problems which in-

clude elasticity and flows in porous media. The fundamental difference between this effort and other efforts in AEH is in the description of the base functions. The approach is computationally expensive due to the solution of simultaneous equations required to obtain these complicated base functions. The multiscale base functions are adaptive to the local properties to account for the refined scale of the heterogeneities. Thus, for general large scale problems, this approach becomes computationally prohibitive.

Woo and Whitcomb [38] present a global/local FEM to estimate local stresses in specific discretized regions using a refined mesh with loads kinematically matched at the subcell boundaries. The method, however, is limited primarily to linear elastic problems due to its use of mechanics of materials to estimate the effective properties and the localized behavior. In contrast, the AEH approach does not employ kinematic conditions when establishing a causal link between the micromechanical behavior and the global response. Instead, the link is established at the level of the primary variable, e.g., the deformation for structural problems, via an asymptotic series approximation. Thus, unlike the AEH approach, the convergence of the solution, the uniqueness of the microlevel stresses, and mathematical consistency of the formulations in the approach of Woo and Whitcomb [38] are not ensured.

In the next section, the background and related efforts in AEH are described. The mathematical basis for the approaches employed in this study can be found in a large breadth of mathematics literature. These are described next.

2.3   Background Literature: Mathematical Basis

Although asymptotic methods have existed for many decades, the application of an asymptotic expansion approach for heterogeneous materials is relatively new. Some early efforts at applying perturbation techniques to field problems in a strict mathematical context are

scattered through the literature beginning in the 1960s and 1970s. The literature observed a sharp increase of published efforts in the late 1970s and early 1980s in AEH as engineers began realizing the viability of the method for transport problems and as the maturity of the methods influenced others in the mathematical community. The increase also coincided with the release of two authoritative texts. The earlier of the two, by Bensoussan et al. [29], provides specific mathematical definitions, theorems, and principles for a large class of general elliptic systems. In addition to the AEH approach, they present other techniques for the treatment of heterogeneous periodic structures in general.

The second text by Sanchez-Palencia [39], much like Bensoussan et al. [29], is detailed in its mathematical analysis. Although much care is taken in presenting the equations, very rarely are the equations actually solved. Yet it is an important development because it provides a new perspective of AEH in its applicability to engineering problems. It effectively demonstrates the utility of AEH for more sophisticated engineering problems by deriving the needed equations for numerous engineering examples. However, both Bensoussan et al. [29] and Sanchez-Palencia [39] favor the functional analysis aspects of AEH and provide little discussion on how to solve the equations, particularly for practical problems.

Other AEH-related efforts in the literature since then consistently and categorically cite Bensoussan et al. [29] and Sanchez-Palencia [39] as their mathematical bases for subsequent novel developments. Other mathematical details can be found in, for instance, Lions [40], Duvaut [41], Oleinik [42], Tartar [43], Jikov et al. [44], Cioranescu and Paulin [45], and Bakhvalov and Panasenko [46].

In the next section, the literature associated with the AEH approach for general linear computational mechanics is described. Linear computational mechanics encompass low Reynold's number flow, heat conduction/diffusion, and linear elasticity.

2.4 Linear Engineering Problems

The majority of efforts, as documented in the mathematics literature, focus on linear problems primarily due to the ease with which linear problems can be studied via functional analysis. Despite the significant number of publications in this area, discussions herein are limited to those efforts that employ AEH in an engineering context. Engineering issues related to AEH, namely computational issues and multiscale equation development, are nontrivial and important facets to understand the behavior of periodic heterogeneous media.

Most developments are presented in elasticity due to the myriad range of engineering situations that can be covered based on this fundamental elliptic PDE. Examples include elastic damage and fracture mechanics. Multidisciplinary problems are also considered in conjunction with the elasticity problem, namely thermoelasticity, which requires the homogenization of the thermomechanical properties. The homogenization of thermal properties can also be found in the literature for efforts in solving the energy equation in non-isothermal fluid flow.

The literature here is arranged according to areas related to linear transport (fluid and heat flow) or linear elasticity.

2.4.1 Transport Problems

The early treatment of the AEH approach can be found in areas related to flow/transport and heat conduction in porous media. The statistically homogeneous nature of porous materials is known to satisfy the periodicity condition required in the AEH approach. A straightforward presentation of AEH for flow through porous media is shown in Keller [47]. The homogenization approach is employed to rederive Darcy's Law yielding sets of equations for the two length scales: micro and macro. In so doing, the approach avoids common heuris-

tic methods of homogenization, such as simple volume averaging, by introducing discrete micromechanical variables via higher order perturbation terms. The velocity, density, pressure, and external body force are expanded in asymptotic series where only the first two terms, representative of the respective macro and micro variables, are carried throughout the formulations. These discrete terms introduce traceable quantities and provide a means of ensuring existence and uniqueness of solutions to the multiple scale linear problems.

Citing the deficiencies of Darcy's Law, namely the inability to handle velocity gradients and boundary layers, Ene [48] presents the AEH approach for the Brinkman equation. Among other more complex engineering situations also considered include flow in a fractured porous medium and fluid-solid interactions.

Chang and Kikuchi [49] applied the homogenization method to analyze the non-isothermal mold filling process used in resin transfer molding and structural reaction injection molding. The approach employs a doubly porous woven fiber preform, the first scale at the scale of individual filaments, the second at the scale of bundled fiber tows, and the third at the scale of the global/macro structure. Stokes flow is assumed for the microscale transport where the resistance of the flow provides an estimate of the permeability tensor at the next length scale. The tensor is then used in Darcy's Law which can then be homogenized once again to provide a global permeability tensor for the Darcy's Law flow assumed to govern the macro mold filling problem. Hence, the homogenization procedure is reiterated to model the pore structures in the two hierarchical regimes.

Flow through porous media is primarily a linear problem because the Reynold's number is typically small. No AEH investigations appear to consider nonlinear inertial effects or convective terms.

Few research efforts seem available for AEH solely for simple heat transfer problems apart from the mathematics literature. The focus here is on engineering problems. The exist-

ing literature in this area appears classifiable into two specific categories: those treating multidisciplinary problems and those considering the complex microstructure geometries of certain types of composites.

Different from related efforts in other mechanics fields, thermal properties depend little on temperature gradients and mostly on the temperatures. That is, it is more common to associate thermal conductivity, k_{ij}, as a function of temperature

$$k_{ij} = k_{ij}(T). \tag{42}$$

Localization of the primary variable is typically uninteresting from a practical point of view because the variable is assumed to adhere to an asymptotic series whose terms after the zeroth order are very small. The higher order terms of the series, representative of the oscillatory temperature variations arising from the periodic distribution of inhomogeneities, are small compared to the zeroth order behavior of the temperature. Therefore, the primary variable at the local level will appear nearly constant. The gradients and heat flux (or strains and stresses in solid mechanics), however, provide greater information and show significant nonuniformity at the local level. In light of these observations, it is expected that the AEH heat transfer literature is limited primarily to homogenization with few considerations of the localized information because the local temperatures appears constant and uninteresting due to the dominance of the first term of the expansion. An investigation exploring these observations were shown by Chung et al. [50].

Thermal problems were treated first analytically by the early mathematical investigations. Many of the relevant references are shown in Bensoussan et al. [29] and Sanchez-Palencia [39]. In contrast to the governing equations in other mechanics areas, the thermal problem is tractable analytically because temperature is the only unknown and is a single degree of freedom.

Aside from the general mathematical considerations, researchers have attempted to under-

30

stand the thermal behavior of complex composite materials. Woven fabrics are employed in the manufacture of printed wiring board substrates. Dasgupta and Agarwal [51] use the two-scale AEH approach to study the orthotropic thermal conductivity of plain-weave fabric composite laminates. An analytical subproblem is studied to augment the numerical approach. Closed-form expressions are proposed to estimate the effective conductivity of the microscale unit cell. The analytical results are compared with the Finite Element (FE) solution of the microscale equations and limited experimental results. The analytical augmentation to AEH appears useful in problems where the solution of the microscale BVP must be avoided. However, two concerns are evident from their paper. First, the solution of the microscale BVP provides the necessary information to perform localization later in an integrated mathematically consistent multiscale analysis whereas their analytical approach provides only a means of homogenization, not localization. Second, the analytical augmentation is tailored for specific microstructure geometries, thus removing the generality of the AEH numerical approach. At the expense of the ability to treat general microstructures, their analytical augmentation to AEH removes the need to solve the microscale equations. This augmentation approach, which does not appear to present significant computational cost savings, is dubious because the solution of the microscale equations in AEH is an integral feature of making the approach general in the present study.

The paper by Chang and Kikuchi [49] discussed earlier also solves the energy equation in a non-isothermal mold filling problem for composites process modeling. The transient heat conduction problem is considered assuming a linear unchanging conductivity tensor and surface convection. The linearity of the problem leaves the heat transfer problem uncoupled from the fluid flow portion of the analysis. It is of the opinion of other investigators that the problem must be considered in the fully coupled context for accurate modeling [52].

Of the developments to date, AEH employed in the study of elastic materials is most numerous in the literature. This is due to the wide range of problems which can be analyzed by studying linear elasticity. In the next section, a brief survey of the literature encompassing

31

elasticity problems for AEH is presented.

2.4.2 Elasticity Problems

The bulk of the developments in AEH appears for the elastic problem. This is due to the larger number of applications feasible modeled by linear elasticity and the general robustness of formulations for continuum mechanics in nonlinear structural mechanics and its adaptability to multiscale situations. The difficulty of problems in the flow and heat transfer areas increases significantly even for small departures from linearity. Such limitations appear not to be present in structural mechanics.

In this section, the literature for linear elastic problems is reviewed. Emphasis is on efforts that employ linear elasticity as the basis for applications to more complicated engineering problems within the AEH framework.

Although the early formulations for simple elasticity are shown precisely in Bensoussan et al. [29] and Sanchez-Palencia [39], interesting and novel developments arise as the level of complexity increases in the elastic engineering problem. Lene [53] proposes an approach for studying damage in elastic UD composites with arbitrary cross section where the damage origin is localized to fiber-fiber and fiber-matrix interfaces. The damage is simulated by a displacement discontinuity applied by numerically inserting a singular element with zero thickness (slipping only) in the damaged region. The magnitude of the discontinuity is specified by a Coulomb friction principle. Throughout the analysis, the material is assumed elastic and additional damage evolution laws from thermodynamic theory are employed to trace the damage through the transient problem.

An optimal shape design methodology is introduced by Bendsöe and Kikuchi [54] that does not limit the problem to equivalent initial and final design topologies and avoids FE re-

32

meshing. The AEH approach is employed to calculate effective elastic properties repeatedly to satisfy specified design requirements. Upon computing the optimal distribution of material in space, an anisotropic mechanism results. The mechanism is constructed by an infimum of periodically distributed small holes in an homogeneous isotropic material.

Adaptive mesh refinement to improve numerical and spatial accuracy is considered by Guedes and Kikuchi [55] for effective linear elastic composite properties. Convergence and error estimate studies are also undertaken in the context of FEM. The AEH approach is employed and explicit details and physical interpretation of the characteristic function or correctors are shown.

The AEH approach has also been applied to biomechanics applications. Hollister et al. [56] employ the homogenization procedure to study the linear elastic material properties of porous trabecular bone structures. Global and local information are estimated and apparent stiffnesses were computed and compared with experiments.

As an extension of an earlier paper for the damage analysis of UD fibers [53], Lene and Paumelle [57] study the damaged properties of woven fabric composites. Again, the approach employs the elastic constitutive equations with the damage modeled as slipping at an interface without separation.

The homogenized properties from the AEH approach are compared with those from mechanics of materials approaches by Hollister and Kikuchi [58]. The strain energy densities are computed and compared for the cases when the homogenization approach is employed for a coarse FE model or the direct solution of the whole refined composite is studied. The mechanics of material approaches are based on flexural and stiffness measurement techniques that represent methods of estimating the bounding material properties for elastic materials as described in Chung and Tamma [59] which provides comparison of effective properties for other types of homogenization approaches in addition to AEH and standard mechanics

methods. Their study shows the agreement between AEH and other approaches for linear elasticity.

In other related works, Kawamoto and Kyoya [60] studied porous rock and pattern bolting of rocks using an earlier AEH development for simple elastic materials [55]. This applications-oriented investigation computed the effective elastic material properties for various volume fractions in a study for geomechanics. Lefik and Schrefler [61] applied AEH to linear elastic beam theory including shear rotations and warping using FEM. Equations of elasticity for bricks and mortar used in masonry structures were homogenized and studied by Papa [62]. The effective elastic properties and the damaged properties are computed via homogenization. Using digital image-based (DIB) geometric modeling, Golanski et al. [63] studied the thermoelastic behavior of layered metal matrix heterogeneous materials: a substrate of low alloy steel attached to a composite layer. In particular, the mismatch in material properties between successive layers and the microstresses in the composite layers was examined. A review of the method for linear elasticity is presented by Chung et al. [64].

The elastic problem has been studied extensively in the literature. Despite the seemingly simple considerations for elastic materials, the multidisciplinary nature of sophisticated problems and the complex computational issues associated with the homogenization approach make the study of elastic materials a cogent beginning for more sophisticated engineering problems. Some of these are described next.

2.5   Inelastic Problems

Stemming from early mathematical derivations by Sanchez-Palencia [39] and Sanchez-Hubert [65], numerous efforts have investigated the curious viscoelastic behavior of heterogeneous materials using AEH. Early mathematical literature for the viscoelastic problem in the con-

text of AEH shows an hereditary effect, the dependence of the present state of deformation on all previous states, occurs due to a physical and mathematical coupling between the non-hereditary phases and the elastic and viscous material tensors. Phases that are history independent appear to produce history dependent effects when composited together. Analogous behavior in other rate-independent inelastic (such as elasto-plastic) investigations is not observable because, regardless of the length scale under consideration, the incremental constitutive (Prandtl-Reuss) equations are Hookean in form. That is, general viscoelastic constitutive laws are non-Hookean:

$$\mathbf{P}\boldsymbol{\sigma} = \mathbf{Q}\boldsymbol{\epsilon}, \tag{43}$$

where $\mathbf{P}$, $\mathbf{Q}$ are differential operators whose coefficients are material properties and $\boldsymbol{\sigma}$, $\boldsymbol{\epsilon}$ are stress and strain tensors. Other types of inelastic constitutive models can typically be expressed in a Hookean form:

$$\boldsymbol{\sigma} = \mathbf{R}(\boldsymbol{\sigma}, U)\dot{\boldsymbol{\epsilon}}, \tag{44}$$

where $\mathbf{R}$ is a tensor whose terms are functions of material properties, stress components $(\boldsymbol{\sigma})$, internal energy (U), or other state variables. A Hooke's law form for the constitutive model possesses only one material property tensor and implies that the AEH approach can be extended forthright to the inelastic problem. The homogenized form of an Hookean constitutive model is Hookean as well. Such an observation is not permitted in non-Hookean forms. As a result of the equation development, mathematical interactions between the multiple terms over multiple phases are likely to occur. Another interpretation is that physical interactions between phases occur due to the simultaneous presence of solid and fluid effects.

Sanchez-Hubert and Sanchez-Palencia [65] showed mathematically that the instantaneous viscoelastic constitutive equation for a Kelvin-Voigt material can be related to long-term aging or long-memory effects via the AEH formulation. That is, the Kelvin-Voigt model applied to the microlevel constituents, when homogenized, may result in a macrolevel stress-strain equation different in form from that of the original microlevel equation.

35

The difference is a long-term aging or dissipative corrector term that manifests itself in the macrolevel equations. Two causes mathematically give rise to the corrector term. The first is the asymptotic expansion of the displacement variables, the central assumption of AEH. The second is the presence of additive rate-dependent and rate-independent terms in the stress-strain relationship. Sanchez-Palencia [39] shows that the coupling results in an additional term in the macro stress strain relationship whose interpretation is that of long memory. Unfortunately, though their investigation provides insights into the mathematical origins of the long-memory effects, the magnitude of those effects or even their practical demonstration were omitted. That is, the relevant equations have never before been solved.

Francfort and Suquet [66] later showed a different formulation with a simpler development of the viscoelastic micro-macro creep equations. Their work extended the earlier developments [39] by investigating convergence to the continuum solution and boundedness of the principal quantities. But despite the depth to which the investigation of the mathematics is presented in Francfort and Suquet [66] and the novelty of the formulations in Sanchez-Palencia [39], many of the computational and numerical details for the viscoelastic multiscale creep problem in practical and engineering applications have only recently been addressed by Chung et al. [67–69].

Viscoelastic methods via AEH for heterogeneous materials have been attempted and are present in the literature. Two efforts are available [70, 71], described below, both of which make several assumptions regarding the multiscale issues.

Dynamic viscoelastic response was investigated where the effective composite properties predicted were compared favorably with limited measurements [70]. The dissipative corrector, however, is avoided by imposing an appropriate harmonic oscillating strain comprised of time-dependent and time-independent components in the dynamic viscoelastic problem. Through the AEH derivation, only the time-independent component is retained hence precluding the time-dependent dissipative corrector effect from appearing.

Shibuya [71] performed the asymptotic expansion of the displacements in the Laplace domain wherein the equilibrium equations governing the fiber and matrix phases are assumed uncoupled. The governing equations are rendered in the Laplace frequency domain where, together with AEH, the viscoelastic response in a single time-step approach can be obtained for Maxwell materials using the elastic-viscoelastic correspondence principle.

Other methods, different from AEH, that treat the viscoelastic problem for more sophisticated constitutive models, employ analytical methods or expeditious assumptions that are inapplicable to general composite microstructures. Thus, despite their availability, especially those that estimate broad-spectrum phase behavior to which the quasi-static problem is a subset, the important limitation is in their assumption for simple shapes in the microstructure. An additional limitation in these existing methods is the decisive decoupling of the primary length scales. The AEH method still remains an open area for viscoelastic materials.

Research in the homogenization of linear problems continues to be of interest in the study of heterogeneous materials. They provide the mathematical and physical foundations upon which extensions to more complex, nonlinear problems can be based. Linear problems are also important in computational mechanics because important implementational and computer issues are easier to identify. Ultimately, however, classes of realistic multidisciplinary nonlinear problems are of greatest interest in the field of computational mechanics. Literature for nonlinear problems employing AEH is described next.

2.6 Nonlinear Engineering Problems

Limited AEH efforts are in the literature for nonlinear engineering situations due to the complicated issues associated with evolution of microlevel properties. To date, most computational mechanics efforts to treat nonlinear problems, apart from the present study, appear

exclusively for solid mechanics. Efforts are divided between geometric and material nonlinearity.

In perhaps one of the earliest demonstrations of a nonlinear engineering problem using computational mechanics and AEH, Guedes [72] employs FEM for quasi-static elasto-plasticity with finite deformations but without updating the microlevel properties between successive numerical iterations. The true elasto-plastic problem must involve change of material properties in the microstructure constituent phases, as recognized in Suquet [73]. As yielding occurs, the material properties must be rehomogenized to accurately model the evolving properties. That procedure was later corrected in a paper by Terada and Kikuchi [31].

Ghosh and co-workers [33, 34] use the Voronoi cell Finite Element Method (VCFEM) to derive the governing equations for two-scale elasto-plastic analysis of heterogeneous materials with AEH. The VCFEM is an alternative to conventional meshing of the heterogeneous microstructure. The analysis is for small displacements with the constitutive model expressed in Hookean form with an instantaneous tangent modulus, making the extension from AEH for elasticity straightforward. The computational approach employs an implicit solution procedure which solves the nonlinear governing equations iteratively.

Galvanetto et al. [74] present an elasto-plastic formulation for plane problems within an asymptotic expansion framework. By attempting to treat general nonlinear problems, their investigation poses restrictions on the forms of the constitutive equations to which the method can be extended. Again, it is apparent that constitutive models adhering to Hookean forms can account for heterogeneous media by extending the AEH approach for elastic materials. This approach has been discussed indirectly in other investigations [31].

Fish et al. [32] present an eigenstrain formulation to account for Hookean constitutive laws with additive strains in an elasto-plastic framework. A two-point integration scheme is proposed to decrease computation time with limited loss in accuracy. The equations are

38

integrated implicitly using an iterative scheme.

Other work in nonlinear AEH are varied. Issues of geometric nonlinearity are considered separately by Smit et al. [75] and Takano et al. [76]. Rate dependent nonlinear composites have been considered by Wu and Ohno [77]. And dynamic transient problems with nonlinear elasto-plastic models have been reported by Chung et al. [78].

Computational methods for heterogeneous media via AEH are still in a state of early development as evidenced in the available literature. Many areas still remain as fertile ground upon which new computational methods can still be developed. Several conclusions from this literature review are described next.

2.7 Demonstration of the Homogenization Method in Elasticity

Asymptotic homogenization approaches, and in particular their associated computational methods, for linear problems are in continued development as evidenced in the literature. Linear problems provide the sturdy foundations upon which nonlinear phenomena can be studied.

The goal of this section is to present AEH in a simple manner for the elastic problem. Elements in this linear formulation provide the foundations to which later developments will be reference. Also discussed are the FE computational issues associated with the model linear elastic problem. These will ultimately convey to any extension of the approach for inelastic/nonlinear problems or problems outside the realm of continuum scales.

The AEH approach for linear elasticity is well established and rigorously derived in the

literature. This section provides only a simple derivation to demonstrate the approach in practical terms for computer implementation. In section 2.7.1, the conventional equations of elasticity are defined formally. Then in section 2.7.2, the multiple scale equations are derived. In section 2.7.3, the relevant FE formulations are described, and the results are presented in section 2.7.4.

2.7.1 Equations of Conventional Elasticity

The PDE system for elasticity is described here for a bounded connected domain $\Omega \in \Re^3$ with smooth boundary $\partial\Omega$ in coordinates x_i (indices denote quantities in $\Re^3$ and the Einstein summation convention is used). The boundary is composed of two parts, $\partial_1\Omega$ and $\partial_2\Omega$, which are the surfaces of non-zero area associated with the Dirichlet and Neumann conditions. The body Ω may further be divisible into two parts, Ω_1 and Ω_2, by a smooth surface, Γ. Figure 9 shows a schematic diagram of the body where $\Omega = \Omega_1 \cup \Omega_2$ and $\partial\Omega = \partial\Omega_1 \cup \partial\Omega_2$.
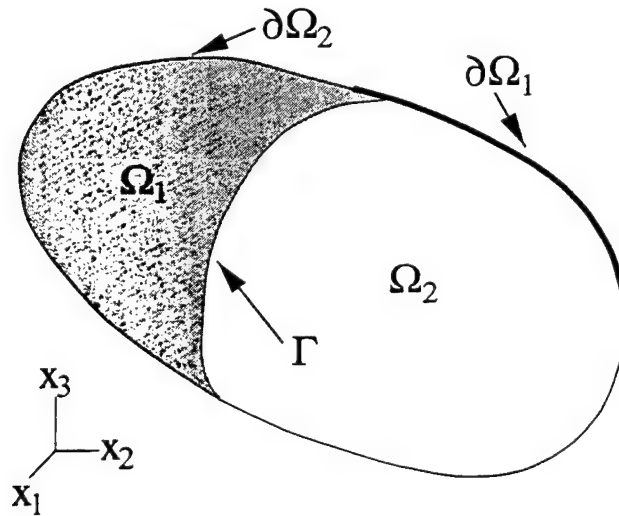
Figure 9. Elastic domain definitions.

2.7.1.1   Boundary Value Problem (BVP)

The BVP is comprised of four key components: (1) equilibrium, (2) compatibility, (3) constitution, and (4) sufficient boundary conditions for well-posedness. The equilibrium condition is specified by

$$\frac{\partial \sigma_{ij}}{\partial x_j} + f_i = 0, \tag{45}$$

where σ_{ij} is the Cauchy stress tensor and f_i is the body force vector. In the framework of linear elasticity with displacements as the unknowns, compatibility is inherently specified by the strain-displacement relationship given by

$$\epsilon_{ij}(\mathbf{u}) = \frac{1}{2}\left(\frac{\partial u_i}{\partial x_j} + \frac{\partial u_j}{\partial x_i}\right), \tag{46}$$

where ϵ_{ij} is the strain tensor and u_i is the displacement. The relationship between stress and strain, in this case Hooke's Law, gives the constitutive equation for the problem.

$$\sigma_{ij} = D_{ijkl}\epsilon_{kl}, \tag{47}$$

where D_{ijkl} is the fourth order elasticity tensor which is piecewise smooth in each phase having discontinuities on the interface Γ. The symmetry and ellipticity of D_{ijkl} are specified by

$$D_{ijkl} = D_{jikl} = D_{ijlk} = D_{klij}; \tag{48}$$

$$D_{ijkl}\epsilon_{ij}\epsilon_{kl} \geq \alpha\epsilon_{ij}\epsilon_{ij} \quad ; \alpha > 0 \qquad \forall \epsilon_{ij}(\mathbf{u}) \ \ (\text{symmetric}). \tag{49}$$

Finally, Dirichlet and Neumann boundary conditions, corresponding to the clamping (u_i) and surface force traction (F_i) boundary conditions on $\partial\Omega$, ensure a unique solution. These are given by

$$u_i = 0 \qquad \text{on } \partial_1\Omega; \tag{50}$$

$$\sigma_{ij}n_j = F_i \qquad \text{on } \partial_2\Omega. \tag{51}$$

41

The BVP can be solved in one of many number of different approaches. The present approach employs FEM to approximate the solution on a discretized general domain. As such, variational forms of the equations expedites the formulations.

2.7.1.2 Variational Problem

The variational formulation of the elasticity problem is presented here only as a manner of formality. The description becomes complete when presented in a functional analysis framework. Additional and more general details are available in Bensoussan et al. [29] and Sanchez-Palencia [39].

To write variational forms of the equations, the Hilbert space for the norm of $(H^1(\Omega))^3$ is defined as

$$V = \left\{ \mathbf{u} \; ; u_i \in H^1(\Omega) \; ; u_i|_{\partial_1 \Omega} = 0 \right\}. \tag{52}$$

The symmetric inner product, by virtue of the symmetry of the material property tensor in equation (48), is given by

$$a(\mathbf{u}, \mathbf{v}) \equiv \int_\Omega D_{ijkl} \epsilon_{ij}(\mathbf{u}) \epsilon_{kl}(\mathbf{v}) d\mathbf{x} \equiv \int_\Omega D_{ijkl} \frac{\partial u_i}{\partial x_j} \frac{\partial v_k}{\partial x_l} d\mathbf{x}. \tag{53}$$

The variational form of the BVP given in equations (45)-(47), (50), and (51) is: Find $u_i \in V$ such that

$$a(\mathbf{u}, \mathbf{v}) = \int_\Omega f_i v_i d\mathbf{x} + \int_{\partial_2 \Omega} F_i v_i d\mathbf{s} \quad \forall v_i \in V. \tag{54}$$

The variational form of the equations can then be extended using an FE approximation. The FE formulations will be presented in the next section in the context of general heterogeneous media.

The conventional equations of elasticity are the governing equations for single phase, homogeneous materials. Methods for heterogeneous materials typically involve an homogenization step. The AEH approach involves an homogenization step that is derived directly from the governing equations. This characteristic of the equations and their developments lends mathematical rigor to the homogenization approach, as frequently described in the literature. The "rigor" will be described in detail in the next section.

2.7.2   Homogenization in Elasticity

This section describes in detail the approach for employing a perturbative asymptotic series in ε for the displacement variables to derive multi-scale equations governing elasticity. We assume that the material under consideration has a microstructure comprised of multiple phases, and the orientation and shapes of the phases are such that they are distributed repetitively, periodically in all three-dimensions throughout the material.

For a more formal mathematical description, let Ω be a bounded domain in $\Re^3$ of coordinates x_i (or $\mathbf{x}$), as depicted in Figure 9. The domain Ω denotes the macrolevel or global structure. In the space of $\Re^3$ coordinates, let there be a fixed parallelepiped Y on coordinates y_i (or $\mathbf{y}$) of edges y_i^o (see Figure 10). All other parallelepipeds in the body are obtained by an integer translation of length ny_i^o where n is some integer. This assemblage of parallelepipeds implies that a single parallelepiped, or unit cell, is Y-periodic in y_i due to the repetition of the cell Y throughout the body.

In a conventional homogeneous material, the tensor of material properties D_{ijkl} is independent of position $\mathbf{x}$. If the material is not homogeneous, however, the material property will depend on $\mathbf{x}$. Moreover, if the heterogeneous material contains a periodic microstructure, where the length of the period is much smaller than any other lengths appearing in the problem, then the material behavior can be approximated by a homogenized material property

43
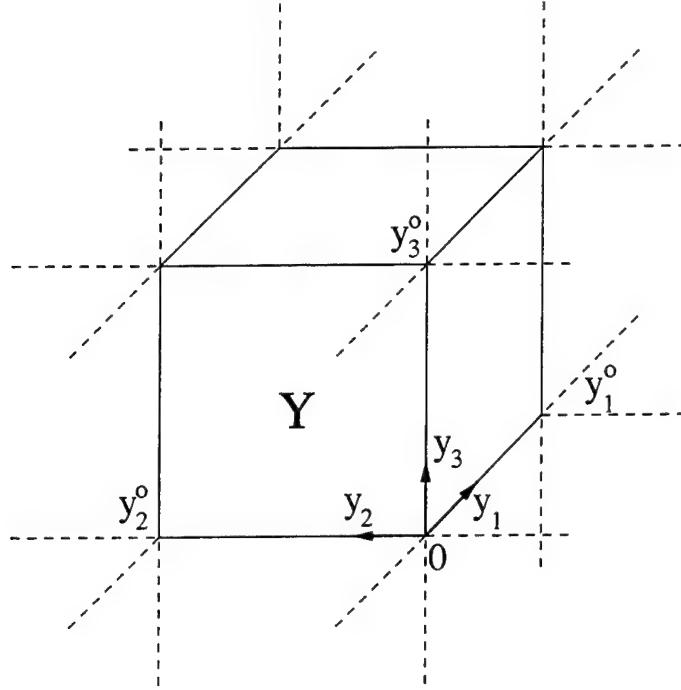
Figure 10. Y-periodic parallelepiped cell.

tensor, D_{ijkl}^h, based only on the salient features of one period. The homogenization method provides a means of computing D_{ijkl}^h such that the global problem can be treated.

The periodicity runs throughout the entire coordinate system x_i. The microstructural variations and the characterization of heterogeneous information are defined in the coordinate system y_i. To characterize the periodicity of the material properties, ε is defined such that

$$D_{ijkl}^\varepsilon(\mathbf{x}) = D_{ijkl}(\frac{\mathbf{x}}{\varepsilon}), \tag{55}$$

where ε is a real positive parameter where $\varepsilon \in (0, \varepsilon_o]$. The function D_{ijkl}^ε is εY-periodic in x_i. The period εY is a repeated array of parallelepipeds in $\Re^3$ whose edges are length εy_i^o.

44

From these developments, equations (45), (50), (51), and (47) are rewritten as

$$\frac{\partial \sigma_{ij}^{\varepsilon}}{\partial x_j^{\varepsilon}} + f_i = 0 \qquad \text{in } \Omega; \tag{56}$$

$$u_i^{\varepsilon} = 0 \qquad \text{on } \partial_1\Omega; \tag{57}$$

$$\sigma_{ij}^{\varepsilon} n_j = F_i \qquad \text{on } \partial_2\Omega; \tag{58}$$

$$\sigma_{ij}^{\varepsilon} = D_{ijkl}^{\varepsilon} \epsilon_{kl}(\mathbf{u}^{\varepsilon}), \tag{59}$$

where the ε script denotes quantities describing the true, high-resolution behavior the material under consideration. The given forces f_i and F_i are noticeably not periodic because they are applied on the surface of the global body Ω.

To summarize thus far, quantities such as the stress, $\sigma_{ij}^{\varepsilon}$, with the script ε, are the stresses in x_i^{ε} which give high-resolution details of the locally periodic nature of the structure. This stress is often impractical to compute due to the large amount of modeling effort needed to create a full size mesh with all the details of the microstructure. Moreover, the computer time needed to solve the problem on the mesh is cost prohibitive. It is prudent, therefore, to introduce an homogenization assumption. This is done by identifying the global body in x_i as an homogenized body with a definitive unit cell(s) in the coordinate system y_i. The local (or micro) coordinates y_i are related to the global (or macro) coordinates x_i via the parameter ε. Thus, the coordinate system y_i is a magnified scale of the microstructure whose absolute lengths are given in the x_i^{ε} coordinate system. And due to the same global body defined in x_i^{ε} and x_i, the distance between any two points in these coordinate systems are equivalent.

The displacements are approximated with an asymptotic series representation in ε given by

$$u_i^{\varepsilon}(\mathbf{x}) = u_i^{(0)}(\mathbf{x}, \mathbf{y}) + \varepsilon u_i^{(1)}(\mathbf{x}, \mathbf{y}) + \varepsilon^2 \cdots, \tag{60}$$

whose terms must be obtained by solving sets of equations, i.e., BVPs. The hierarchical equations will be described next. The Y-periodicity of the material requires that the stresses, strains and displacements also be Y-periodic. The functions $u_i^{(j)}(x, y)$ (j=1,2,...) are assumed

45

smooth functions that are Y-periodic in the variable y_i such that $y_i = x_i/\varepsilon$ and defined for $x_i \in \Omega, y_i \in \Re^3$ independent of ε. Thus, conversion of lengths between the magnified scale y_i and the original length scale x_i^ε is computed using ε. Henceforth, it is common practice to refer to any quantity with y-dependence as Y-periodic. Any quantity that is *solely* dependent on x with the script ε notation is εY-periodic.

Moreover, derivatives in x_i^ε must now be expanded in a chain rule for the space x_i possessing a periodic microstructure in y_i. The derivatives are now over two length scales given by

$$\frac{\partial}{\partial x_i^\varepsilon} = \frac{\partial}{\partial x_i} + \frac{1}{\varepsilon}\frac{\partial}{\partial y_i}. \tag{61}$$

The strains in equation (46) are therefore rewritten as

$$
\begin{aligned}
\epsilon_{ij}\left(\mathbf{u}^\varepsilon\right) &= \frac{1}{2}\left(\frac{\partial u_i^\varepsilon}{\partial x_j} + \frac{\partial u_j^\varepsilon}{\partial x_i}\right) \\
&= \frac{1}{2}\left(\frac{\partial u_i^{(0)}}{\partial x_j} + \frac{1}{\varepsilon}\frac{\partial u_i^{(0)}}{\partial y_j} + \frac{\partial u_j^{(0)}}{\partial x_i} + \frac{1}{\varepsilon}\frac{\partial u_j^{(0)}}{\partial y_i}\right. \\
&\quad + \varepsilon\frac{\partial u_i^{(1)}}{\partial x_j} + \frac{\partial u_i^{(1)}}{\partial y_j} + \varepsilon\frac{\partial u_j^{(1)}}{\partial x_i} + \frac{\partial u_j^{(1)}}{\partial y_i} \\
&\quad \left. + \varepsilon^2\frac{\partial u_i^{(2)}}{\partial x_j} + \varepsilon\frac{\partial u_i^{(2)}}{\partial y_j} + \varepsilon^2\frac{\partial u_j^{(2)}}{\partial x_i} + \varepsilon\frac{\partial u_j^{(2)}}{\partial y_i} + \cdots\right) \\
&= \frac{1}{2\varepsilon}\left(\frac{\partial u_i^{(0)}}{\partial y_j} + \frac{\partial u_j^{(0)}}{\partial y_i}\right) + \frac{1}{2}\left(\frac{\partial u_i^{(0)}}{\partial x_j} + \frac{\partial u_j^{(0)}}{\partial x_i} + \frac{\partial u_i^{(1)}}{\partial y_j} + \frac{\partial u_j^{(1)}}{\partial y_i}\right) \\
&\quad + \frac{\varepsilon}{2}\left(\frac{\partial u_i^{(1)}}{\partial x_j} + \frac{\partial u_j^{(1)}}{\partial x_i} + \frac{\partial u_i^{(2)}}{\partial y_j} + \frac{\partial u_j^{(2)}}{\partial y_i}\right) + \cdots \\
&= \frac{1}{\varepsilon}\epsilon_{ij}^{(-1)}(\mathbf{x},\mathbf{y}) + \epsilon_{ij}^{(0)}(\mathbf{x},\mathbf{y}) + \varepsilon\epsilon_{ij}^{(1)}(\mathbf{x},\mathbf{y}) + \varepsilon^2\cdots .
\end{aligned}
\tag{62}
$$

Hooke's Law in equation (47) also can be written in the expanded form as

$$
\begin{aligned}
\sigma_{ij}^{\varepsilon} &= D_{ijkl}^{\varepsilon}(\mathbf{x})\epsilon_{kl}\left(\mathbf{u}^{\varepsilon}\right) \\
&= D_{ijkl}(\mathbf{y})\left[\frac{1}{2\varepsilon}\left(\frac{\partial u_i^{(0)}}{\partial y_j}+\frac{\partial u_j^{(0)}}{\partial y_i}\right)+\frac{1}{2}\left(\frac{\partial u_i^{(0)}}{\partial x_j}+\frac{\partial u_j^{(0)}}{\partial x_i}+\frac{\partial u_i^{(1)}}{\partial y_j}+\frac{\partial u_j^{(1)}}{\partial y_i}\right)\right. \\
&\quad\left.+\frac{\varepsilon}{2}\left(\frac{\partial u_i^{(1)}}{\partial x_j}+\frac{\partial u_j^{(1)}}{\partial x_i}+\frac{\partial u_i^{(2)}}{\partial x_j}+\frac{\partial u_j^{(2)}}{\partial y_i}\right)+\cdots\right] \\
&= \frac{1}{\varepsilon}\sigma_{ij}^{(-1)}(\mathbf{x},\mathbf{y})+\sigma_{ij}^{(0)}(\mathbf{x},\mathbf{y})+\varepsilon\sigma_{ij}^{(1)}(\mathbf{x},\mathbf{y})+\varepsilon^2\cdots\ .
\end{aligned}
\tag{63}
$$

Substituting equation (63) into (57) gives a new set of hierarchical BVPs. These hierarchical BVPs are the multiple equations relevant to each scale in the multiple scale problem under consideration. The substitution yields

$$
\begin{aligned}
\varepsilon^{-1}\frac{\partial\sigma_{ij}^{(-1)}}{\partial x_j}+\varepsilon^{-2}\frac{\partial\sigma_{ij}^{(-1)}}{\partial y_j}+\varepsilon^{0}\frac{\partial\sigma_{ij}^{(0)}}{\partial x_j}+\varepsilon^{-1}\frac{\partial\sigma_{ij}^{(0)}}{\partial y_j} \\
+\varepsilon^{1}\frac{\partial\sigma_{ij}^{(1)}}{\partial x_j}+\varepsilon^{0}\frac{\partial\sigma_{ij}^{(1)}}{\partial y_j}+\varepsilon^{2}\frac{\partial\sigma_{ij}^{(2)}}{\partial x_j}+\varepsilon^{1}\frac{\partial\sigma_{ij}^{(2)}}{\partial y_j}+\cdots+f_i=0,
\end{aligned}
\tag{64}
$$

and upon rearranging terms, yields

$$
\begin{aligned}
\varepsilon^{-2}\frac{\partial\sigma_{ij}^{(-1)}}{\partial y_j}+\varepsilon^{-1}\left(\frac{\partial\sigma_{ij}^{(-1)}}{\partial x_j}+\frac{\partial\sigma_{ij}^{(0)}}{\partial y_j}\right)+\varepsilon^{0}\left(\frac{\partial\sigma_{ij}^{(0)}}{\partial x_j}+\frac{\partial\sigma_{ij}^{(1)}}{\partial y_j}+f_i\right) \\
+\varepsilon^{1}\left(\frac{\partial\sigma_{ij}^{(1)}}{\partial x_j}+\frac{\partial\sigma_{ij}^{(2)}}{\partial y_j}\right)+\varepsilon^2\cdots=0.
\end{aligned}
\tag{65}
$$

The equations must be valid for all $\varepsilon\rightarrow 0$. Therefore, the coefficients of the powers of ε must be zero identically. This implies that the first three coefficients are written as

$$
\varepsilon^{-2}:\qquad\qquad\frac{\partial\sigma_{ij}^{(-1)}}{\partial y_j}=0\ ;
\tag{66}
$$

$$
\varepsilon^{-1}:\qquad\qquad\frac{\partial\sigma_{ij}^{(-1)}}{\partial x_j}+\frac{\partial\sigma_{ij}^{(0)}}{\partial y_j}=0\ ;
\tag{67}
$$

$$\varepsilon^0 : \qquad \frac{\partial \sigma_{ij}^{(0)}}{\partial x_j} + \frac{\partial \sigma_{ij}^{(1)}}{\partial y_j} + f_i = 0 \quad . \tag{68}$$

Equations (66)–(68) are the hierarchical boundary value problems.

In summary thus far, three key operations have been performed. In the first operation, the displacements in ε-space were replaced by the series approximation in equation (60). In the second operation, the chain rule in equation (61) was used for derivatives. The chain rule is a consequence of the decomposition of the true structure in x_i^ε into an homogenized body in x_i (in which lengths are identical to those in the coordinate system x_i^ε) with a representative unit cell in y_i. The unit cell is characterized in a coordinate system that is a magnified scale of the microstructure that originally resides in x_i^ε. In the third operation, the displacements and chain rule were substituted into the conventional BVP for elasticity, and by setting the coefficients for the powers of ε to zero, three equations (66)–(68) were developed. The first and second equations are discussed in the next section in the derivation of a microlevel equation. The subsequent section employs the micro equation to derive a coupled multiscale BVP for linear elasticity.

2.7.2.1   Micro Equation

The micro equation refers to the equation governing the elastic phenomena on the domain characterized by the y_i coordinate system (the x_i coordinate system characterizes the macro domain). The micro equation is derived from equations (66) and (67) where the first equation defines the macro displacement variable which is then used to solve the second equation to give the first order perturbative variable. The present formulation is for a dual-scale heterogeneous material where it is implied that continuum level descriptions are applicable to both length scales.

Substituting for the first three orders for stresses and invoking the symmetry associated with

48

the material property tensor gives the following alternate forms of equations (66)-(68).

$$\frac{\partial}{\partial y_j} D_{ijkl} \frac{\partial u_k^{(0)}}{\partial y_l} = 0; \tag{69}$$

$$\frac{\partial}{\partial x_j} D_{ijkl} \frac{\partial u_k^{(0)}}{\partial y_l} + \frac{\partial}{\partial y_j} D_{ijkl} \left(\frac{\partial u_k^{(0)}}{\partial x_l} + \frac{\partial u_k^{(1)}}{\partial y_l} \right) = 0; \tag{70}$$

$$\frac{\partial}{\partial x_j} D_{ijkl} \left(\frac{\partial u_k^{(0)}}{\partial x_l} + \frac{\partial u_k^{(1)}}{\partial y_l} \right) + \frac{\partial}{\partial y_j} D_{ijkl} \left(\frac{\partial u_k^{(1)}}{\partial x_l} + \frac{\partial u_k^{(2)}}{\partial y_l} \right) + f_i = 0. \tag{71}$$

By virtue of the Y-periodicity of $u_i^{(0)}(\mathbf{x}, \mathbf{y})$ and the ellipticity (and positivity characteristics) of D_{ijkl}, it is evident that

$$\frac{\partial u_i^{(0)}}{\partial y_j} = 0. \tag{72}$$

This important result reveals that $u_i^{(0)}$ is a constant in y_i, or stated differently, $u_i^{(0)}$ is the global solution, the displacement of the macrolevel body and independent of y_i. With this in mind, equation (70) is simplified to

$$\frac{\partial}{\partial y_j} D_{ijkl} \left(\frac{\partial u_k^{(0)}}{\partial x_l} + \frac{\partial u_k^{(1)}}{\partial y_l} \right) = 0. \tag{73}$$

Equation (73) is an equation that relates the zeroth and first order displacements. Based on the global solution, $u_i^{(0)}$, the perturbative displacements, $u_i^{(1)}$, can be obtained from the equation

$$\frac{\partial}{\partial y_j} \left(D_{ijkl} \frac{\partial u_k^{(1)}}{\partial y_l} \right) = -\frac{\partial u_k^{(0)}}{\partial x_l} \frac{\partial D_{ijkl}}{\partial y_j}. \tag{74}$$

In practice, however, the solution of equation (74) is cumbersome in an FE sense if $u_i^{(0)}$ varies over x_i. Such a scenario requires the repeated solution for $u_i^{(1)}$ for every $u_i^{(0)}$, a task that is computationally onerous. Or stated differently, if one employs a straight-forward approach, the solution of equation (74) must be repeatedly obtained for each global element.

Fortunately, a simpler and more efficient approach is available. To help introduce the simpler version of the same problem, the Y-periodic Hilbert space V_Y is defined as

$$V_Y = \left\{ \mathbf{u} \; ; \; u_i \in H^1_{\text{loc}}(\Re^3) \, Y - \text{periodic} \right\}, \tag{75}$$

where the script loc refers to the *local* Y-periodicity depicted in Figure 11. In Figure 11, the solutions at points α_1 and α_2 are approximately equal due to their local proximity in x_i, though not the same, and their respective locations within each period, y_i, which are the same. The solutions at α_1 and β_2 are different because their locations in y_i are entirely different despite their local proximity in x_i. The solutions at β_2 and β_3 are also different despite their similar locations y_i. The difference is due to their large distance apart, much larger than the size of a single period, εy_i^o.

It is proposed that the solution of the perturbative displacement takes the form

$$u_i^{(1)} = \chi_i^{kl} \frac{\partial u_k^{(0)}}{\partial x_l} + \tilde{u}_i^{(1)}(\mathbf{x}), \tag{76}$$

where $\tilde{u}_i^{(1)}(\mathbf{x})$ is a constant of integration independent of y_i and χ_i^{kl} is the solution to the auxiliary variational problem given by: Find $\chi_i^{kl} \in V_Y$ such that

$$\int_Y D_{ijkl} \frac{\partial \chi_k^{mn}}{\partial y_l} \frac{\partial v_i}{\partial y_j} d\mathbf{y} = \int_Y v_j \frac{\partial D_{ijmn}}{\partial y_i} d\mathbf{y} \quad \forall v_i \in V_Y. \tag{77}$$

The function χ_i^{kl} is often termed the elastic corrector. Its namesake is described later in the development of the homogenized global equations. Other terms in the literature describe χ_i^{kl} as the characteristic function or, more classically, its gradient is the so-called misfit strain.

It is immediately evident that, via a superposition principle, the solution of equation (77) eventually yields a solution to equation (74). Equation (74) is often called the micro-equation because it relates the global solution to the perturbative solution and is solved over the domain of the unit cell. It is also the equation governing the smaller of the two length scales and illustrates the coupling between micro/local ($u_i^{(1)}$) and macro/global ($u_i^{(0)}$).

Figure 11. Local periodicity.

From equations (62) and (63), approximate microlevel strains and stresses can be computed using the solution for $u_i^{(1)}$. The expression for microlevel strains is given by substituting equation (76) into (62) and taking the zeroth order terms of ε which gives

$$
\begin{aligned}
\epsilon_{ij}^{(0)}(\mathbf{x}, \mathbf{y}) &= \frac{1}{2}\left(\frac{\partial u_i^{(0)}}{\partial x_j} + \frac{\partial u_j^{(0)}}{\partial x_i} + \frac{\partial u_i^{(1)}}{\partial x_j} + \frac{\partial u_j^{(1)}}{\partial x_i}\right) \\
&= \frac{1}{2}\left(\frac{\partial u_i^{(0)}}{\partial x_j} + \frac{\partial u_j^{(0)}}{\partial x_i} + \frac{\partial \chi_i^{mn}}{\partial y_j}\frac{\partial u_m^{(0)}}{\partial x_n} + \frac{\partial \chi_j^{mn}}{\partial y_i}\frac{\partial u_j^{(0)}}{\partial x_i}\right) \\
&= \left(\delta_{im}\delta_{jn} + \frac{\partial \chi_i^{mn}}{\partial y_j}\right)\frac{\partial u_m^{(0)}}{\partial x_n} \qquad \text{(symmetric about ij).} \qquad (78)
\end{aligned}
$$

51

In a similar way, the microlevel stresses can by obtained from the expression

$$\sigma_{ij}^{(0)}(\mathbf{x}, \mathbf{y}) = D_{ijkl}(\mathbf{y})\epsilon_{ij}^{(0)}(\mathbf{x}, \mathbf{y})$$

$$= D_{ijkl}(\mathbf{y})\left(\delta_{im}\delta_{jn} + \frac{\partial \chi_i^{mn}}{\partial y_j}\right)\frac{\partial u_m^{(0)}}{\partial x_n}. \tag{79}$$

Localization is performed by employing equation (78) to yield the microlevel strain details. Similarly, equation (79) gives the microlevel stresses. Localization refers to the process of obtaining microlevel information, or information on the y_i coordinate system from the global solution $(u_i^{(0)})$.

In summary thus far, the corrector χ_i^{kl} was introduced as a means of expressing the perturbative displacement $u_i^{(1)}$ in a closed-form relationship with the global displacement $u_i^{(0)}$. It is of key importance to distinguish between the global displacement $u_i^{(0)}$ and the microstress $\sigma_{ij}^{(0)}$. Although both share the same script notation for the zeroth order, the gradient of the global displacement in x_i^ϵ, by virtue of the chain rule of equation (61), does not immediately give the global stress. This inequality can be expressed by

$$\frac{\partial u_i^{(0)}}{\partial x_j^\epsilon} \neq \frac{\partial u_i^{(0)}}{\partial x_j}. \tag{80}$$

But mathematical consistency of the formulations can be demonstrated by showing that the gradient of $u_i^{(0)}$ in x_i gives the volume average of the gradients in x_i^ϵ. This is characterized by

$$\frac{1}{|Y|}\int_Y \sigma_{ij}^{(0)}(\mathbf{x}, \mathbf{y})d\mathbf{y} = \frac{\partial u_i^{(0)}}{\partial x_j}, \tag{81}$$

where $|Y|$ is the volume of the unit cell. That is, the average of the microstress in equation (79) gives the global stress.

2.7.2.2 Single-Point Localization Paradox

Equations (78) and (79) exemplify a key deficiency of the AEH approach. Despite the equations being "micro equations," length scale information, namely the scale parameter ε, is conspicuously absent. This precludes the exchange of length scale information across multiple scales. The absence of ε is attributable to the first order approximation of the asymptotic series in ε. The gradients of the first order displacement for strains and stresses are therefore zeroth order in ε. The physical interpretation is that the AEH approach involves point-wise localization. Upon homogenization, the scale and details of the microstructure are "smeared" away. When one returns to compute microlevel information via localization, the microstrains and stresses are computed at a single point in the global body. An entire unit cell exists at the single point, x_i. Thus, the point-valued global strain is then used to compute the local strains (and stresses) over all y_i.

A paradox is therefore evident. The scale parameter ε is a quantity that magnifies the coordinate system of the microstructure. But the microstructure is assumed mathematically disconnected from the global body. The scale parameter is not used to relate a position in y_i to the original heterogeneous body in the ε-space. Thus, if two points (x_i^1 and x_i^2) are selected arbitrarily close, both will have an entire unit cell Y. The two unit cells may therefore overlap, hence the paradox. We presently call this the single-point localization paradox and is depicted schematically in Figure 12.

It is reassuring, however, that in equation (78), the strain term outside of the parentheses is the only term dependent on x_i. The other terms are constants or depend on y_i. Thus, in the limit as the two points approach each other ($x_i^1 \to x_i^2$), the global strain at the point is single-valued. Even if two selected points in x_i are very close and have two different unit cells associated with them, the microstrains computed over those two unit cells become the same as $x_i^1 \to x_i^2$. That is, if x_i^1 and x_i^2 are very close but not the same, the difference in computed microstrains may be trivially small. An analogous argument can be made for microstresses.
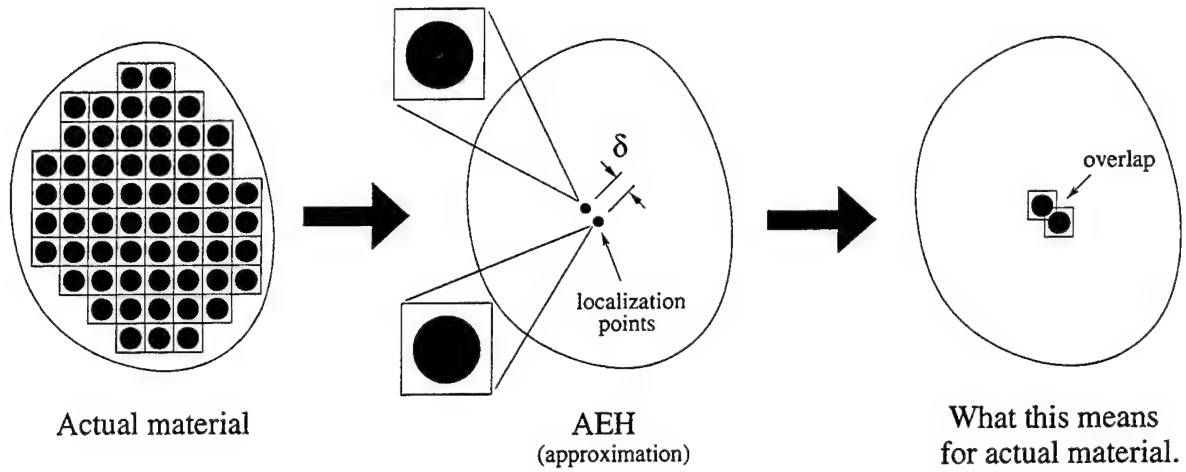
53

Figure 12. The single-point localization paradox. The approximations of the
AEH approach remove length scale information at the microlevel.
This allows for unit cells to overlap conceptually and leads to the
localization paradox.

The single-point localization paradox implies that equations (78) and (79) are only quantitative "estimates" of the local strain and stress. To have an exact prediction entails the solution of the fully refined problem with all microscale details of the structure modeled using a prohibitively large number of degrees of freedom. Such is the trade-off between solving an homogenized solution with estimates of the local behavior and an extremely large single scale high resolution problem possessing a large number of degrees of freedom. The local estimates are merely representative of the behavior. In an FE context, this local region is an element or the region near the quadrature point where the gradient terms of equations (78) and (79) are computed.

2.7.2.3   Macro Equation

Equation (76) is now used to complete the derivation of the effectively homogenized equations for linear elasticity. That is, the effective macro BVP is formulated here. Substituting

equation (76) into (71) gives

$$\frac{\partial}{\partial x_j} D_{ijkl} \left[\frac{\partial u_k^{(0)}}{\partial x_l} + \frac{\partial \chi_k^{mn}}{\partial y_l} \frac{\partial u_m^{(0)}}{\partial x_n} \right]$$
$$+ \frac{\partial}{\partial y_j} D_{ijkl} \left[\frac{\partial}{\partial x_l} \left(\chi_k^{mn} \frac{\partial u_m^{(0)}}{\partial x_n} \right) + \frac{\partial \tilde{u}_k^{(1)}}{\partial x_l} + \frac{\partial u_k^{(2)}}{\partial y_l} \right] + f_i = 0. \tag{82}$$

If $u_i^{(2)}$ is to be Y-periodic, then by virtue of the definition of Y-periodicity, equation (82) admits a unique solution for $u_i^{(2)}$ up to an additive constant if and only if

$$\int_Y \frac{\partial}{\partial y_j} D_{ijkl} \frac{\partial u_k^{(2)}}{\partial y_l} d\mathbf{y} = 0. \tag{83}$$

Substituting equation (82) into (83) yields

$$\int_Y \left\{ \frac{\partial}{\partial x_j} D_{ijkl} \left[\frac{\partial u_k^{(0)}}{\partial x_l} + \frac{\partial \chi_k^{mn}}{\partial y_l} \frac{\partial u_m^{(0)}}{\partial x_n} \right] + f_i \right\} d\mathbf{y} = 0 \tag{84}$$

and upon rearrangement and dividing both sides by the volume of the unit cell $|Y|$ gives

$$\frac{\partial}{\partial x_j} \left\{ \frac{1}{|Y|} \int_Y D_{ijkl} \left[\delta_{km} \delta_{ln} + \frac{\partial \chi_k^{mn}}{\partial y_l} \right] d\mathbf{y} \right\} \frac{\partial u_m^{(0)}}{\partial x_n} + f_i = 0 \tag{85}$$

Equation (85) and equations (50) and (51) constitute the homogenized BVP in elasticity. The material property tensor is now

$$D_{ijmn}^h = \frac{1}{|Y|} \int_Y D_{ijkl} \left[\delta_{km} \delta_{ln} + \frac{\partial \chi_k^{mn}}{\partial y_l} \right] d\mathbf{y}. \tag{86}$$

Thus, the average zeroth order stress, also the macrolevel effective stress, is given by

$$\left\langle \sigma_{ij}^{(0)} \right\rangle = D_{ijkl}^h \frac{\partial u_k^{(0)}}{\partial x_l}, \tag{87}$$

$$= D_{ijkl}^h \left\langle \epsilon_{kl}^{(0)} \right\rangle, \tag{88}$$

where the volume average notation is implied by the brackets:

$$\langle\ \rangle = \frac{1}{|Y|} \int_Y (\ )\, d\mathbf{y}. \tag{89}$$

Equation (86) provides the motivation for referring to χ_i^{kl} as a corrector function because of its corrective feature in the equation. In its absence, equation (86) gives the standard volume average of the material properties, characteristic of the Rule-of-Mixtures approach for estimating homogenized properties of heterogeneous materials. Thus the corrector effectively "corrects" for the presence of multiple phases within the unit cell and their collective interactions everywhere else in the global body via periodic boundary conditions on ∂Y. The gradient of χ_i^{kl} can also be interpreted as a misfit strain because it accounts for the mismatch strains resulting in the multiple phase microstructure. However, this study chooses the "corrector" terminology for its physical interpretation where χ_i^{kl} corrects the heterogeneous material from the otherwise conventional homogeneous understanding of the governing equations.

This concludes the derivation of the multiscale BVP for linear elasticity. The equation for the microscale is given in equation (77) and the equation for the macroscale is given in equation (85). Solving equation (77) gives χ_i^{kl} which is then used in equation (86) to calculate the effective homogenized properties. The homogenized properties are used in equation (85) to compute the global solution, $u_i^{(0)}$. Once the global solution is obtained, the perturbative displacement term, $u_i^{(1)}$, can be computed using equation (76). Moreover, the microlevel information can be computed using χ_i^{kl} and the localization equations given in equation (78) for strains and equation (79) for stresses. The homogenization-localization cycle demonstrated provides the integral link allowing causal relation of the continuum BVP across multiple-length scales.

Although the mathematical formulations are well-defined and discussed extensively in the literature, the practical implementational issues are often nebulous. In the next section, FE equations are formed and presented along with a computational, implementational procedure which provides the conceptual understanding required to employ AEH in general numerical methods.

2.7.3 Finite Elements, Elasticity, and the Homogenization Approach

This section provides a practical approach for computing the corrector, χ_i^{kl}, the effective material properties, D_{ijkl}^h, and the localized perturbative displacement term, $u_i^{(1)}$, in the framework of FEM. The description and the utility of the AEH approach differ subtly from the earlier mathematical descriptions when placed in the context of numerical methods. This section attempts to discuss these differences and present a simple approach for employing the method for relatively complicated heterogeneous problems.

2.7.3.1 Computing the Corrector

The solution of the variational equation given in equation (77) gives the corrector, χ_i^{kl}. The variational equation is rewritten here for convenience: Find $\chi_i^{kl} \in V_Y$ such that

$$\int_Y D_{ijkl} \frac{\partial \chi_k^{mn}}{\partial y_l} \frac{\partial v_i}{\partial y_j} d\mathbf{y} = \int_Y v_j \frac{\partial D_{ijmn}}{\partial y_i} d\mathbf{y} \quad \forall v_i \in V_Y.$$

For simplicity, consider the material under investigation to be in the class of orthotropic materials with nine independent components in the material property tensor. Henceforth, Voigt notation will be employed which exploits the symmetry of the strains and allows the following notational simplification to be made:

$$\begin{Bmatrix} \epsilon_{11} \\ \epsilon_{22} \\ \epsilon_{33} \\ 2\epsilon_{12} \\ 2\epsilon_{13} \\ 2\epsilon_{23} \end{Bmatrix} \rightarrow \begin{Bmatrix} \epsilon_1 \\ \epsilon_2 \\ \epsilon_3 \\ \epsilon_4 \\ \epsilon_5 \\ \epsilon_6 \end{Bmatrix}. \tag{90}$$

Furthermore, the appropriate piecewise linear Sobolev spaces are implied for the test and trial functions. A less rigorous engineering description is favored here over a mathematical FE procedure in terms of function spaces. Additional details can be found in numerous FE references [55, 79–82]. The standard FE representation for element strain, $\{\epsilon\}$, is given by

$$\{\epsilon\} = [B]\{u\}, \tag{91}$$

where $[B]$ is the element strain matrix and $\{u\}$ is the vector of nodal displacements. The element stresses are given by

$$\{\sigma\} = [D][B]\{u\}, \tag{92}$$

where $[D]$ is the matrix of material properties and $\{\sigma\}$ is the vector form of the symmetric stress tensor. Thus, the FE analogue of equation (77) is given in element form by

$$\int_{Y^e} [B]^T [D][B] d\mathbf{y}^e [\chi] = \int_{Y^e} [B]^T [D] d\mathbf{y}^e, \tag{93}$$

where the script e denotes element quantities associated with the discretized FE domain of the unit cell, namely the body Y^e. Equation (93) can also be written for a 3-D problem as

$$
\begin{array}{ccc}
[K^e] & [\chi] = & [F^D] \\
[n^e_{\text{dof}} \times n^e_{\text{dof}}] & [n^e_{\text{dof}} \times 6] & [n^e_{\text{dof}} \times 6]
\end{array}
, \tag{94}
$$

where

$$[K^e] = \int_{Y^e} [B]^T [D][B] d\mathbf{y}^e \quad \text{and} \quad [F^D] = \int_{Y^e} [B]^T [D] d\mathbf{y}^e, \tag{95}$$

and n^e_{dof} is the number of nodal degrees of freedom of each element in Y^e.

2.7.3.2 The RHS Matrix $[F^D]$

The corrector is noticeably a matrix, not a vector as is the case for displacements in conventional elasticity. This is a result of the multiple right-hand side vectors signifying the load,

58

$[F^D]$. Each column of the load "matrix" corresponds to a column in the material property matrix, $[D]$. Stated differently, equation (93) is actually a set of six matrix equations for 3-D elasticity. These can be summarized in a conventional sense of solving for a single column of unknowns $\chi^{(n)}$ as

$$[K^e]\{\chi^{(n)}\} = \int_{Y^e} [B]^T \{D^{(n)}\} dy^e, \tag{96}$$

where $n = 1 \cdots 6$, implying a total of six solutions of the problem, with

$$\{D^{(1)}\} = \begin{Bmatrix} D_{11} \\ D_{21} \\ D_{31} \\ 0 \\ 0 \\ 0 \end{Bmatrix}, \{D^{(2)}\} = \begin{Bmatrix} D_{12} \\ D_{22} \\ D_{32} \\ 0 \\ 0 \\ 0 \end{Bmatrix}, \{D^{(3)}\} = \begin{Bmatrix} D_{13} \\ D_{23} \\ D_{33} \\ 0 \\ 0 \\ 0 \end{Bmatrix},$$

$$\{D^{(4)}\} = \begin{Bmatrix} 0 \\ 0 \\ 0 \\ D_{44} \\ 0 \\ 0 \end{Bmatrix}, \{D^{(5)}\} = \begin{Bmatrix} 0 \\ 0 \\ 0 \\ 0 \\ D_{55} \\ 0 \end{Bmatrix}, \{D^{(6)}\} = \begin{Bmatrix} 0 \\ 0 \\ 0 \\ 0 \\ 0 \\ D_{66} \end{Bmatrix}. \tag{97}$$

The six solutions provide the six columns of $[\chi]$ in equation (94).

Thus, for a given elastic problem of a heterogeneous body, the approach requires the solution of six sets of equations to compute the corrector. Each solution corresponds to a particular "mode" or "character" of the unit cell: three normal modes and three shear modes.

To obtain a unique numerical solution, a zero constraint on χ must be applied somewhere within the FE model of the unit cell. This can be done arbitrarily because only the corrector gradient is needed in obtaining the homogenized properties. For explicit computation of the

59

perturbative displacement $u_i^{(1)}$, it is optimal to choose a node exploiting the symmetry of the parallelepiped. In the present study, the zero constraint is applied on a corner node where any three edges intersect.

2.7.3.3   Periodic Boundary Conditions

Additionally, boundary conditions must be applied to simulate the periodicity as required by the AEH approach. Periodicity is enforced by requiring nodal value equality on opposing boundaries of the unit cell model. To illustrate this, consider the 3-D parallelepiped as depicted in Figure 13. Boundary conditions for all degrees of freedom at the relevant nodes on opposing faces of the following form must be applied

$$\chi_i(0, y_2, y_3) = \chi_i(y_1^o, y_2, y_3), \tag{98}$$

$$\chi_i(y_1, 0, y_3) = \chi_i(y_1, y_2^o, y_3), \tag{99}$$

$$\chi_i(y_1, y_2, 0) = \chi_i(y_1, y_2, y_3^o). \tag{100}$$

In practice, a simple linear algebra operation on the assembled stiffness matrix, $[K]$, is all that is required to impose these boundary conditions. Hinton et al. [83] provide an approach that reduces the order of the stiffness matrix in accomplishing this task.

The periodicity assumption is crucial to the numerical procedure because it imposes the condition originally specified theoretically in equations (55) and (75). The explicit dependence of the equations on x_i and/or y_i are predicated on the definition of X in $\Re^3$ and the periodicity definition of Y. These conditions are tantamount to enforcing the assumption that each given unit cell is embedded in an array of identical unit cells. Methods of enforcing other types of periodicity conditions are discussed in Whitcomb [26] and Chung [84]. Though no studies in the literature appear to investigate the merits of one set of periodicity conditions over another, it traditionally understood that the periodicity breaks down near boundaries
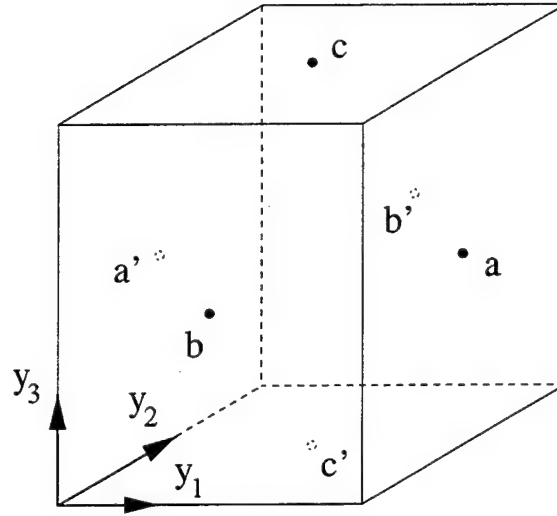
$$\chi_i(\text{a}) = \chi_i(\text{a'})$$
$$\chi_i(\text{b}) = \chi_i(\text{b'}) \quad \text{i=1,2,3}$$
$$\chi_i(\text{c}) = \chi_i(\text{c'})$$

Figure 13. Periodic boundary conditions. Nodal values for χ on opposing faces are equal.

or regions of global discontinuities [37].

However, the assumption of periodicity is necessary in sophisticated approaches because it indirectly accounts for the presence and interactions of the other unit cells. Without such conditions, only dilute concentrations of inclusions are permissible, the correctness of the present formulations notwithstanding.

Finally, to obtain a solution with rigid body modes removed, a zero displacement condition must be applied arbitrarily in the body Y^e. The effective properties are independent of the location where the zero condition is applied. The relative magnitudes of the nodal values of $[\chi]$, however, are easiest to interpret when the zero condition is applied at a location that exploits the cubic symmetry of the unit cell in Figure 13. The present study enforces this condition at an arbitrary corner where any three edges intersect. Then, by virtue of the

periodicity assumption, all corners also have zero displacement.

Once the corrector, $[\chi]$, is determined at the nodes of the unit cell FE model, the effective property matrix of the model can be computed. In the next section, an approach for computing the homogenized effective elastic properties of the unit cell is described.

2.7.3.4   Computing the Homogenized Property Matrix

The computation of the homogenized property matrix in FEM comes from a direct modification of equation (86) which gives

$$[D^h] = \sum_{e=1}^{n_{elm}} \frac{V_e}{V_{tot}}[D^e]\left([I] + [B^e][\chi^e]\right), \qquad (101)$$

where $[D^h]$ is the homogenized property matrix for the unit cell, n_{elm} is the number of elements in the unit cell, V_e is the volume of the element, V_{tot} is the total volume of the unit cell, $[I]$ is the identity matrix, $[B^e]$ is the element strain matrix, and $[\chi^e]$ is the matrix of nodal $[\chi]$ values connected to that element. Summing over all the elements provides the volume average over the unit cell with the added correction that $[\chi^e]$ provides. The script e in all of the terms denotes the micro element in Y^e.

The last term of equation (101) is the so-called corrector term which accounts for the presence of the inhomogeneities in the microstructure. It also accounts for the interactions between a given cell, Y^e, and the periodic array of cells surrounding it. This is what is referred to earlier in section 2.7.2.1 as the misfit strain, in keeping with micromechanical elasticity theories [85, 86].

The gradients of $[\chi^e]$ are computed at the integration points of the elements in Y^e where they are numerically most accurate. For linear problems, the gradients at the integration points can be averaged to provide a single gradient for the entire element. The gradient of

$[\chi^e]$ in equation (101) is this average in the present context of elasticity.

It is of interest to note that the integral in equation (86), due to the division by the unit cell volume, adds no dimensionality to the homogenized properties. This implies that the effective property matrix is only a function of the relative lengths of inclusions and matrix.

The effective material property matrix is then employed in the global equations as the material property matrix of the global element. It is therefore implied that each global element possesses one unit cell representative of the microstructure in that global region of the structure. After the global solution is obtained, the local gradients within the representative unit cell can be computed. The next section describes the approach for computing this "localization" information.

2.7.3.5 Computing the Perturbative Term

The perturbative term, $u_i^{(1)}$, is determined at the nodes of the body in Y^e. The term is a function of the global deformation gradient which varies from one global element to another. Thus, if the gradients through the global body are not uniform, then the perturbative displacements will also vary accordingly. This can also be interpreted as the local periodicity assumption permitting variations of the microlevel information from one location in the global body to another.

In the integrated multiple scale approaches of this study, the local information is computed using the deformation gradient at the numerical integration points of the global element. Thus, the integration points of the global elements serve as conduits of information through which passes the macro information to the micro domain.

In equation (76), the perturbative displacement was given as

$$u_i^{(1)} = \chi_i^{kl} \frac{\partial u_k^{(0)}}{\partial x_j} + \tilde{u}_i^{(1)}(\mathbf{x}).$$

The boundary conditions used to compute χ_i^{kl} described in section 2.7.3.3 implies that the constant of integration of equation (76), $\tilde{u}_i^{(1)}$, is zero. Then, the nodal perturbative displacements in a 3-D problem are given by

$$
\begin{array}{cccc}
\{u^{(1)}\} = & [\chi] & [B^g] & \{u^{(0)}\} \\
\{n_{\text{DOF}} \times 1\} & [n_{\text{DOF}} \times 6] & [6 \times n_{\text{dof}}^g] & \{n_{\text{dof}}^g\}
\end{array}
, \tag{102}
$$

where $\{u^{(1)}\}$ is the vector of nodal perturbative displacements at the microlevel, $[\chi]$ is the matrix of nodal corrector values at the microlevel, $[B^g]$ is the strain matrix of the global element for which the microlevel unit cell is being considered, and n_{DOF} is the total number of degrees of freedom in the FE mesh for the body in Y^e.

Finally, the microlevel strains and stresses can be computed using equations (78) and (79) from the perturbative displacements given in equation (102). In the next section, the specific procedural steps are outlined.

2.7.3.6 Computational Procedure

The procedural steps for homogenization and localization of a linear elastic problem are described here. It is assumed for simplicity that the global geometry possesses only one microstructural representative unit cell. That is, the FE problem involves the solutions of the governing equations over two meshes – the global body mesh and the local unit cell mesh. Should the microstructure vary at different locations within the global body, it is understood that the procedure must be extended to account for multiple unit cell meshes.

In the following steps, the dimensions of the matrices are provided for a 3-D scenario. The matrix sizes can be changed according to the dimensional of the problem. The distinction

64

between global FE quantities and local quantities are specified by script g or e, respectively.

Step 1. Create the FE model of the global body in X^e.

Step 2. Create the FE model of the microstructural body in Y^e.

Step 3. Solve for the corrector χ_i^{jk} in the variational equation given by equation (77) or the discretized corrector in equation (93):

$$
\underset{[n_{\text{dof}}^e \times 6]}{\int_{Y^e} [B^e]^T} \ \underset{[6 \times 6]}{[D^e]} \ \underset{[6 \times n_{\text{dof}}^e]}{[B^e] d\mathbf{y^e}} \ \underset{[n_{\text{dof}}^e \times 6]}{[\chi]} = \underset{[n_{\text{dof}}^e \times 6]}{\int_{Y^e} [B^e]^T} \ \underset{[6 \times 6]}{[D^e] d\mathbf{y^e}} \ .
$$

The RHS terms are given in equation (97) and the symmetric boundary conditions are imposed according to equations (98)-(100).

Step 4. Compute the effective elastic tensor by substituting the correctors determined in step 3 into equation (86) or (101):

$$
\underset{[6 \times 6]}{[D^h]} = \sum_{e=1}^{n_{\text{elm}}} \frac{V_e}{V_{\text{tot}}} \ \underset{[6 \times 6]}{[D^e]} (\ \underset{[6 \times 6]}{[I]} + \ \underset{[6 \times n_{\text{dof}}^e]}{[B^e]} \ \underset{[n_{\text{dof}}^e \times 6]}{[\chi^e]}) \ .
$$

The result of this step is the homogenized material property tensor or *homogenization*.

Step 5. Solve the global problem for $u_i^{(0)}$ using the homogenized properties of step 4 subject to boundary conditions and loads on the global body. The solution is obtained from equation (85) or the discretized form given by

$$
\underset{[n_{\text{dof}}^g \times 6]}{\int_{X^e} [B^g]^T} \ \underset{[6 \times 6]}{[D^h]} \ \underset{[6 \times n_{\text{dof}}^e]}{[B^g] d\mathbf{x^e}} \ \underset{\{n_{\text{dof}}^e\}}{\{u^{(0)}\}} = \underset{[n_{\text{dof}}^g \times 3]}{\int_{X^e} [N]^T} \ \underset{\{3\}}{\{f\} d\mathbf{x^e}} \ . \tag{103}
$$

The values of $u_i^{(0)}$ from this step give the traditional global solution analogous to the conventional response of an homogeneous material.

Step 6. Compute the average local strains at the desired discrete locations in X^e (usually at quadrature points) via equation (78) on an element-by-element basis over Y^e which is given by

$$\left\{\epsilon^{(0)}\right\}(\mathbf{x}, \mathbf{y}) = ([I] + [B^e][\chi])[B^g]\left\{u^{(0)}\right\}, \qquad (104)$$

where the script g and e are used to denote the FE strain matrices for the global element and the local element, respectively. Note that the gradient term, $\partial u^{(0)}/\partial x$ or $[B^g]\left\{u^{(0)}\right\}$, is constant in y_i. This means that for a given microstructural unit cell, $[B^g]$ is a constant.

Step 7. Compute the local stresses via equation (79) also on an element-by-element basis over Y^e:

$$\left\{\sigma^{(0)}\right\}(\mathbf{x}, \mathbf{y}) = [D^e]([I] + [B^e][\chi])[B^g]\left\{u^{(0)}\right\}. \qquad (105)$$

The material property tensor $[D]$ in equation (105) varies according to y_i. This step, together with step 6, completes the *localization* procedure that yields the local strain and stress information.

2.7.4   Comparisons With Other Homogenization Methods

This section is divided into two subsections. The first subsection discusses the similarities between AEH and classical homogenization approaches to develop an analogy to facilitate the understanding of the AEH homogenization approach. In the second subsection, simple comparisons between the present homogenization approach and other homogenization approaches are presented in the context of inplane plate stiffness.

2.7.4.1   Classical Approach Analogy

There exists a rich body of literature in the understanding of effective properties of composites [13, 85–89]. Many so-called classical approaches employ analytical techniques which place assumptions on the simply shaped geometry of the microstructure. The assumption on geometry and isotropy of the phases permits the development of closed form approximations for the effective properties. They consequently preclude considerations for complex substrate geometries, such as woven fabrics, and are limited to spherical, cylindrical, ellipsoidal or other types of simply shaped inclusions. Others depart from a classical methodology, and instead, opt for numerical techniques or analytical methods derived from classical approaches to accommodate the complex microstructure of advanced high performance composites [24–28, 38]. Some approaches ostensibly claim causal links between the local and global behaviors [38] much like the advocated AEH approach of this study.

However, there are three key distinctions that set the present AEH approach apart from other computational homogenization methods. The first is the ability of the AEH approach to provide homogenized properties for linear *and* nonlinear continuum BVPs. The second is the capability of estimating local response at very small length scales within the framework of seamlessly integrated multiscale mathematical derivations. Approaches such as Woo and Whitcomb [38] provide a means of estimating global and local response but use kinematic balances between length scales based on no mathematical development that inherently restricts the schemes to the elastic regime. The third is the similarities between the AEH approach and classical homogenization approaches. Analogies with classical approaches can be drawn due to the rigorous equation development of the AEH approach, and this is the topic of study in this section. Although it is beyond the scope of the present study to review all classical homogenization approaches – elasticity, heat transfer, etc. – there are inherent features over a broad range of homogenization schemes that are of interest for comparison purposes with the present computational method.

67

The comparisons and analogies drawn here are only to qualitatively examine the correctors described in earlier sections in a classical mechanics context. The equation morphology of correctors can draw parallels within the framework of the general theory of eigenstrains [85] and, for a more specific case, Eshelby's formulation [86, 90]. The rigorous treatment of these parallel observations is the subject of another investigation. The objective here is to loosely show the physical inferences permitted by these comparisons for didactic purposes.

2.7.4.1.1 General Theory of Eigenstrains In a strict sense, an eigenstrain refers to any general non-elastic strain such as thermal expansion, phase transformation, or misfit strains [85]. Presently, in the context of the correctors $[\chi]$ which is employed to effectively "correct" the homogenized material properties by

$$[D^h] = \sum_{e=1}^{n_{\mathrm{elm}}} \frac{V_e}{V_{\mathrm{tot}}} [D^e] \left([I] + [B^e][\chi^e]\right), \tag{106}$$

it is evident that computing the average stresses based on the effective elastic properties yields

$$\{\sigma^{(0)}\} = \sum_{e=1}^{n_{\mathrm{elm}}} \frac{V_e}{V_{\mathrm{tot}}} [D^e] \left([I] + [B^e][\chi^e]\right) \{\epsilon^{(0)}\}. \tag{107}$$

In Mura's general theory of eigenstrains, the fundamental assumption regarding linear elasticity is that the total strain (ϵ) is the linear superposition of the elastic strain (ϵ^e) and the eigenstrain (ϵ^*), given by (for notational simplicity, the zeroth order script of the asymptotic series is henceforth omitted)

$$\{\epsilon\} = \{\epsilon^e\} + \{\epsilon^*\}. \tag{108}$$

The elastic strain is related to the stress by Hooke's Law which gives

$$\{\sigma\} = [D]\{\epsilon^e\} = [D]\left(\{\epsilon\} - \{\epsilon^*\}\right). \tag{109}$$

By comparing equation (107) with equation (109), it is immediately evident that the second strain component upon distributed multiplication in equation (107) is analogous with the

eigenstress component in equation (109). The eigenstress is the constitutive counterpart of the aforementioned eigenstrain. In the present context of heterogeneous materials, the eigenstrain is precisely the misfit strain which accounts for the inhomogeneous stress distribution that arises from the presence of an inclusion in a homogeneous matrix. As a consequence, in keeping with the physical descriptions of Mura [85], the stress and strain fields are "disturbed" from the trivial state in the AEH approach due to the fictitious eigenstrain (re: corrector) in the homogeneous material that accounts for the additional inclusion phase and the subsequent interactions between other inclusions.

2.7.4.1.2 Eshelby's Formulation

A more specific case of the eigenstrain interpretation is seen by parallel comparison with Eshelby's formulation for isotropic inclusions [86, 90]. In Eshelby's original formulations, the inclusions and matrix are of the same material. The premise of the approach is to equate the strain energy of a body in which a local region is subject to inhomogeneous loads (inclusion) with that of an homogeneous body containing a particular distribution of body forces to account for the inclusion. Misfit strains are those that result from the body forces that account for the presence of the inclusion, thereby disturbing the homogeneous matrix from its initial state and inducing a strain field.

The problem of an inhomogeneous material loaded externally by an applied field is decomposed into the sum of two problems. The first is that of a homogeneous material subject to the same external loads as the original problem. The second is the homogeneous material in the absence of external fields subject to a misfit strain (ϵ^*) that accounts for the presence of the inclusion. The induced strain ($\hat{\epsilon}$) caused by the presence of the inclusion can be obtained by transforming the misfit strain field via the transformation given by

$$\{\hat{\epsilon}\} = [E]\{\epsilon^*\}, \tag{110}$$

where $[E]$ is the so-called Eshelby tensor. The decomposition of the problem implies that

the internal energies are additive. By comparing the energies of the various problems, the true energy of the heterogeneous problem was derived as the sum of the internal energy of the same problem with the inclusion removed plus an additional interaction energy. That is,

$$U = U_o + \frac{1}{2}U_{\text{INT}}, \tag{111}$$

where U is the energy of the heterogeneous problem, U_o is for the homogeneous problem where the matrix has been removed, and U_{INT} is the interaction energy. The interaction energy for a problem with applied tractions is defined by

$$U_{\text{INT}} = \int_S (t_i^0 u_i - t_i u_i^0)dS, \tag{112}$$

where S is the surface of the inclusion and t_i and u_i are the surface tractions and the deformation, respectively. The script 0 denotes the fictitious problem where only the matrix is considered in the absence of the inclusion.

In the AEH approach, in the context of FEM, the total internal energy is given as the sum over Y^e of the internal energy in each element given by

$$U = \sum_{\neq \text{ elm}} V_e \left\{ \epsilon^{(0)} \right\}^T [D] \left([I] + [B^e][\chi^e] \right) \left\{ \epsilon^{(0)} \right\}, \tag{113}$$

where the ellipticity and symmetry of the terms have been used. In a more abbreviated form, equation (113) can be written as

$$U = U_{\text{D}} + U_{\text{corr}}, \tag{114}$$

where the energy components are self-evident by comparison to equation (113). Via non-rigorous manipulations, it can be shown that equation (114) becomes

$$U = (U_{\text{D}} + U_{\text{m}}) - (U_{\text{m}} - U_{\text{corr}}), \tag{115}$$

where U_{m} is a "catch-all" term whose value can be tuned by comparing with equation (111) such that $U_o = U_{\text{D}} + U_{\text{m}}$. Then, it is clear that the interpretation of the misfit strain is applicable to the AEH approach.

Clearly the derivation for the corrector of the present AEH approach is different from that for the interaction energy in Eshelby's formulations. But the additional interaction energy shows precise parallels in the interpretation of the equation forms and lends credence to the "corrector" interpretation of χ in equation (77). This superficial comparison of the equations is meant only to reveal the additive nature of the corrector and show its consistency with interpretations of classical homogenization approaches.

Moreover, other computational approaches such as those defined, for instance, by Foye [24, 25], Whitcomb [26], Gowayed and Yi [27], and Woo and Whitcomb [38], are not as easily comparable to classical approaches. Though the mechanics of material schemes employed therein are more intuitive from a force-balance perspective, it is precisely for this reason they cannot be extended to the nonlinear regime and show the rigorous coupling across length scales.

In the next section, quantitative comparisons are undertaken to show the agreement of the AEH approach with other numerical and analytical homogenization approaches for plate-like composites in linear elasticity. Though the AEH approach possess features not found in other computational homogenization approaches, it is still expected that for linear problems agreements with existing results can be obtained.

2.7.4.2 Numerical Comparisons

In this section, quantitative comparisons are presented between several homogenization methods. The homogenized inplane stiffness of a woven fabric plate structure is used for the comparison. The homogenized results from the AEH approach are compared with the so-called Strain Energy Balance, Finite Element Plate Approximation, and Area Averaging approaches. In addition, two analytical methods due to Ishikawa and Chou [91] for the so-called mosaic and crimp models are used to further verify the results with well-accepted

71

theories for woven fabric composites. The purpose here is to demonstrate the different effective elastic properties of composite materials obtainable using other homogenization methods and to show the definitive localization feature of the AEH approach. The distinction between the present work and other homogenization approaches, therefore, is illustrated quantitatively. The results presented in this section are directly from a published paper [59] and the associated thesis [84] on the effective homogenized elastic properties of woven fabric composites.

The present considerations are for general composites and therefore focus on methods which can homogenize, say, woven/undulating stiff cylindrical inclusions embedded in a soft matrix. In light of the scope of this section, homogenization approaches which can estimate effective properties of complex geometries are considered. In principle, these approaches are similar to classical mechanics approaches such as those described in Refs. [85, 86] in that only homogenization is feasible. This illustrates the key component of AEH absent in other existing approaches – AEH possesses the ability to establish a causal link between the continuum BVPs across the relevant length scales.

A full comparative study of selected homogenization schemes was conducted using the finite element meshes of the microstructure depicted in Figures 14(a)–(j). The study compares only the inplane Young's modulus because of the limitations inherent in using the plate approximation (see Chung [84]). Figures 15(a)–(b) show the moduli for the mosaic and crimp models and compare the results from the four homogenization schemes. The mosaic and crimp models are theoretical idealizations of the woven geometry of fibers used in woven fabric composites. They were originally proposed by Chou [92] for analytical methods.

Values for n_g used were 2, 3, 4, 5, 10, and ∞. It is clear by observation of these geometries that they are implicitly 50% fill tows by volume and 50% warp tows. The longitudinal (fill) and transverse (warp) material properties of the fiber bundles are representative of an epoxy graphite composite in Table 1.

72

(a) Mosaic model, $n_g=2$

(b) Crimp model, $n_g=2$

(c) Mosaic model, $n_g=3$

(d) Crimp model, $n_g=3$

(e) Mosaic model, $n_g=4$

(f) Crimp model, $n_g=4$

(g) Mosaic model, $n_g=5$

(h) Crimp model, $n_g=5$

(i) Mosaic model, $n_g=10$

(j) Crimp model, $n_g=10$
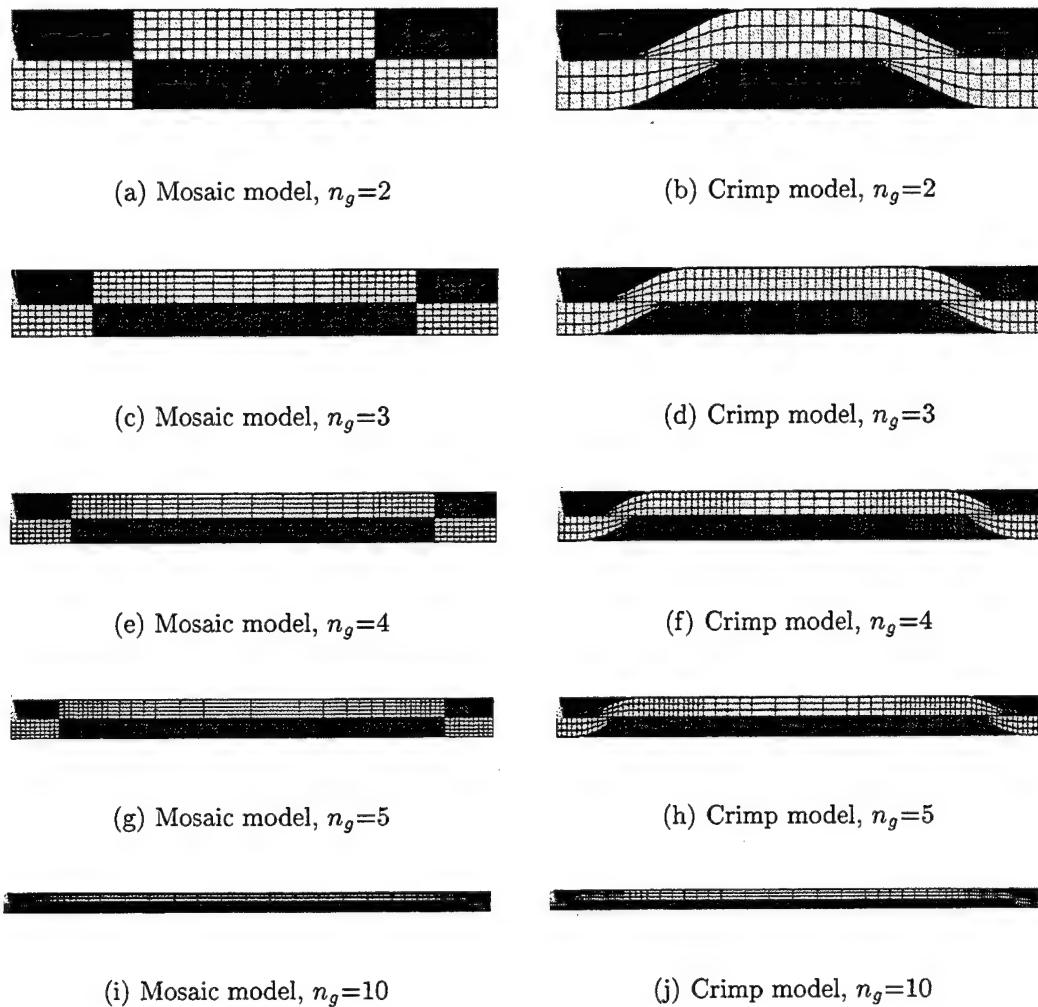
Figure 14. Finite element meshes of mosaic and crimp models for various weaviness parameter, n_g.

The results indicate that the AEH approach for linear elasticity yields results within the bounds of the analytical mosaic and crimp models. Furthermore, the AEH numerical results agree well with the other computational homogenization approaches. These results are indicative of the good agreement expected for other classes of linear problems. Nonlinear problems typically can be decomposed into a series of smaller linear problems in numerical implementation. In light of this, the mathematical consistency of the formulations further suggest the viability of AEH for treating problems in the nonlinear regime.
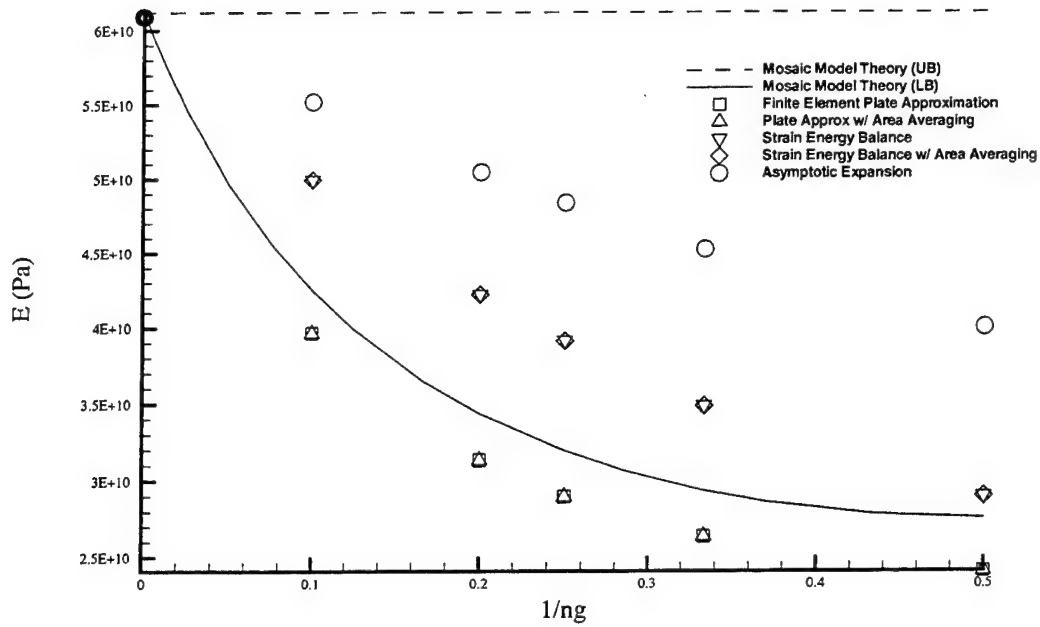
(a) Mosaic Model
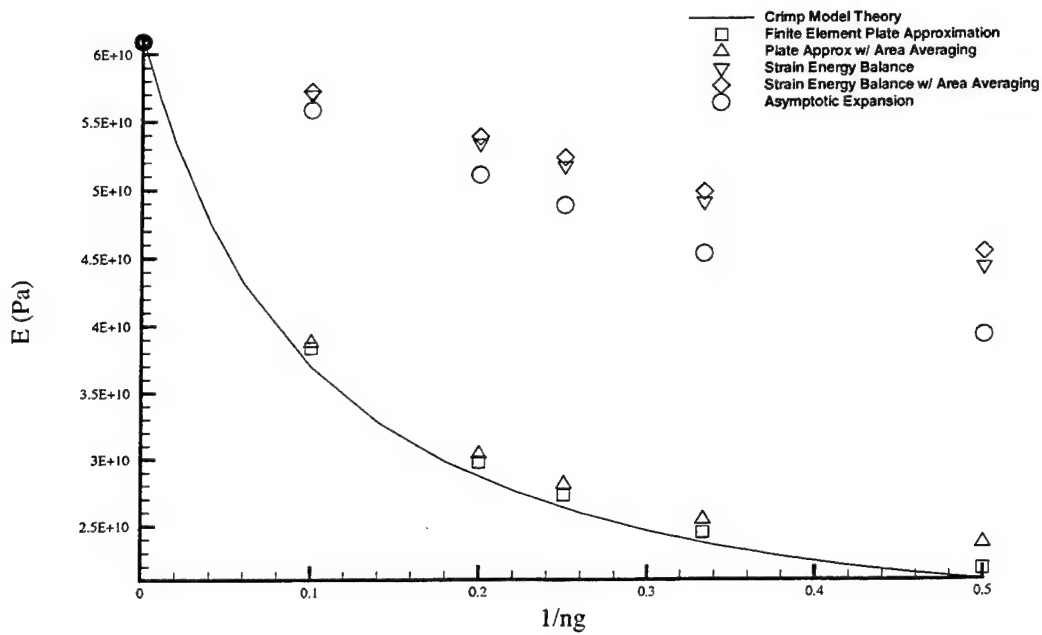
(b) Crimp Model

Figure 15. Comparisons of inplane moduli for the mosaic and crimp models for varying weaviness parameter, $1/n_g$.

74

Table 1. Constituent elastic material properties for epoxy/graphite composite.

Property	Longitudinal	Transverse
E_x (GPa)	113.0	8.82
E_y (GPa)	8.82	8.82
E_z (GPa)	8.82	8.82
ν_{xy}	0.0235	0.495
ν_{yz}	0.495	0.495
ν_{xz}	0.0235	0.495
G_{xy} (GPa)	4.46	2.95
G_{yz} (GPa)	2.95	2.95
G_{xz} (GPa)	4.46	2.95

Consider now the global problem depicted schematically in Figure 16. The FE model of this geometry is depicted in Figure 17 with 2,541 nodes and 2,000 elements. Two types of microstructures are employed in this section. The first microstructure is representative of an orthogonal non-woven fiber composite depicted in Figure 18 with 1,917 nodes and 1,472 element. The second model is representative of a plain woven fabric composite depicted in Figure 19 with 1,819 nodes and 1,408 elements. Constituent material properties for this example are listed in Table 2. Each material component is assumed isotropic. The objective here is to compute both the global deformation and stresses while simultaneously computing the approximate local stresses at the element locations depicted in Figure 16. The stresses are approximate due to the homogenization assumption which smears the inhomogeneous medium, simulating homogeneity, and the subsequent localization which uses the solutions obtained from the smeared behavior. Element no. 1,110 is located in a region that is expected to be of lower overall stresses than element no. 1,990. The bar will experience stress gradients due to the three-dimensionality of the problem. The dimensions of the bar are 2 m × 1 m × 1 m.
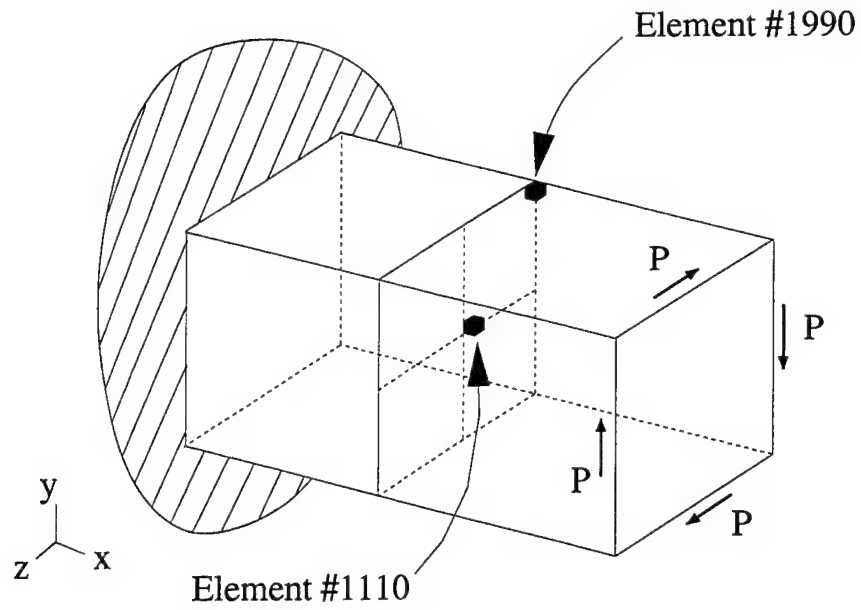
Figure 16. Bar twist problem (macro).
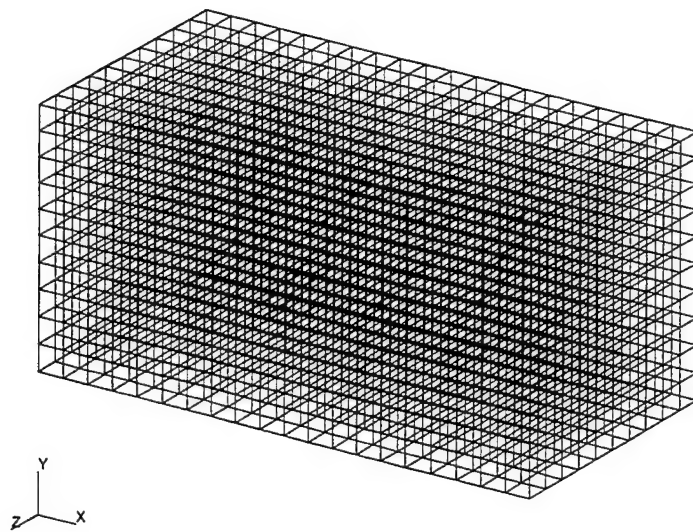
Figure 17. FE model of global (macro) bar twist problem.
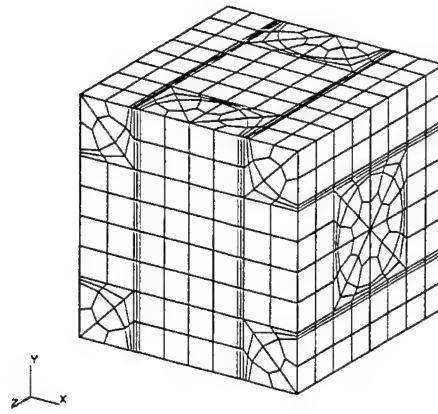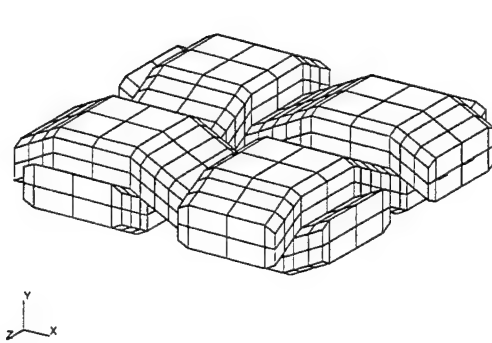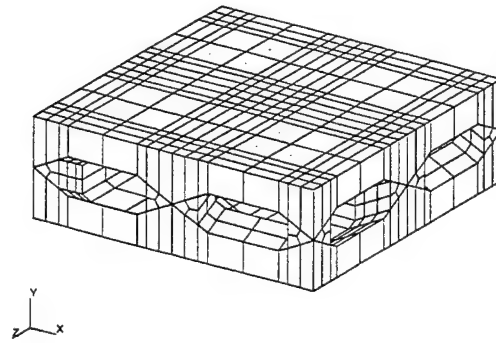
Figure 18. FE model of (micro) orthogonal non-woven fiber composite.
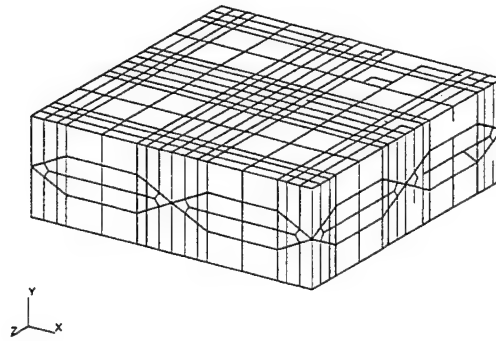
(a) 2D plain weave composite

(b) Fiber component

(c) Matrix component

Figure 19. Plain weave composite (micro) FE models.

Table 2. Constituent properties.

	E (GPa)	G (GPa)	ν
Epoxy resin	3.5	1.3	0.35
E-Glass	72.0	27.7	0.30
Ti-metalβ21-S	112.0	41.8	0.34
SCS-6	393.0	157.2	0.25

For the 3-D orthogonal non-woven and the 2-D plain weave composites, the elastic material tensors are computed. For the orthogonal non-woven fiber composite, the elastic tensor is given by

$$
\left[D^h\right]_{\text{orthog}} = \begin{bmatrix}
21.1 & 5.3 & 5.3 & 0 & 0 & 0 \\
5.3 & 21.1 & 5.3 & 0 & 0 & 0 \\
5.3 & 5.3 & 21.1 & 0 & 0 & 0 \\
0 & 0 & 0 & 3.4 & 0 & 0 \\
0 & 0 & 0 & 0 & 3.4 & 0 \\
0 & 0 & 0 & 0 & 0 & 3.4
\end{bmatrix} (GPa). \tag{116}
$$

For the 2-D plain weave composite, the elastic tensor is given by

$$
\left[D^h\right]_{\text{weave}} = \begin{bmatrix}
28.5 & 5.0 & 8.3 & 0 & 0 & 0 \\
5.0 & 12.3 & 5.0 & 0 & 0 & 0 \\
8.3 & 5.0 & 28.5 & 0 & 0 & 0 \\
0 & 0 & 0 & 3.3 & 0 & 0 \\
0 & 0 & 0 & 0 & 3.3 & 0 \\
0 & 0 & 0 & 0 & 0 & 6.9
\end{bmatrix} (GPa). \tag{117}
$$

The corrector provides a measure of the heterogeneity of the microstructure, namely, the interaction between the inclusion and the matrix. In Figures 20 and 21 the "mode" shapes are illustrated via isocontours where the grey-scales represent the magnitudes of the corrector term.
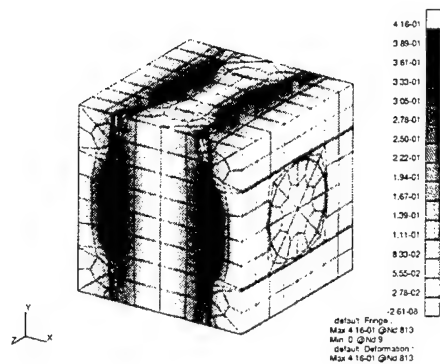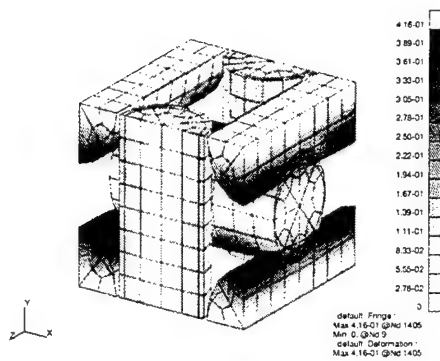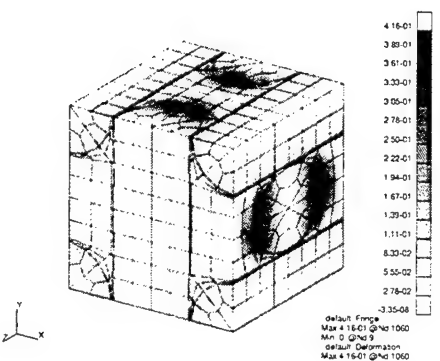
(a) Mode 11
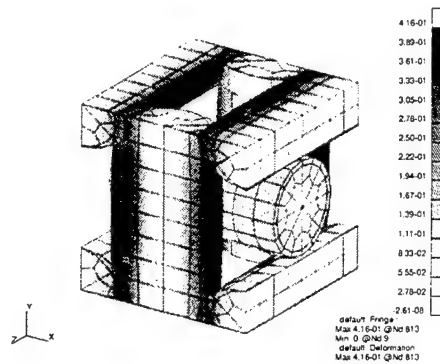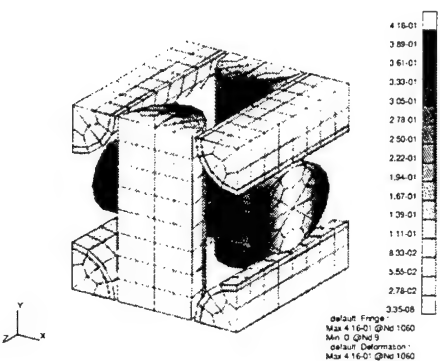
(b) Fiber cut-out in mode 11
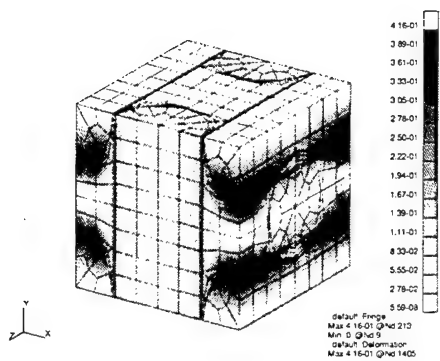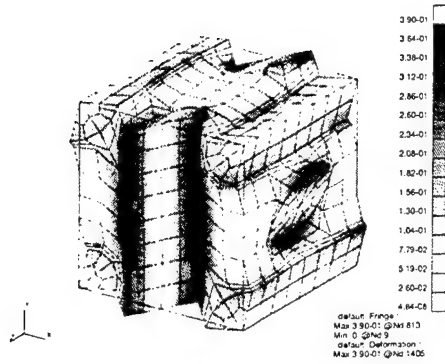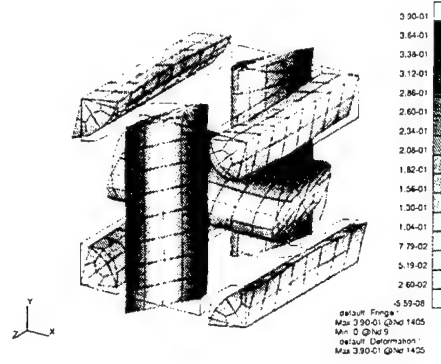
(c) Mode 22

(d) Fiber cut-out in mode 22
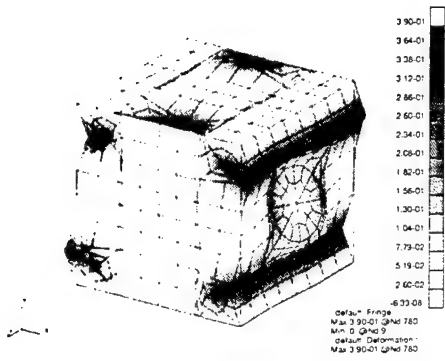
(e) Mode 33

(f) Fiber cut-out in mode 33

Figure 20. Corrector mode shapes for orthogonal non-woven microstructure (magnified 10% of model scale).
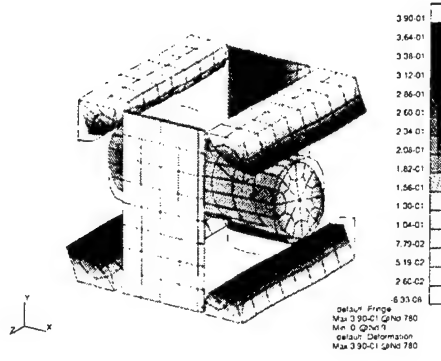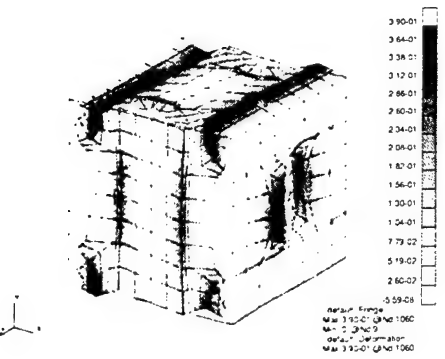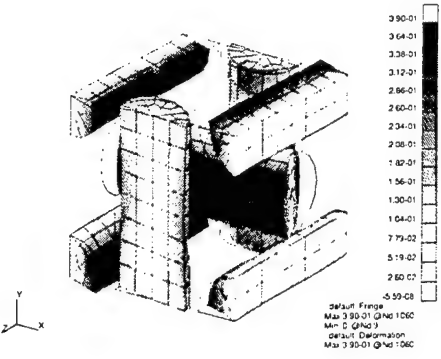
(a) Mode 12

(b) Fiber cut-out in mode 12
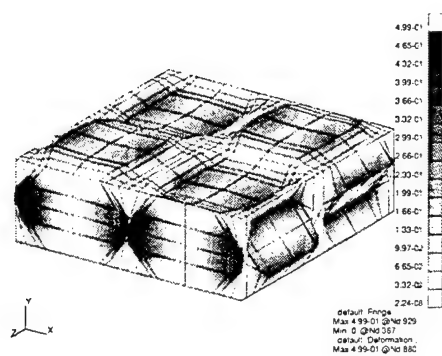
(c) Mode 23

(d) Fiber cut-out in mode 23

(e) Mode 13

(f) Fiber cut-out in mode 13

Figure 20. Corrector mode shapes for orthogonal non-woven microstructure
(magnified 10% of model scale)(continued).

80

(a) Mode 11

(b) Fiber cut-out in mode 11

(c) Mode 22

(d) Fiber cut-out in mode 22

(e) Mode 33

(f) Fiber cut-out in mode 33

Figure 21. Corrector mode shapes for plain weave microstructure (magnified 10% of model scale).

(a) Mode 12

(b) Fiber cut-out in mode 12

(c) Mode 23
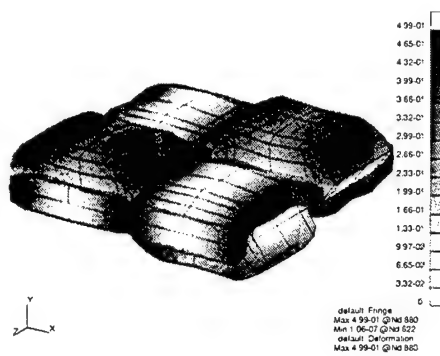
(d) Fiber cut-out in mode 23
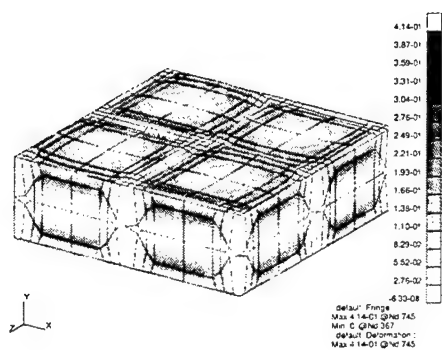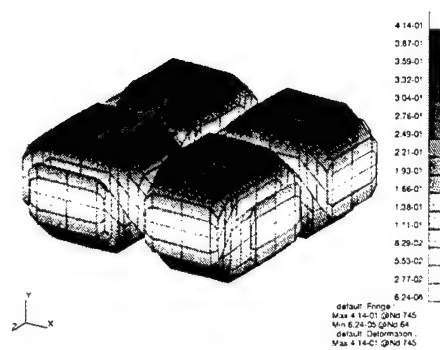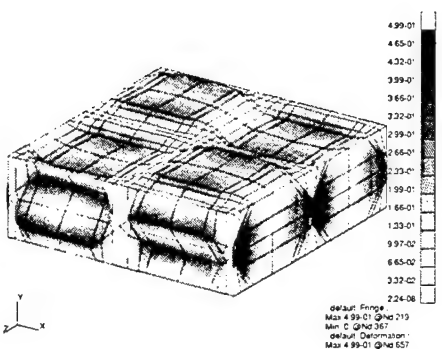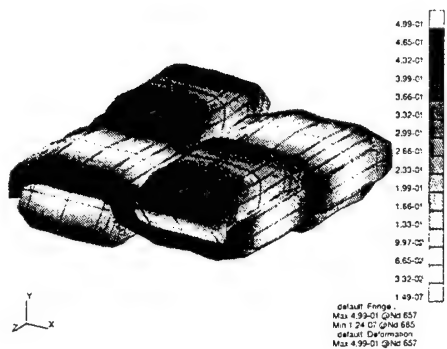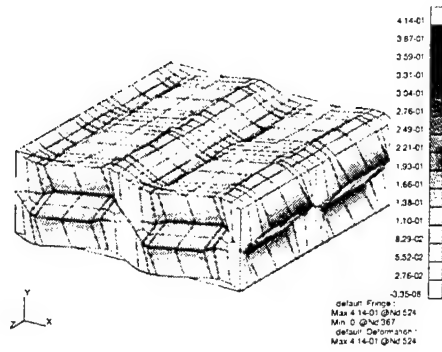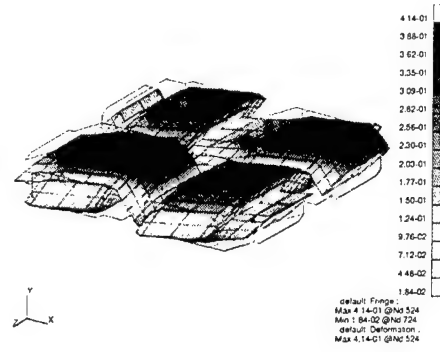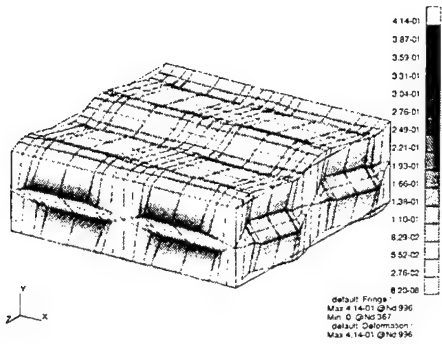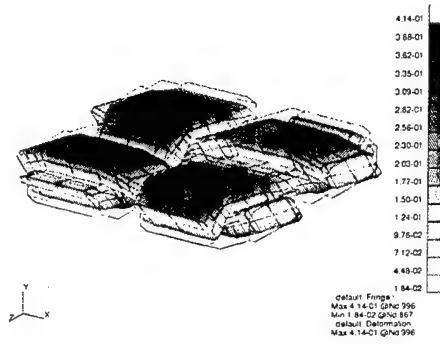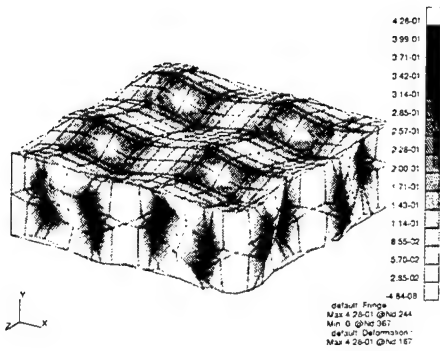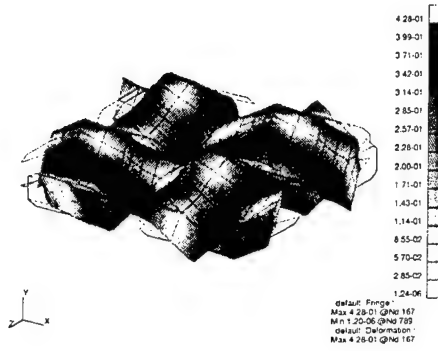
(e) Mode 13

(f) Fiber cut-out in mode 13

Figure 21. Corrector mode shapes for plain weave microstructure (magnified 10% of model scale)(continued).

In Figure 20(b) the fibers extend in the x-direction corresponding to the χ^{11} mode shape. The fibers *expand* in the 11-direction as a result of its stiffer behavior. This is in accordance with equation (77) where the "loads" are defined by the magnitude of the property difference across the phase boundaries. In this case, the stiff fiber has higher elastic constants which "loads" the softer matrix in the 11-direction. In the event where the matrix is of a stiffer elastic material than the inclusion, the difference in properties is negative indicating that the matrix "loads" the fibers. In either event, the loading gives the appearance of the stiffer material expanding while the softer material contracts. Analogous observations can be made for Figures 20(d) and (f), and Figures 21(b), (d), and (f).

Noteworthy in Figures 20 and 21 are the periodic shapes of the modes. Each unit cell can be placed adjacent to identical cells in all three dimensions. This characteristic reflects the Y-periodicity, or the translational symmetry of the unit cell. They appear to fit seamlessly together, as in a jigsaw puzzle, making a continuous array. The symmetry was enforced mathematically by application of the periodic boundary conditions.

The global bar twisting solutions are illustrated in Figures 22(a) and (b) for the non-woven and woven microstructures, respectively. A line load of $P = 10$ kN/m is applied counterclockwise around the edges of the bar's tip. The associated Von Mises stresses and strains are illustrated in Figures 23(a) and (b) and Figures 24(a) and (b). The isotropic effective properties of the non-woven microstructure yields isotropic macro behavior of the bar. The plain weave microstructure is transversely isotropic, and this behavior is reflected in Figures 23(b) and 24(b) at the tip where the respective stresses and strains are not distributed uniformly around the perimeter of the cross section. The stresses and strains at the bar tip with the non-woven microstructure, however, are distributed evenly.

In addition to the standard global behavior, which is obtainable using conventional elasticity theory, the present approach provides a means of estimating the microstress response. The microstresses are computed at the two locations indicated in Figure 16. The first location at
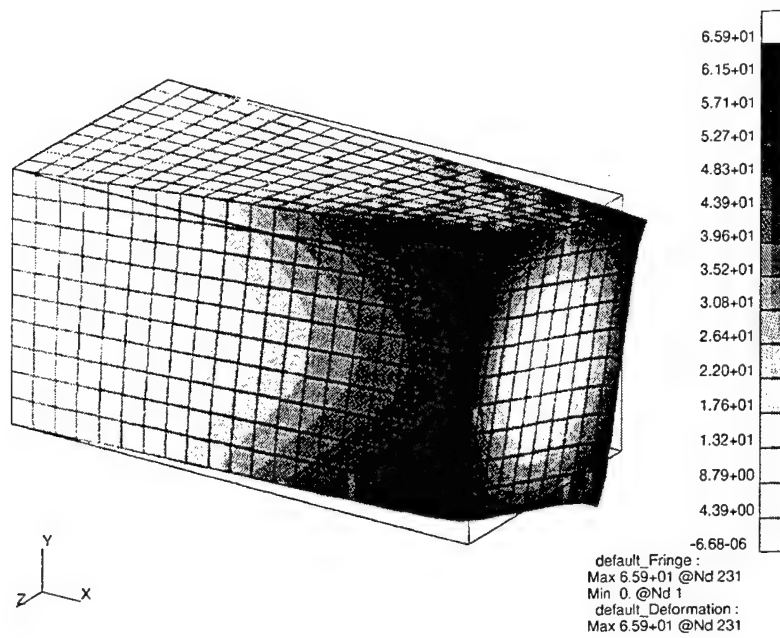
(a) Non-woven microstructure
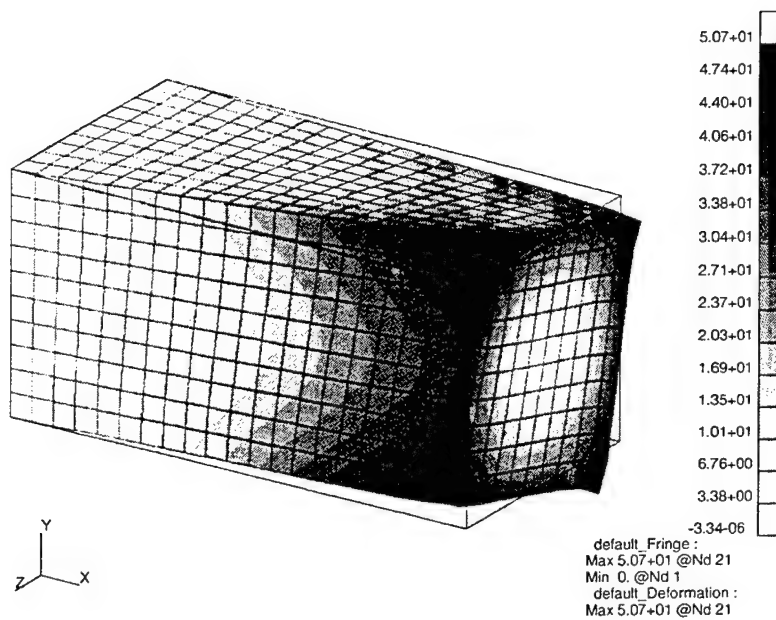
(b) Plain weave microstructure

Figure 22. Final bar deformation shapes and magnitude contours (in millimeters).

84
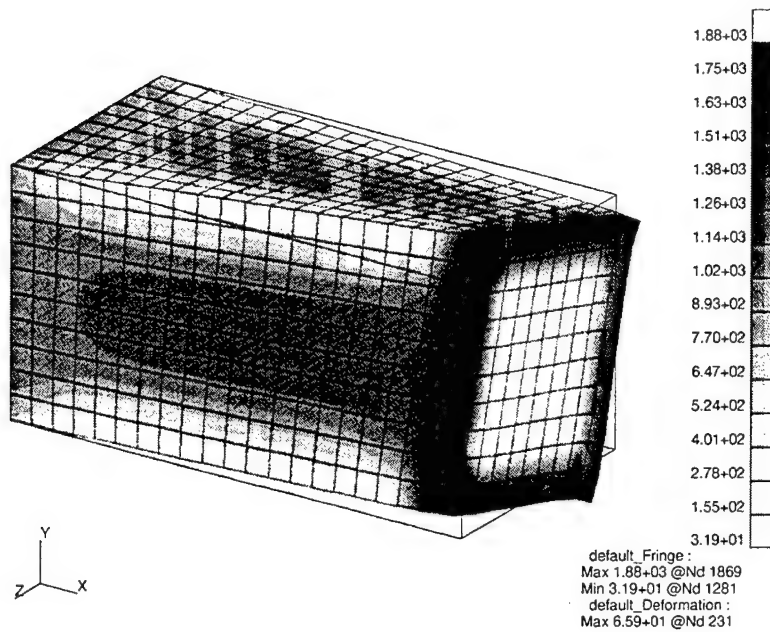
(a) Non-woven microstructure
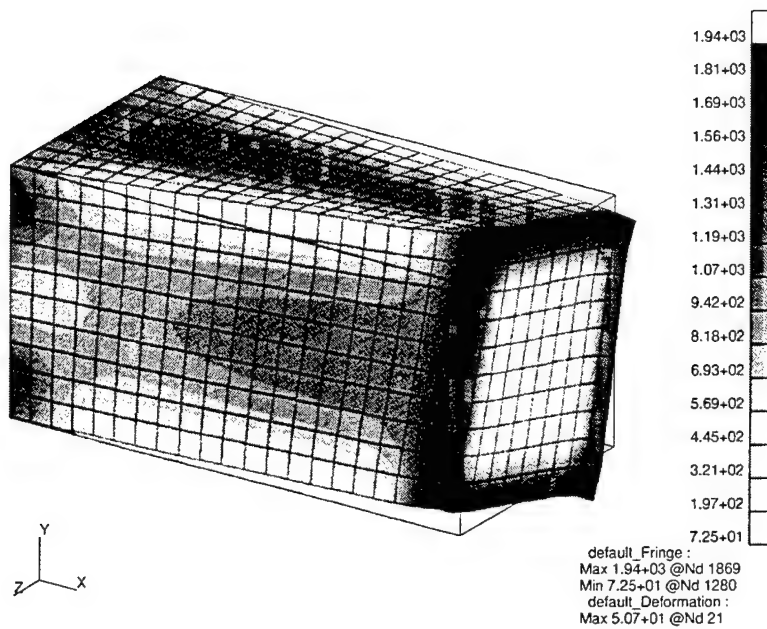
(b) Plain weave microstructure

Figure 23. Von Mises stress magnitudes (in Pascals).
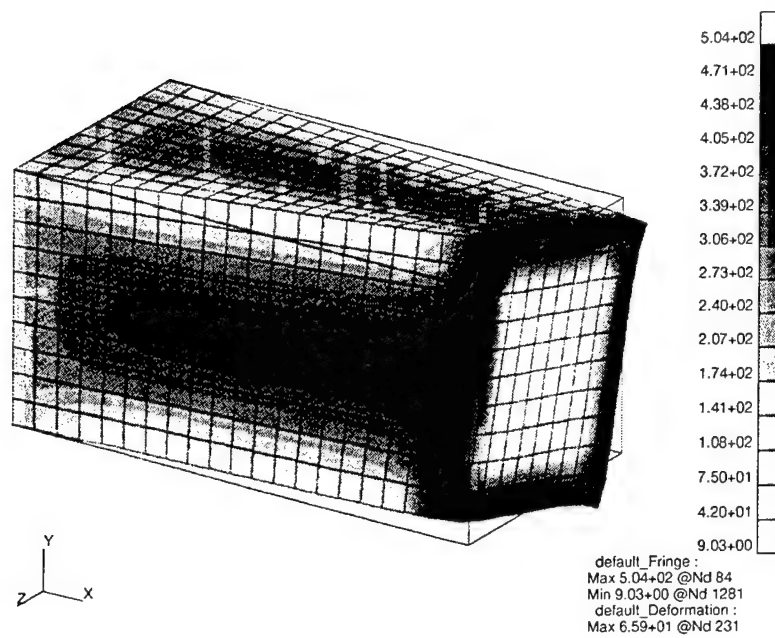
(a) Non-woven microstructure
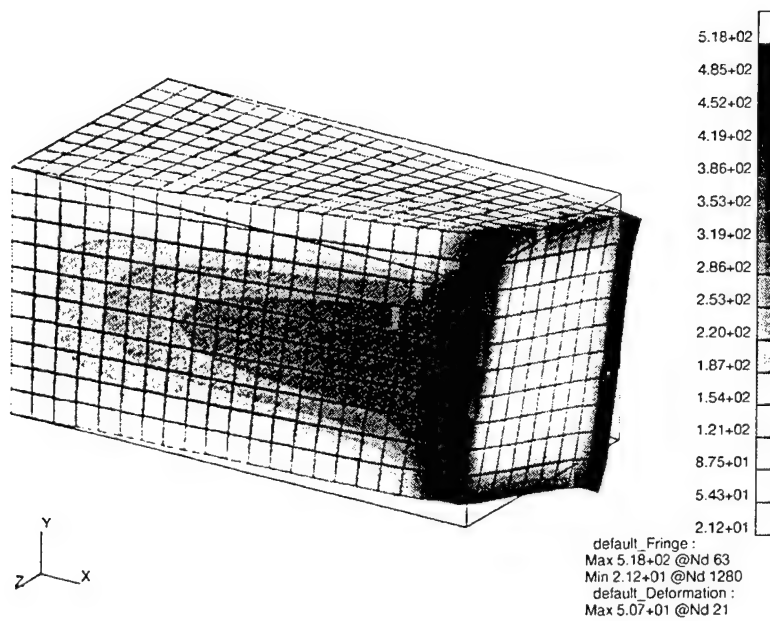
(b) Plain weave microstructure

Figure 24. Von Mises strain magnitudes ($\times 10^{-3}$m/m).

element no. 1,110 is near the center axis of the bar which is the region of lowest stress in the cross-section plane. The second location at element no. 1,990 is closer to the outer surface of the bar where it is expected to experience larger stresses. Although the microstresses can be approximated anywhere, the two locations are chosen presently to demonstrate the differences in microstresses using the AEH approach. In contrast, a similar problem involving a high resolution mesh would require significant modeling effort and solution time.

The microstress contours for the appropriate geometries are depicted in Figures 25 and 26. The differences in the stresses are evident between Figures 25(a) and (c) in the legends to the right of each figure. The stresses in Figure 25(c) are clearly greater than those in Figure 25(a). Whereas the median microstress at element no. 1,110 is 8.115 Pa, the median microstress at element no. 1,990 is 53.9 Pa. Analogous observations can be made for their respective fiber cut-outs in Figures 25(b) and (d) or for the plain weave microstructure in Figure 26.

The average of the microstresses over the unit cell gives the global stress because the Y-periodic correctors cancel when volume averaged in equation (79). This is what gives the AEH approach mathematical consistency between scales.

Finally, although the present discussions have not fully exploited the microstructural information obtained by the present approach, further studies can be conducted to interpolate greater refinement of microlevel detail. Figure 27 depicts a possible area of investigation to extract stress details at smaller scales by identifying and manipulating stress information inside the cell. This topic can be treated in the context of scientific visualization in future research.

In contrast to a the linear elastic problems considered in this section which involves a single step of homogenization and/or localization, time-dependent problems may require repeated homogenization. This is especially in cases where the material properties of the
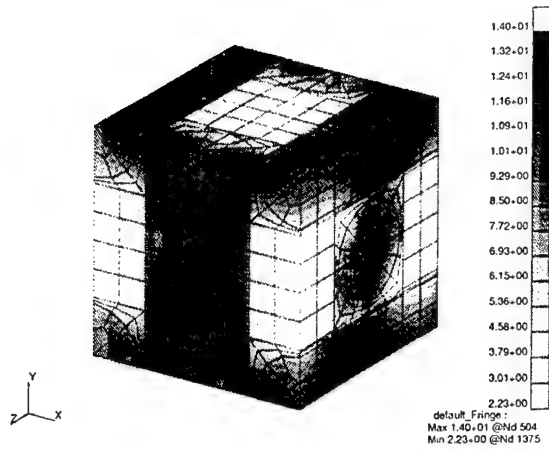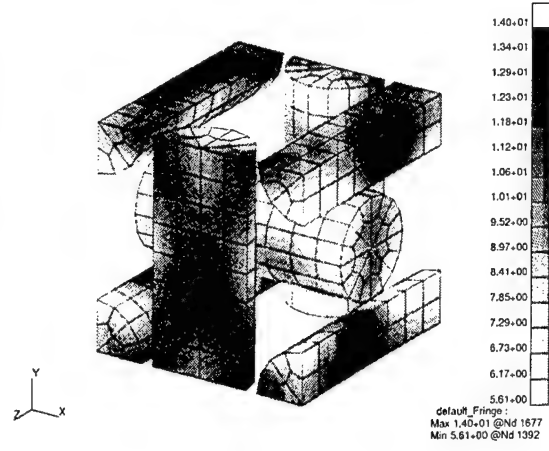
87

(a) At element no. 1110

(b) Fiber microstresses at element no. 1110
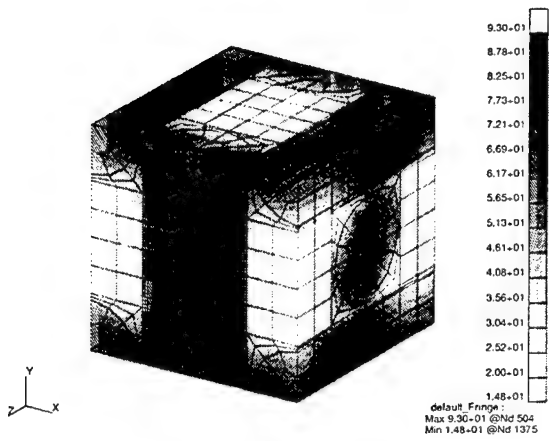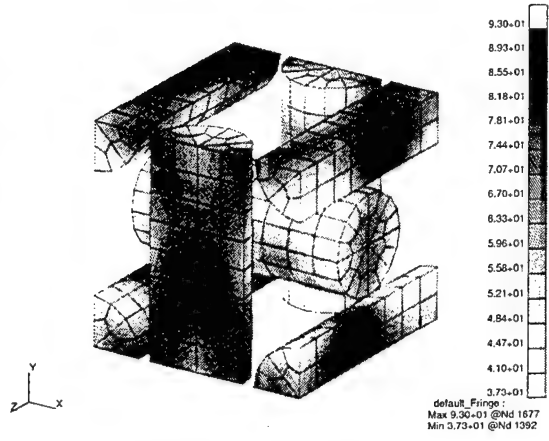
(c) At element no. 1990

(d) Fiber microstresses at element no. 1990

Figure 25. Approximate microstresses for non-woven microstructure (in Pascals).

constituents change with time. In the next section, a linear form of a time-dependent problem is considered in the viscoelastic regime where the BVP is a function of time due to the time-dependence of the constitutive equation. However, despite the unchanging nature of the linear material properties, the global problem still requires the rehomogenization of a
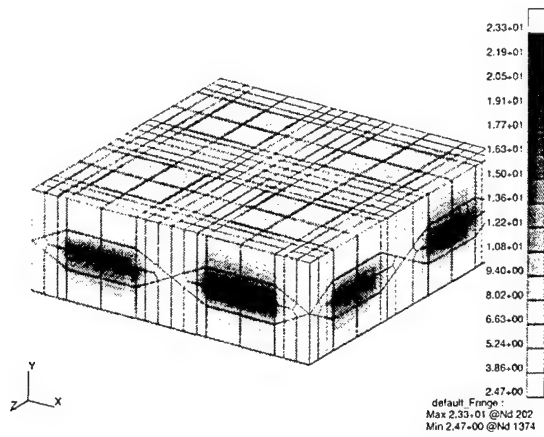
(a) At element no. 1110
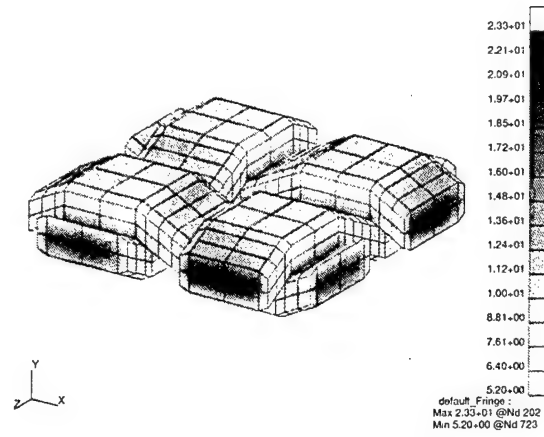
(b) Fiber microstresses at element no. 1110
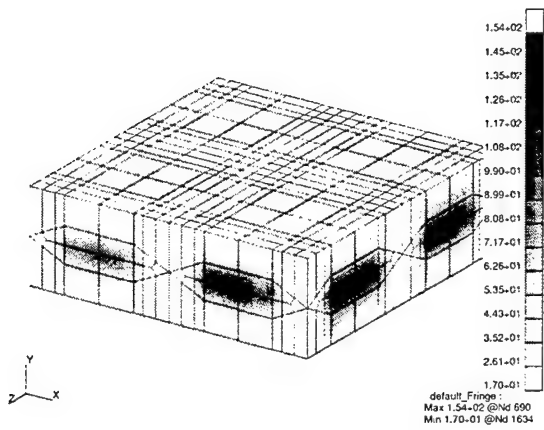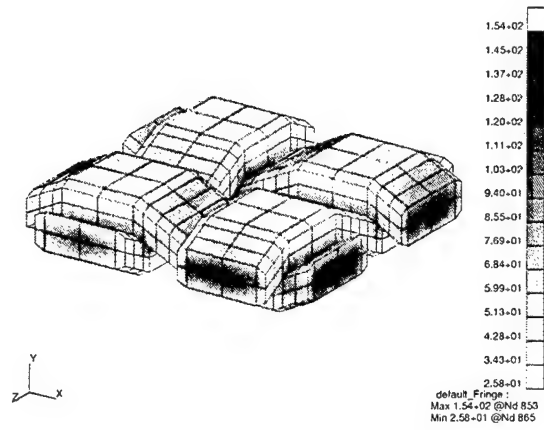
(c) At element no. 1990

(d) Fiber microstresses at element no. 1990

Figure 26. Approximate microstresses for plain weave microstructure (in Pascals).

limited number of quantities due to non-intuitive effects that occur when time-dependent multiple term constitutive models are homogenized.
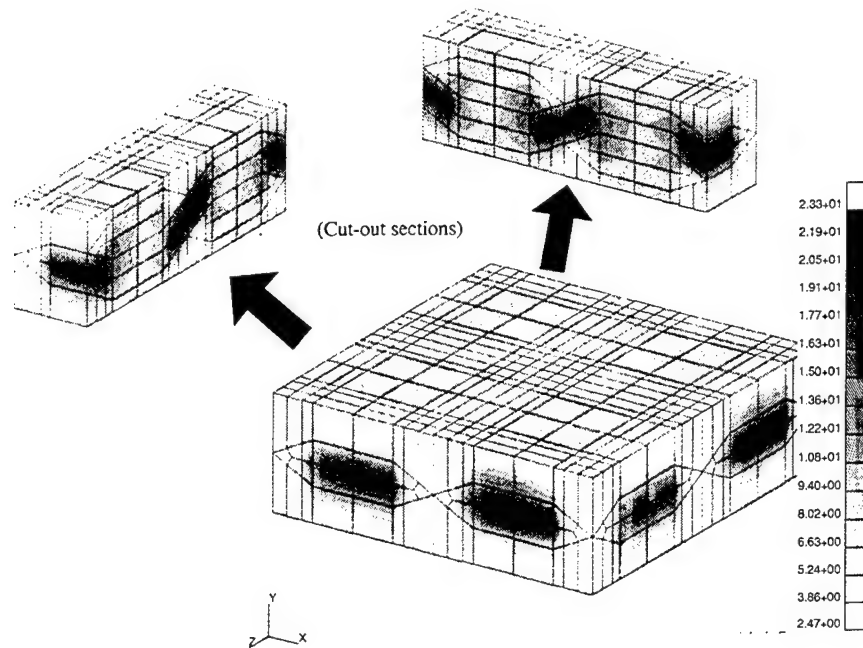
Figure 27. Additional microstress details by further refinement and inspection of the microstructure.

2.8 Conclusions From the Literature Review

Four primary conclusions can be drawn from the literature for AEH: (1) computational methods for linear and elastic engineering problems are well established and based on mathematically consistent derivations found in the mathematics literature; (2) some problems originally posed and discussed cursorily in the mathematics literature, such as in Bensoussan et al. [29] and Sanchez-Palencia [39], have yet to be fully investigated, understood, and demonstrated/proven for practical situations; (3) computational methods for inelastic and nonlinear mechanics remain fertile areas for growth and novel developments, and (4) despite the ostensible label of multiscale, AEH is traditionally applied only to scales where continuum equations apply, and no efforts show applicability to scales smaller such as at the

atomistic level.

It is clear that AEH remains an active area of research for computational mechanics. In the next section, the AEH method serves as the framework for a new method of linking atomistic scales to continuum scales. To date, no documented efforts have shown either theoretically or in application that this is possible.

3. Formulation of a Multiscale Atomistic-Continuum Homogenization Method

3.1 Overview

A large amount of interest has recently focused on the multiscale problem involving atoms and continua. It is widely accepted that many effects on the continuum germinate at the atomic level. Events such as fracture, fatigue, and inelastic material response can be traced back to the evolution of the atomic structure of the material.

Methodologies for linking a continuum to an atomistic domain can be found in the literature as early 1971 [1]. Finite element methods were later employed in Mullins and Dokainish [2] using a numerically decoupled domain approach with spatially overlapping atomistic and continuum regions. A review of some of these methods can be found by Cleri et al. [3]. Among these early analytic and computational studies, frequent issues regarding the treatment of the interface arose which were primarily handled through creative use of kinematic constraints.

More recently Tadmor et al. [4] developed an entirely FE-based formulation, the so-called quasicontinuum method. Similar efforts were made through the so-called handshaking or coupling-of-length-scales (CLS) method by Broughton et al. [5] by increasing the atomic resolution via the tight-binding (TB) method. And the dynamic problem was studied with a generalized scaling approach in coarse-grained molecular dynamics (CGMD) by Rudd and Broughton [6] to better handle the propagation of waves through the atomistic-FE interface and the FE far field.

Multiscale methods, such as those previously described, have traditionally been limited mainly to localized regions of interest. For example, the applications to which these methods have been applied involve small sets of dislocations and cracks and very few limited analyses of their mutual interactions. The localized regions on which these simulations are run typically span, at most, several microns. The limiting assumption in these works is the use of kinematic constraints to tie together the equations and disparate length scales. Driving the resolution of the discretized continuum finite elements intrinsically restricts the size of the continuum and leads to smaller overall dimensions of the problem which can only be overcome by large use of computer resources. Furthermore, the kinematic constraints on the atoms and continua lead to incompatibility issues arising at the interface such as ghost forces [7].

The asymptotic expansion homogenization method has been widely studied by applied mathematicians for many years. Numerous authoritative texts on the basic theory can be found in the literature, for instance, by Bensoussan et al. [29], Sanchez-Palencia [39], and Bakhvalov and Panasenko [93]. And despite the prolific research in the field, no attempts have been documented for extending the theory to atoms.

In this part of the report, a computational framework for homogenization of the atomistic problem is presented. Using two concurrent domains, one for the macroscale continuum domain and one for the atomic scale domain, concurrent self-consistent sets of equations are derived. Atoms in arbitrary configurations and structures of unlimited size are permitted. Through the asymptotic expansion homogenization technique, a set of hierarchical equations are derived based on hyperelasticity. At the local level, the atomistic equations are used under the assumption of the harmonic approximation to generate the effective properties needed to solve the effective global level equations. The Cauchy-Born rule [12] is applied to the atoms to enforce the gross deformation of the continuum on the atoms. This circumvents the need to apply kinematic constraints by making use of the weak averaging properties of homogenization and causes the small scale equations to be linear.

The contents of this part are as follows. In section 3.2, the conventional continuum equations are shown eventually leading to a variational form based on the principle of virtual work. Then, in section 3.3, the multiscale equations are developed resulting in two sets of equations which govern the local and global length scales. By introducing the atomistic potential in sections 3.4 and 3.5 the details of the atomistic formulations are presented and are cast in a variational form for use in the multiscale homogenization method. In section 3.6, the derivatives of the atomistic energy potential needed to complete the derivation of the method are provided in a general form. In section 3.7, 1-D demonstrative examples are worked and shown. Closing remarks are discussed in section 3.8. Additional details of the derivative of the Tersoff-Brenner type II potential are shown in the Appendix.

3.2   Continuum Formulations

This section describes the kinematics, stress definitions, and linear momentum conservation laws needed to develop the homogenization method from atomistic principles.

3.2.1   Kinematics

Consider an open set V in $\Re^3$ that deforms to the configuration v in $\Re^3$. Points in V are denoted $\mathbf{X} = (X_1, X_2, X_3) \in V$ and are called material points, while points in v are denoted $\mathbf{x} = (x_1, x_2, x_3) \in v$ and are called spatial points. The deformation is a one-to-one mapping through ϕ so that $x = \phi(X)$. The deformation gradient is defined by

$$\mathbf{F} = \frac{\partial \phi}{\partial \mathbf{X}} = \frac{\partial \mathbf{x}}{\partial \mathbf{X}} = \nabla_0 \mathbf{x}, \qquad F_{ij} = \frac{\partial \phi_i}{\partial X_j} = \frac{\partial x_i}{\partial X_j}, \tag{118}$$

where ∇_0 signifies the gradient taken with respect to V. The determinant of F is termed the Jacobian and is defined by $J = \det \mathbf{F}$. The right Cauchy-Green strain tensor is defined

94

by

$$C = F^T F, \tag{119}$$

and the Green strain tensor is defined by

$$E = \frac{1}{2}(C - I). \tag{120}$$

3.2.2 Stress and Equilibrium

The material representation for the conservation of linear momentum is defined by

$$\nabla_0 \cdot P + f_0 = 0, \tag{121}$$

where P is the first Piola-Kirchoff stress tensor and f_0 is the body force per unit of undeformed volume. In rate form, it is given by

$$\nabla_0 \cdot \dot{P} + \dot{f}_0 = 0. \tag{122}$$

Using the principle of virtual work, equation (122) can be rewritten as

$$\int_V \left(\nabla_0 \cdot \dot{P} \right) \delta u dV + \int_V \dot{f}_0 \cdot \delta u dV = 0, \qquad \forall \delta u, \tag{123}$$

where δu is the virtual displacement. Then, using the definition for traction with respect to the undeformed body, equation (123) can be rewritten as

$$\int_V \dot{P} : \nabla_0 \delta u dV = \int_{\partial V} \dot{t}_0 \cdot \delta u dA + \int_V \dot{f}_0 \cdot \delta u dV. \tag{124}$$

We invoke the notion of hyperelasticity by assuming that the atomistic potential, $\mathcal{W}$, which is a function of the atom positions, can be expressed in terms of strain. Intrinsically, this assumes that the strain energy density (or the free energy at zero temperature) is equivalent

95

to the atomistic energy potential. Following classical continuum mechanics, one can then define the first Piola-Kirchoff stress as

$$\mathbf{P} = \frac{\partial \mathcal{W}}{\partial \mathbf{F}}, \qquad P_{ij} = \frac{\partial \mathcal{W}}{\partial F_{ij}}, \qquad (125)$$

and the first Lagrangian elasticity tensor as

$$\mathcal{C} = \frac{\partial^2 \mathcal{W}}{\partial \mathbf{F} \partial \mathbf{F}} = \frac{\partial \mathbf{P}}{\partial \mathbf{F}}, \qquad \mathcal{C}_{ijkl} = \frac{\partial^2 \mathcal{W}}{\partial F_{ij} \partial F_{kl}} = \frac{\partial P_{ij}}{\partial F_{kl}}. \qquad (126)$$

A relationship is needed between stress and strain. From equation (126), one can see that in hyperelastic materials, $\mathbf{P}$ is related to $\mathbf{F}$ through

$$\dot{\mathbf{P}} = \mathcal{C} : \dot{\mathbf{F}}, \qquad \dot{P}_{ij} = \mathcal{C}_{ijkl} \dot{F}_{kl}, \qquad (127)$$

where

$$\dot{\mathbf{F}} = \partial \dot{\mathbf{u}} / \partial \mathbf{X} = \partial \mathbf{v} / \partial \mathbf{X}, \qquad (128)$$

and where $\dot{\mathbf{u}} = \mathbf{v}$ denotes the velocity.

Substituting equation (127) into (124) and using (128) yields

$$\int_V \mathcal{C} :: (\nabla_0 \delta \mathbf{u} \otimes \nabla_0 \mathbf{v}) \, dV = \int_{\partial V} \dot{\mathbf{t}}_0 \cdot \delta \mathbf{u} dA + \int_V \dot{\mathbf{f}}_0 \cdot \delta \mathbf{u} dV, \qquad \forall \delta \mathbf{u}, \qquad (129)$$

and the equivalent indicial form,

$$\int_V \mathcal{C}_{ijkl} \frac{\partial \delta u_i}{\partial X_j} \frac{\partial v_k}{\partial X_l} dV = \int_{\partial V} \dot{t}_{0_i} \delta u_i dA + \int_V \dot{f}_{0_i} \delta u_i dV. \qquad (130)$$

This is the virtual work equation associated with hyperelasticity. The two-scale approach is described next. It is devised so that traditional finite element continuum equations can be solved in the coarse scale and atomistic equations can be solved in the fine scale.

3.3 Homogenization

The homogenization framework enables the *weak* coupling of the continuum to the atoms. By taking the limit of the time-independent asymptotic expansion parameter $\varepsilon \to 0$, we

exploit the weak convergence properties of the scheme so as to decouple the length scales. Hence the term "weak coupling." At the fine scale, the domain contains only atoms with periodic conditions prescribed on the boundary and all atom displacements are measured relative to a fixed point in the local frame of reference.

The homogenization method is based on the assumption that two scales exist - a coarse scale and a fine scale. Coordinates in the coarse material scale are $\mathbf{X} = (X_1, X_2, X_3)$, and those in the fine material scale are $\mathbf{Y} = (Y_1, Y_2, Y_3)$. Likewise, the spatial coordinates are the lowercase analogues. The two scales are related by the scale parameter

$$\mathbf{Y} = \frac{\mathbf{X}}{\varepsilon}. \tag{131}$$

Therefore, we assume that the ratio of scales remains the same before and after deformation. The aim is to obtain two sets of coupled equations. The asymptotic series assumption decomposes the displacements as

$$\mathbf{u}(\mathbf{X}) = \mathbf{u}^{[0]}(\mathbf{X}) + \mathbf{u}^{[1]}(\mathbf{X}) \tag{132}$$
$$= \mathbf{u}^{[0]}(\mathbf{X}) + \varepsilon \mathbf{u}^{[1]}(\mathbf{Y}), \tag{133}$$

where $\mathbf{u}^{[0]}$ represents the displacement at the coarse scale and $\mathbf{u}^{[1]}$ represents the perturbed displacements due to inhomogeneity at the fine scale. Square brackets denote the order of the term in the asymptotic series. The representation of the total displacement at the fine scale is given by Takano et al. [76] as

$$\frac{1}{\varepsilon}\mathbf{u}(\mathbf{X}) = \mathbf{u}^{\text{micro}}(\mathbf{Y})$$
$$= \mathbf{F}(\mathbf{u}^{[0]}(\mathbf{X}))\mathbf{Y} + \mathbf{u}^{[1]}(\mathbf{Y}). \tag{134}$$

The variable $\mathbf{X}$ in equation (134) is a fixed value with respect to $\mathbf{Y}$. That is, the deformation gradient of a point in the coarse scale gets mapped onto a fine scale grid. This point is typically a quadrature point in a finite element sense.

The time derivatives are analogous to equations (133) and (134). They are given as

$$\dot{\mathbf{u}}(\mathbf{X}) = \mathbf{v}(\mathbf{X})$$
$$= \mathbf{v}^{[0]}(\mathbf{X}) + \varepsilon \mathbf{v}^{[1]}(\mathbf{Y}), \tag{135}$$
$$\dot{\mathbf{u}}^{\text{micro}}(\mathbf{Y}) = \mathbf{v}^{\text{micro}}(\mathbf{X})$$
$$= \mathbf{F}(\mathbf{v}^{[0]}(\mathbf{X}))\mathbf{Y} + \mathbf{v}^{[1]}(\mathbf{Y}). \tag{136}$$

Substituting equations (133) and (135) into (130) yields

$$\int_V \mathcal{C} :: \left[\nabla_X \left(\delta \mathbf{u}^{[0]}(\mathbf{X}) + \varepsilon \delta \mathbf{u}^{[1]}(\mathbf{Y}) \right) \otimes \nabla_X \left(\mathbf{v}^{[0]}(\mathbf{X}) + \varepsilon \mathbf{v}^{[1]}(\mathbf{Y}) \right) \right] dV$$
$$= \int_{\partial V} \left(\delta \mathbf{u}^{[0]}(\mathbf{X}) + \varepsilon \delta \mathbf{u}^{[1]}(\mathbf{Y}) \right) \cdot \dot{\mathbf{t}}_0 dA$$
$$+ \int_V \left(\delta \mathbf{u}^{[0]}(\mathbf{X}) + \varepsilon \delta \mathbf{u}^{[1]}(\mathbf{Y}) \right) \cdot \dot{\mathbf{f}}_0 dV, \qquad \forall \delta \mathbf{u}^{[0]}, \delta \mathbf{u}^{[1]} \tag{137}$$

Note that by use of the chain rule and equation (131),

$$\nabla_X \phi(\mathbf{X}, \mathbf{Y}) = \nabla_X \phi + \frac{\partial \mathbf{Y}}{\partial \mathbf{X}} \nabla_Y \phi$$
$$= \nabla_X \phi + \frac{1}{\varepsilon} \nabla_Y \phi. \tag{138}$$

Therefore,

$$\nabla_X \left(\mathbf{u}^{[0]}(\mathbf{X}) + \varepsilon \mathbf{u}^{[1]}(\mathbf{Y}) \right) = \nabla_X \mathbf{u}^{[0]}(\mathbf{X}) + \nabla_Y \mathbf{u}^{[1]}(\mathbf{Y}). \tag{139}$$

Using equation (139) in (137) and taking the average over Y gives

$$\int_V \frac{1}{|Y|} \int_Y \mathcal{C} :: \left[\left(\nabla_X \delta \mathbf{u}^{[0]}(\mathbf{X}) + \nabla_Y \delta \mathbf{u}^{[1]}(\mathbf{Y}) \right) \otimes \left(\nabla_X \mathbf{v}^{[0]}(\mathbf{X}) + \nabla_Y \mathbf{v}^{[1]}(\mathbf{Y}) \right) \right] dY dV$$
$$= \int_{\partial V} \left(\delta \mathbf{u}^{[0]}(\mathbf{X}) + \varepsilon \delta \mathbf{u}^{[1]}(\mathbf{Y}) \right) \cdot \dot{\mathbf{t}}_0 dA + \int_V \left(\delta \mathbf{u}^{[0]}(\mathbf{X}) + \varepsilon \delta \mathbf{u}^{[1]}(\mathbf{Y}) \right) \cdot \dot{\mathbf{f}}_0 dV, \quad (140)$$
$$\forall \delta \mathbf{u}^{[0]}, \delta \mathbf{u}^{[1]}.$$

Then, in the limit as $\varepsilon \to 0$, equation (140) is satisfied only if the following two equations

are satisfied,

$$\frac{1}{|Y|} \int_V \int_Y \mathcal{C} :: \left[\nabla_X \delta \mathbf{u}^{[0]}(\mathbf{X}) \otimes \left(\nabla_X \mathbf{v}^{[0]}(\mathbf{X}) + \nabla_Y \mathbf{v}^{[1]}(\mathbf{Y}) \right) \right] dY dV$$
$$= \int_{\partial V} \delta \mathbf{u}^{[0]}(\mathbf{X}) \cdot \dot{\mathbf{t}}_0 dA + \int_V \delta \mathbf{u}^{[0]}(\mathbf{X}) \cdot \dot{\mathbf{f}}_0 dV, \qquad \forall \, \delta \mathbf{u}^{[0]}, \tag{141}$$

$$\frac{1}{|Y|} \int_V \int_Y \mathcal{C} :: \left[\nabla_Y \delta \mathbf{u}^{[1]}(\mathbf{Y}) \otimes \left(\nabla_X \mathbf{v}^{[0]}(\mathbf{X}) + \nabla_Y \mathbf{v}^{[1]}(\mathbf{Y}) \right) \right] dY dV = 0, \qquad \forall \, \delta \mathbf{u}^{[1]}. \tag{142}$$

By recourse to the finite element method, the solution of equation (141) is straightforward assuming $\mathcal{C}$ and $\mathbf{v}^{[1]}$ are known. It is then evident that due to the dependence of (142) on $\mathbf{v}^{[0]}$, equations (141) and (142) are coupled and must be solved concurrently.

In the next two sections, a method is first shown for solving equation (142) for $\mathbf{v}^{[1]}$, then in the following section, the formulation that enables the atomistic information to be fed into equation (141) is derived. Then by linearizing the equations, a Newton-Raphson scheme can be employed to achieve the needed concurrency.

3.4 Atomistic Equation

Distinct and distinguishable atoms are assumed to reside in the local level cell. By the Cauchy-Born rule [12], at a point $\mathbf{X}$, $\mathbf{F}(\mathbf{u}^{[0]})$ is assumed to give the energy minimizing configuration of the atoms. For simplicity, we assume that the atoms are arranged in a lattice.* Then, the positions of the atoms $\mathbf{Y}$ are given from the lattice coordinates $\mathbf{m}$ by

$$\mathbf{Y}_{(\mathbf{m})} = \mathbf{m} \mathbf{e}_i : \quad \mathbf{m} \in \mathcal{L}, \mathcal{L} = \mathbb{Z}^3, \mathbb{Z} \leq \mathbb{N}, \tag{143}$$

where $\mathbf{e}_i$ are the primitive translation vectors and $\mathbb{N}$ is the integer multiple of atoms contained in the unit cell. To avoid confusion in notation, atom labels are noted in parentheses

---

*Note that there is no restriction to perfect lattices. In fact, by use of computers, arbitrary arrangements of atoms can be considered as long as the assumption of the Cauchy-Born rule still applies.

henceforth and are not subject to the conventional summation rules associated with indicial notation. The displacement of the atoms are

$$\mathbf{q_{(m)}}: \quad \mathbf{m} \in \mathcal{L}. \tag{144}$$

Upon deformation, the new positions of the atoms are given by

$$\mathbf{y_{(m)}} = \mathbf{Y_{(m)}} + \mathbf{q_{(m)}}. \tag{145}$$

The deformation gradient is defined by

$$\mathbf{F} = \frac{\partial \mathbf{y}}{\partial \mathbf{Y}}. \tag{146}$$

The vector separating two atoms i and j in the reference configuration is given by

$$\mathbf{R}_{(ij)} = \mathbf{Y}_{(j)} - \mathbf{Y}_{(i)}, \tag{147}$$

where $\mathbf{Y}_{(j)}$ denotes the position of atom j and $\mathbf{Y}_{(i)}$ the position of atom i. The vector separating two atoms in the deformed configuration is given by

$$\mathbf{r}_{(ij)} = \mathbf{y}_{(j)} - \mathbf{y}_{(i)}. \tag{148}$$

Then the Cauchy-Born rule can be stated in a more precise manner by

$$\begin{aligned}
\mathbf{r}_{(ij)} &= \mathbf{F}\mathbf{Y}_{(j)} - \mathbf{F}\mathbf{Y}_{(i)} \\
&= \mathbf{F}\mathbf{R}_{(ij)}.
\end{aligned} \tag{149}$$

For the energy associated with the deformation of the atoms, we use the so-called type II parameterization of the Tersoff-Brenner potential [94, 95]. It takes the form,

$$\mathcal{W} = \frac{1}{n_a} \left[E_b(\mathbf{Y} + \mathbf{q}) - E_b(\mathbf{Y}) \right], \tag{150}$$

where $\mathcal{W}$ is the energy density of the frozen system, n_a is the number of atoms, and E_b is

the binding energy given for a pure carbon system by

$$E_b(\mathbf{r}) = \sum_i \sum_{j(>i)} \left[V_R\left(r_{(ij)}\right) - \bar{B} V_A\left(r_{(ij)}\right) \right], \tag{151}$$

$$\bar{B} = \frac{1}{2} \left(B_{(ij)} + B_{(ji)} \right), \tag{152}$$

$$V_R(r) = \frac{f_{(ij)}(r) D^{(e)}}{(S-1)} e^{-\sqrt{2S}\beta(r - R^{(e)})}, \tag{153}$$

$$V_A(r) = \frac{f_{(ij)}(r) D^{(e)} S}{(S-1)} e^{-\sqrt{\frac{2}{S}}\beta(r - R^{(e)})}, \tag{154}$$

$$f_{(ij)}(r) = \begin{cases} 1, & r < R^{[1]} \\ \frac{1}{2} \left\{ 1 + \cos\left[\frac{\pi(r - R^{[1]})}{(r - R^{(2)})} \right] \right\}, & R^{[1]} < r < R^{(2)} \\ 0, & r > R^{(2)} \end{cases}, \tag{155}$$

$$B_{(ij)} = \left[1 + \sum_{k(\neq i,j)} G(\theta_{(ijk)}) f_{(ik)}\left(r_{(ik)}\right) \right]^{-\delta}, \tag{156}$$

$$G(\theta) = a_o \left\{ 1 + \frac{c_o^2}{d_o^2} - \frac{c_o^2}{d_o^2 + (1 + \cos\theta)^2} \right\}, \tag{157}$$

with the constants given in Table 3.

Table 3. Parameters for Tersoff-Brenner potential.

$R^{(e)}$	1.39 Å
$D^{(e)}$	6.0 eV
S	1.22
β	2.1 Å
δ	0.5
$R^{(1)}$	1.7 Å
$R^{(2)}$	2.0 Å
a_o	0.00020813
c_o^2	330^2
d_o^2	3.5^2

Given that the energy can be written as a function of the atom displacements, equation

101

(142) can be expressed in a form conducive to atom representations. We equate $\mathbf{v}^{[1]}$ to the rate of atom displacement and attempt to solve the equivalent form

$$\frac{\partial}{\partial Y_j} \mathcal{C}_{ijkl} \frac{\partial v_k^{[1]}}{\partial Y_l} = -\frac{\partial \mathcal{C}_{ijkl}}{\partial Y_j} \frac{\partial v_k^{[0]}}{\partial X_l}. \tag{158}$$

under periodic boundary conditions. The solution to equation (158) is found as the zero of $\partial \mathcal{R}$ in the equation

$$\partial \mathcal{R} = \mathcal{K} \mathbf{v}^{[1]} - \mathcal{D} \cdot \nabla_0 \mathbf{v}^{[0]}(\mathbf{x}), \tag{159}$$

where $\mathcal{K}$ is the $n_a \times n_a$ Hessian and is given by

$$\mathcal{K} = \frac{\partial^2 \mathcal{W}}{\partial \mathbf{q} \partial \mathbf{q}}, \tag{160}$$

where $\mathbf{q}$ is the vector of atom displacements of size $3n_a$ (in three dimensions), and $\mathcal{D}$ is a third order unsymmetric tensor that is obtained from the first derivative of the Euler-Lagrange equation with respect to the local deformation gradient, given by

$$\mathcal{D} = -\frac{\partial^2 \mathcal{W}}{\partial \mathbf{q} \partial \mathbf{F}}. \tag{161}$$

The size of $\mathcal{D}$ depends on the dimensionality of the problem. In three dimensions, it can be expressed as an $n_a \times 9$ matrix where 9 corresponds to the number of independent components of $\mathbf{F}$.

Under the Cauchy-Born hypothesis that the atomic primitive vectors deform homogeneously according to the gross deformation of the continuum, equation (159) is a linear equation. That is, the atom positions needed to compute $\mathcal{K}$ are determined solely by $\nabla_0 \mathbf{v}^{[0]}$ and is independent of $\mathbf{v}^{[1]}$.* However, if necessary, a mixed strategy can be used incorporating molecular dynamics to compute the true energy minimizing atom configuration at the fine scale.

---

*This is not to say that $\mathbf{v}^{[1]}$ and $\mathbf{v}^{[0]}$ are independent. The distinction being made here is between interscale and intrascale coupling. The coupling is interscale but not intrascale.

3.5 Multiscale Equation

Once equation (159) has been solved for $\mathbf{v}^{[1]}$, the remaining task is to formulate a tractable global scale boundary value problem. The key distinction between this investigation and conventional continuum formulations, such as hyperelasticity, is the conspicuous incorporation of $\mathbf{v}^{[1]}$, a fine-scale/atomistic quantity, in the global scale equations, and the definition of the material property tensor completely in terms of atomistic variables.

We return to equation (141) recognizing that $\mathbf{v}^{[1]}$ is now known. Incorporating the definition for the first Lagrangian elasticity tensor from equation (126) yields

$$\frac{1}{|Y|} \int_V \int_Y \frac{\partial^2 \mathcal{W}}{\partial \mathbf{F} \partial \mathbf{F}} :: \left[\nabla_X \boldsymbol{\delta} \mathbf{u}^{[0]}(\mathbf{X}) \otimes \left(\nabla_X \mathbf{v}^{[0]}(\mathbf{X}) + \nabla_Y \mathbf{v}^{[1]}(\mathbf{Y}) \right) \right] dY dV$$
$$= \int_{\partial V} \boldsymbol{\delta} \mathbf{u}^{[0]}(\mathbf{X}) \cdot \dot{\mathbf{t}}_0 dA + \int_V \boldsymbol{\delta} \mathbf{u}^{[0]}(\mathbf{X}) \cdot \dot{\mathbf{f}}_0 dV, \qquad \forall \, \boldsymbol{\delta} \mathbf{u}^{[0]}. \tag{162}$$

Then using the definition of $\mathbf{F}$ in equation (118) and assuming a first order Taylor series representation for the time derivative gives,

$$\frac{1}{|Y|} \int_V \int_Y \frac{\partial^2 \mathcal{W}}{\partial \mathbf{F} \partial \mathbf{F}} :: \left(\nabla_X \boldsymbol{\delta} \mathbf{u}^{[0]}(\mathbf{X}) \otimes \nabla_X \mathbf{v}^{[0]}(\mathbf{X}) \right) dY dV$$
$$= \int_{\partial V} \boldsymbol{\delta} \mathbf{u}^{[0]}(\mathbf{X}) \cdot \dot{\mathbf{t}}_0 dA + \int_V \boldsymbol{\delta} \mathbf{u}^{[0]}(\mathbf{X}) \cdot \dot{\mathbf{f}}_0 dV$$
$$- \frac{1}{|Y|} \int_V \int_Y \frac{\partial^2 \mathcal{W}}{\partial \mathbf{F} \partial \mathbf{q}} :: \left(\nabla_X \boldsymbol{\delta} \mathbf{u}^{[0]}(\mathbf{X}) \otimes \mathbf{v}^{[1]}(\mathbf{Y}) \right) dY dV, \qquad \forall \, \boldsymbol{\delta} \mathbf{u}^{[0]}. \tag{163}$$

The solution to equation (163) yields $\mathbf{v}^{[0]}$ that takes into consideration the effect of the atoms. It is noteworthy that the last term is zero when the energy distribution over Y is constant, i.e., when the atom arrangement forms a perfect lattice. This reduces the problem to a classical harmonic approximation where the first Lagrangian elasticity tensor is assumed to model the material behavior. In equation (163), the last term serves as a corrective force in regions of highly energetic atoms, i.e. non-locality regions, to account for defects and lattice inhomogeneities. Note also that the atomistic energy density and its derivatives intrinsically

account for invariance properties of the atoms. For example, by switching the positions of two atoms of the same species, the energy remains constant.

3.6   The Euler-Lagrange Equations and the Hessian

In this section, the analytic forms of the Euler-Lagrange equations and Hessian are derived for a general potential. The nontrivial algebra typically needed to obtain equations (160) and (161) for the specific case of the Tersoff-Brenner potential are shown in greater detail in the Appendix, and only general forms are derived here. The Euler-Lagrange equation is the first derivative of the Lagrangian with respect to the degrees of freedom. In this problem, the Lagrangian is the negative of the atomistic energy density. The Euler-Lagrange equation is therefore given by

$$
\begin{aligned}
\mathcal{E} &= \frac{\partial \mathcal{W}}{\partial \mathbf{q}_{(m)}} \\
&= \frac{1}{n_a} \frac{\partial E_b}{\partial \mathbf{q}_{(m)}},
\end{aligned}
\tag{164}
$$

and using the chain rule for derivatives, it is

$$
\begin{aligned}
\mathcal{E} &= \frac{1}{n_a} \frac{\partial E_b}{\partial \mathbf{q}_{(m)}} \\
&= \frac{1}{n_a} \left(\frac{\partial E_b}{\partial \mathbf{r}_{(ij)}} \frac{\partial \mathbf{r}_{(ij)}}{\partial \mathbf{q}_{(m)}} + \frac{\partial E_b}{\partial \mathbf{r}_{(ik)}} \frac{\partial \mathbf{r}_{(ik)}}{\partial \mathbf{q}_{(m)}} + \frac{\partial E_b}{\partial \mathbf{r}_{(jk)}} \frac{\partial \mathbf{r}_{(jk)}}{\partial \mathbf{q}_{(m)}} \right).
\end{aligned}
\tag{165}
$$

The Hessian is obtained by taking an additional derivative of the Euler-Lagrange equations.

Specifically, we again make use of the chain rule to obtain

$$
\begin{aligned}
\mathcal{K} &= \frac{\partial^2 \mathcal{W}}{\partial \mathbf{q}_{(n)} \partial \mathbf{q}_{(m)}} \\
&= \frac{1}{n_a} \frac{\partial^2 E_b}{\partial \mathbf{q}_{(n)} \partial \mathbf{q}_{(m)}} \\
&= \frac{1}{n_a} \left[\frac{\partial^2 E_b}{\partial \mathbf{r}_{(ij)} \partial \mathbf{r}_{(ij)}} :: \left(\frac{\partial \mathbf{r}_{(ij)}}{\partial \mathbf{q}_{(n)}} \otimes \frac{\partial \mathbf{r}_{(ij)}}{\partial \mathbf{q}_{(m)}} \right) + \frac{\partial^2 E_b}{\partial \mathbf{r}_{(ij)} \partial \mathbf{r}_{(ik)}} :: \left(\frac{\partial \mathbf{r}_{(ij)}}{\partial \mathbf{q}_{(n)}} \otimes \frac{\partial \mathbf{r}_{(ik)}}{\partial \mathbf{q}_{(m)}} \right) \right. \\
&\quad + \frac{\partial^2 E_b}{\partial \mathbf{r}_{(ik)} \partial \mathbf{r}_{(ij)}} :: \left(\frac{\partial \mathbf{r}_{(ik)}}{\partial \mathbf{q}_{(n)}} \otimes \frac{\partial \mathbf{r}_{(ij)}}{\partial \mathbf{q}_{(m)}} \right) + \frac{\partial^2 E_b}{\partial \mathbf{r}_{(ik)} \partial \mathbf{r}_{(ik)}} :: \left(\frac{\partial \mathbf{r}_{(ik)}}{\partial \mathbf{q}_{(n)}} \otimes \frac{\partial \mathbf{r}_{(ik)}}{\partial \mathbf{q}_{(m)}} \right) \\
&\quad + \frac{\partial^2 E_b}{\partial \mathbf{r}_{(jk)} \partial \mathbf{r}_{(jk)}} :: \left(\frac{\partial \mathbf{r}_{(jk)}}{\partial \mathbf{q}_{(n)}} \otimes \frac{\partial \mathbf{r}_{(jk)}}{\partial \mathbf{q}_{(m)}} \right) + \frac{\partial^2 E_b}{\partial \mathbf{r}_{(ij)} \partial \mathbf{r}_{(jk)}} :: \left(\frac{\partial \mathbf{r}_{(ij)}}{\partial \mathbf{q}_{(n)}} \otimes \frac{\partial \mathbf{r}_{(jk)}}{\partial \mathbf{q}_{(m)}} \right) \\
&\quad + \frac{\partial^2 E_b}{\partial \mathbf{r}_{(jk)} \partial \mathbf{r}_{(ij)}} :: \left(\frac{\partial \mathbf{r}_{(jk)}}{\partial \mathbf{q}_{(n)}} \otimes \frac{\partial \mathbf{r}_{(ij)}}{\partial \mathbf{q}_{(m)}} \right) + \frac{\partial^2 E_b}{\partial \mathbf{r}_{(ik)} \partial \mathbf{r}_{(jk)}} :: \left(\frac{\partial \mathbf{r}_{(ik)}}{\partial \mathbf{q}_{(n)}} \otimes \frac{\partial \mathbf{r}_{(jk)}}{\partial \mathbf{q}_{(m)}} \right) \\
&\quad \left. + \frac{\partial^2 E_b}{\partial \mathbf{r}_{(jk)} \partial \mathbf{r}_{(ik)}} :: \left(\frac{\partial \mathbf{r}_{(jk)}}{\partial \mathbf{q}_{(n)}} \otimes \frac{\partial \mathbf{r}_{(ik)}}{\partial \mathbf{q}_{(m)}} \right) \right].
\end{aligned}
\tag{166}
$$

Second derivatives of the inter-atom vectors are zero, i.e.,

$$
\begin{aligned}
\frac{\partial^2 \mathbf{r}_{(ij)}}{\partial \mathbf{q}_{(m)} \partial \mathbf{q}_{(n)}} &= \frac{\partial^2}{\partial \mathbf{q}_{(m)} \partial \mathbf{q}_{(n)}} \left(\mathbf{Y}_{(j)} + \mathbf{q}_{(j)} - \mathbf{Y}_{(i)} + \mathbf{q}_{(i)} \right) \tag{167} \\
&= \mathbf{0} \qquad \forall (m, n). \tag{168}
\end{aligned}
$$

Next, the appropriate right hand side expressions are derived for equation (159) and (161). This involves the use of the chain rule again to obtain

$$
\begin{aligned}
\frac{\partial^2 \mathcal{W}}{\partial \mathbf{q}_{(m)} \partial \mathbf{F}} &= \frac{1}{n_a} \left[\frac{\partial^2 E_b}{\partial \mathbf{r}_{(ij)} \partial \mathbf{r}_{(ij)}} :: \left(\frac{\partial \mathbf{r}_{(ij)}}{\partial \mathbf{F}} \otimes \frac{\partial \mathbf{r}_{(ij)}}{\partial \mathbf{q}_{(m)}} \right) + \frac{\partial^2 E_b}{\partial \mathbf{r}_{(ij)} \partial \mathbf{r}_{(ik)}} :: \left(\frac{\partial \mathbf{r}_{(ik)}}{\partial \mathbf{F}} \otimes \frac{\partial \mathbf{r}_{(ij)}}{\partial \mathbf{q}_{(m)}} \right) \right. \\
&\quad + \frac{\partial^2 E_b}{\partial \mathbf{r}_{(ik)} \partial \mathbf{r}_{(ij)}} :: \left(\frac{\partial \mathbf{r}_{(ij)}}{\partial \mathbf{F}} \otimes \frac{\partial \mathbf{r}_{(ik)}}{\partial \mathbf{q}_{(m)}} \right) + \frac{\partial^2 E_b}{\partial \mathbf{r}_{(ik)} \partial \mathbf{r}_{(ik)}} :: \left(\frac{\partial \mathbf{r}_{(ik)}}{\partial \mathbf{F}} \otimes \frac{\partial \mathbf{r}_{(ik)}}{\partial \mathbf{q}_{(m)}} \right) \\
&\quad + \frac{\partial^2 E_b}{\partial \mathbf{r}_{(ij)} \partial \mathbf{r}_{(jk)}} :: \left(\frac{\partial \mathbf{r}_{(jk)}}{\partial \mathbf{F}} \otimes \frac{\partial \mathbf{r}_{(ij)}}{\partial \mathbf{q}_{(m)}} \right) + \frac{\partial^2 E_b}{\partial \mathbf{r}_{(jk)} \partial \mathbf{r}_{(ij)}} :: \left(\frac{\partial \mathbf{r}_{(ij)}}{\partial \mathbf{F}} \otimes \frac{\partial \mathbf{r}_{(jk)}}{\partial \mathbf{q}_{(m)}} \right) \\
&\quad + \frac{\partial^2 E_b}{\partial \mathbf{r}_{(ik)} \partial \mathbf{r}_{(jk)}} :: \left(\frac{\partial \mathbf{r}_{(jk)}}{\partial \mathbf{F}} \otimes \frac{\partial \mathbf{r}_{(ik)}}{\partial \mathbf{q}_{(m)}} \right) + \frac{\partial^2 E_b}{\partial \mathbf{r}_{(jk)} \partial \mathbf{r}_{(ik)}} :: \left(\frac{\partial \mathbf{r}_{(ik)}}{\partial \mathbf{F}} \otimes \frac{\partial \mathbf{r}_{(jk)}}{\partial \mathbf{q}_{(m)}} \right) \\
&\quad \left. + \frac{\partial^2 E_b}{\partial \mathbf{r}_{(jk)} \partial \mathbf{r}_{(jk)}} :: \left(\frac{\partial \mathbf{r}_{(jk)}}{\partial \mathbf{F}} \otimes \frac{\partial \mathbf{r}_{(jk)}}{\partial \mathbf{q}_{(m)}} \right) \right],
\end{aligned}
\tag{169}
$$

and by definition,

$$
\frac{\partial \mathbf{r}_{(ij)}}{\partial \mathbf{F}} = \mathbf{R}_{(ij)}, \qquad \frac{\partial \mathbf{r}_{(ik)}}{\partial \mathbf{F}} = \mathbf{R}_{(ik)}.
\tag{170}
$$

105

Finally, we use a similar approach to define the first Lagrangian elasticity tensor. This is the traditional way of estimating the elastic properties of a solid. Using the chain rule once again gives

$$
\begin{aligned}
\frac{\partial^2 \mathcal{W}}{\partial \mathbf{F} \partial \mathbf{F}} = \frac{1}{n_a} \Bigg[& \frac{\partial^2 E_b}{\partial \mathbf{r}_{(ij)} \partial \mathbf{r}_{(ij)}} :: \left(\frac{\partial \mathbf{r}_{(ij)}}{\partial \mathbf{F}} \otimes \frac{\partial \mathbf{r}_{(ij)}}{\partial \mathbf{F}} \right) + \frac{\partial^2 E_b}{\partial \mathbf{r}_{(ij)} \partial \mathbf{r}_{(ik)}} :: \left(\frac{\partial \mathbf{r}_{(ik)}}{\partial \mathbf{F}} \otimes \frac{\partial \mathbf{r}_{(ij)}}{\partial \mathbf{F}} \right) \\
& + \frac{\partial^2 E_b}{\partial \mathbf{r}_{(ik)} \partial \mathbf{r}_{(ij)}} :: \left(\frac{\partial \mathbf{r}_{(ij)}}{\partial \mathbf{F}} \otimes \frac{\partial \mathbf{r}_{(ik)}}{\partial \mathbf{F}} \right) + \frac{\partial^2 E_b}{\partial \mathbf{r}_{(ik)} \partial \mathbf{r}_{(ik)}} :: \left(\frac{\partial \mathbf{r}_{(ik)}}{\partial \mathbf{F}} \otimes \frac{\partial \mathbf{r}_{(ik)}}{\partial \mathbf{F}} \right) \\
& + \frac{\partial^2 E_b}{\partial \mathbf{r}_{(ij)} \partial \mathbf{r}_{(jk)}} :: \left(\frac{\partial \mathbf{r}_{(jk)}}{\partial \mathbf{F}} \otimes \frac{\partial \mathbf{r}_{(ij)}}{\partial \mathbf{F}} \right) + \frac{\partial^2 E_b}{\partial \mathbf{r}_{(jk)} \partial \mathbf{r}_{(ij)}} :: \left(\frac{\partial \mathbf{r}_{(ij)}}{\partial \mathbf{F}} \otimes \frac{\partial \mathbf{r}_{(jk)}}{\partial \mathbf{F}} \right) \quad (171) \\
& + \frac{\partial^2 E_b}{\partial \mathbf{r}_{(ik)} \partial \mathbf{r}_{(jk)}} :: \left(\frac{\partial \mathbf{r}_{(jk)}}{\partial \mathbf{F}} \otimes \frac{\partial \mathbf{r}_{(ik)}}{\partial \mathbf{F}} \right) + \frac{\partial^2 E_b}{\partial \mathbf{r}_{(jk)} \partial \mathbf{r}_{(ik)}} :: \left(\frac{\partial \mathbf{r}_{(ik)}}{\partial \mathbf{F}} \otimes \frac{\partial \mathbf{r}_{(jk)}}{\partial \mathbf{F}} \right) \\
& + \frac{\partial^2 E_b}{\partial \mathbf{r}_{(jk)} \partial \mathbf{r}_{(jk)}} :: \left(\frac{\partial \mathbf{r}_{(jk)}}{\partial \mathbf{F}} \otimes \frac{\partial \mathbf{r}_{(jk)}}{\partial \mathbf{F}} \right) \Bigg] .
\end{aligned}
$$

The first Lagrangian elasticity tensor is used in equation (163) whose solution gives $\mathbf{v}^{[0]}$. In a perfect lattice, equation (171) provides the only atomistic material information needed to solve the macroscopic continuum problem. The next section illustrates this by showing that the perturbation is zero for a uniform crystal.

3.7   Example Problems

3.7.1   Example I: Perfect 1-D Atomic Lattice

To illustrate the calculation, a 1-D analytical example is presented. The Tersoff-Brenner potential is used to represent the energetics of a 1-D single-species chain of carbon atoms. The objective here is to solve equations (158) and (159) for $v^{[1]}$ and demonstrate a simple case of a perfect lattice using this method.

One atom comprises the periodic unit cell, but to account for the effects of triples, two "fictitious" atoms are assumed to extend beyond the boundaries of the cell on each side as illustrated in Figure 28. Periodic conditions apply at the cell boundaries. The equilibrium
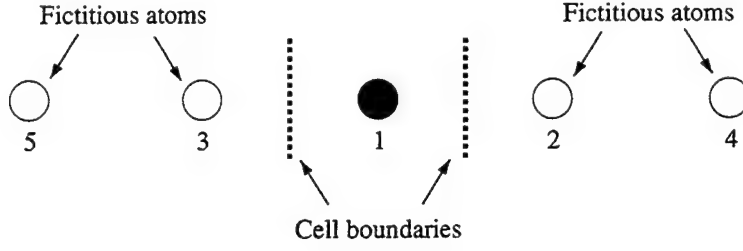
Figure 28. Unit cell of 1-D carbon chain. The atoms are labeled by identify-
ing numbers.

lattice constant for the one-dimensional chain is $r_o = 1.86868\text{Å}$. The following two conditions stem from the 1-D assumption,

$$\theta = \pi, \tag{172}$$

$$R^{(1)} < r < R^{(2)}. \tag{173}$$

This simplifies the expressions in the Appendix. The resulting Hessian for three arbitrary collinear atoms (i, j, k) is obtained as

$$\left[\mathcal{K}^{(ijk)}\right] = \begin{bmatrix} \mathcal{K}_{11}^{(ijk)} & \mathcal{K}_{12}^{(ijk)} & \mathcal{K}_{13}^{(ijk)} \\ \mathcal{K}_{21}^{(ijk)} & \mathcal{K}_{22}^{(ijk)} & \mathcal{K}_{23}^{(ijk)} \\ \mathcal{K}_{31}^{(ijk)} & \mathcal{K}_{32}^{(ijk)} & \mathcal{K}_{33}^{(ijk)} \end{bmatrix}, \tag{174}$$

where $\mathcal{K}_{mn}^{(ijk)} = \mathcal{K}_{nm}^{(ijk)}$ and the terms are defined by

$$\mathcal{K}_{11}^{(ijk)} = V_R'' - \bar{B}V_A'' + a_o\delta V_A' B_{(ij)}^{1+\frac{1}{\delta}} f_{(ik)}' + \frac{\delta}{2}(\delta+1)V_A B_{(ij)}^{1+\frac{2}{\delta}} \left(a_o f_{(ik)}'\right)^2$$
$$+ \frac{a_o\delta}{2} V_A B_{(ij)}^{1+\frac{1}{\delta}} f_{(ik)}'', \tag{175}$$

$$\mathcal{K}_{12}^{(ijk)} = -V_R'' + \bar{B}V_A'' - \frac{a_o\delta}{2} V_A' B_{(ij)}^{1+\frac{1}{\delta}} f_{(ik)}', \tag{176}$$

$$\mathcal{K}_{13}^{(ijk)} = -\frac{a_o\delta}{2} V_A' B_{(ij)}^{1+\frac{1}{\delta}} f_{(ik)}' - \frac{\delta}{2}(\delta+1)V_A B_{(ij)}^{1+\frac{2}{\delta}} \left(a_o f_{(ik)}'\right)^2 - \frac{a_o\delta}{2} V_A B_{(ij)}^{1+\frac{1}{\delta}} f_{(ik)}'', \tag{177}$$

$$\mathcal{K}_{22}^{(ijk)} = V_R'' - \bar{B}V_A'', \tag{178}$$

$$\mathcal{K}_{23}^{(ijk)} = \frac{a_o\delta}{2} V_A' B_{(ij)}^{1+\frac{1}{\delta}} f_{(ik)}', \tag{179}$$

$$\mathcal{K}_{33}^{(ijk)} = \frac{\delta}{2}(\delta+1)V_A B_{(ij)}^{1+\frac{2}{\delta}} \left(a_o f_{(ik)}'\right)^2 + \frac{a_o\delta}{2} V_A B_{(ij)}^{1+\frac{1}{\delta}} f_{(ik)}''. \tag{180}$$

Upon assembly of the two unique pairs (31,12) and their associated triples (123,132) in Figure 28, the final assembled Hessian of the global system is given by the matrix,

$$[\mathcal{K}] = \begin{bmatrix} \mathcal{K}_{11} & \mathcal{K}_{12} & \mathcal{K}_{13} \\ \mathcal{K}_{21} & \mathcal{K}_{22} & \mathcal{K}_{23} \\ \mathcal{K}_{31} & \mathcal{K}_{32} & \mathcal{K}_{33} \end{bmatrix}, \tag{181}$$

which is assembled through the operation,

$$[\mathcal{K}] = \bigsqcup_{(m)}^{(i,j,k)} \bigsqcup_{(n)}^{(i,j,k)} \left[\mathcal{K}^{(ijk)} \right] = \mathcal{K}_{mn}, \tag{182}$$

where $\bigsqcup$ is the addition operator over all unique pair and triple combinations of (i, j, k) and (m) and (n) are displacement degrees of freedom for each atom. In equation (182), $[\mathcal{K}]$ is symmetric once again and its components are obtained in detail for the problem shown in Figure 28 as follows,

$$\mathcal{K}_{11} = \mathcal{K}_{11}^{(123)} + \mathcal{K}_{22}^{(315)} + \mathcal{K}_{33}^{(241)}, \tag{183}$$

$$\mathcal{K}_{12} = \mathcal{K}_{12}^{(123)} + \mathcal{K}_{13}^{(241)}, \tag{184}$$

$$\mathcal{K}_{13} = \mathcal{K}_{13}^{(123)} + \mathcal{K}_{12}^{(315)}, \tag{185}$$

$$\mathcal{K}_{22} = \mathcal{K}_{22}^{(123)} + \mathcal{K}_{11}^{(241)}, \tag{186}$$

$$\mathcal{K}_{23} = \mathcal{K}_{23}^{(123)}, \tag{187}$$

$$\mathcal{K}_{33} = \mathcal{K}_{33}^{(123)} + \mathcal{K}_{11}^{(315)}. \tag{188}$$

This constitutes the stiffness matrix $\mathcal{K}$ in equation (159).

The next step is to calculate the right-hand side of equation (158) which is equivalent to calculating $\mathcal{D}$ and multiplying by the global rate of the deformation gradient. Using equations (161) and (169) the right hand side for three arbitrary collinear atoms (i, j, k) is obtained as

$$\{\mathcal{D}^{(ijk)}\} = \left\{ \begin{array}{c} \mathcal{D}_1^{(ijk)} \\ \mathcal{D}_2^{(ijk)} \\ \mathcal{D}_3^{(ijk)} \end{array} \right\}, \tag{189}$$

where the components are defined by

$$\mathcal{D}_1^{(ijk)} = R_{(ij)}\left(V_R'' - \bar{B}V_A''\right) + \left(R_{(ik)} - R_{(ij)}\right)\left(\frac{a_o\delta}{2}V_A'B_{(ij)}^{1+\frac{1}{\delta}}f_{(ik)}'\right)$$
$$+ R_{(ik)}\left(\frac{\delta}{2}(\delta+1)V_AB_{(ij)}^{1+\frac{2}{\delta}}\left(a_of_{(ik)}'\right)^2 + \frac{a_o\delta}{2}V_AB_{(ij)}^{1+\frac{1}{\delta}}f_{(ik)}''\right), \tag{190}$$

$$\mathcal{D}_2^{(ijk)} = -R_{(ij)}\left(V_R'' - \bar{B}V_A''\right) - R_{(ik)}\left(\frac{a_o\delta}{2}V_A'B_{(ij)}^{1+\frac{1}{\delta}}f_{(ik)}'\right), \tag{191}$$

$$\mathcal{D}_3^{(ijk)} = -R_{(ij)}\left(\frac{a_o\delta}{2}V_A'B_{(ij)}^{1+\frac{1}{\delta}}f_{(ik)}'\right) - R_{(ik)}\left(\frac{\delta}{2}(\delta+1)V_AB_{(ij)}^{1+\frac{2}{\delta}}\left(a_of_{(ik)}'\right)^2 + \frac{a_o\delta}{2}V_AB_{(ij)}^{1+\frac{1}{\delta}}f_{(ik)}''\right). \tag{192}$$

As earlier, the assembly operation

$$\{\mathcal{D}\} = \bigsqcup_{(m)}^{(i,j,k)} \left\{\mathcal{D}^{(ijk)}\right\} = \mathcal{D}_m, \tag{193}$$

yields the right-hand side of the global system given by,

$$\{\mathcal{D}\} = \left\{ \begin{array}{c} \mathcal{D}_1 \\ \mathcal{D}_2 \\ \mathcal{D}_3 \end{array} \right\}, \tag{194}$$

where the components are

$$\mathcal{D}_1 = \mathcal{D}_1^{(123)} + \mathcal{D}_2^{(315)} + \mathcal{D}_3^{(241)}, \tag{195}$$

$$\mathcal{D}_2 = \mathcal{D}_2^{(123)} + \mathcal{D}_1^{(241)}, \tag{196}$$

$$\mathcal{D}_3 = \mathcal{D}_3^{(123)} + \mathcal{D}_1^{(315)}. \tag{197}$$

Under the assumption of a 1-D perfect lattice, we have $R_{(ij)} = R_{(ik)}$, and consequently, $\mathcal{D}_1 = 0$. Then, we can satisfy the periodicity condition and the rigid body constraint by setting $v_{(2)}^{[1]} = v_{(3)}^{[1]} = 0$. The solution is therefore,

$$v_{(1)}^{[1]} = v_{(2)}^{[1]} = v_{(3)}^{[1]} = 0. \tag{198}$$

In light of equation (198), the last term in equation (163) is zero and the material properties are obtained from the atomistic energy density solely through equation (171). This result

shows that in a defect-free lattice, the homogenization method coincides with the conventional atomistic hyperelasticity problem. The next section shows an example in which a defect causes an inhomogeneous energy distribution leading to a situation where homogenization is needed to average out the energy.

3.7.2 Example II: 1-D Atomic Lattice With Defect

Consider the problem shown in Figure 29 where the center atom is displaced by a distance L from its original energy minimizing configuration. This displacement of the center atom constitutes the defect. With this change, the assumption in equation (173) no longer applies and the key stiffness matrix term in equation (183) is now

$$
\begin{aligned}
\mathcal{K}_{11} =& V''_{R_{(12)}} - \bar{B}_{(12)} V''_{A_{(12)}} + a_o \delta V'_{A_{(12)}} B^{1+\frac{1}{\delta}}_{(12)} f'_{(13)} \\
&+ \frac{\delta}{2}(\delta + 1) V_{A_{(12)}} B^{1+\frac{2}{\delta}}_{(12)} \left(a_o f'_{(13)} \right)^2 + \frac{a_o \delta}{2} V_{A_{(12)}} B^{1+\frac{1}{\delta}}_{(12)} f''_{(13)} \\
&+ V''_{R_{(13)}} - \bar{B}_{(13)} V''_{A_{(13)}} + a_o \delta V'_{A_{(13)}} B^{1+\frac{1}{\delta}}_{(13)} f'_{(12)} \\
&+ \frac{\delta}{2}(\delta + 1) V_{A_{(13)}} B^{1+\frac{2}{\delta}}_{(13)} \left(a_o f'_{(12)} \right)^2 + \frac{a_o \delta}{2} V_{A_{(13)}} B^{1+\frac{1}{\delta}}_{(13)} f''_{(12)},
\end{aligned}
\tag{199}
$$

and likewise, equation (195) becomes,

$$
\begin{aligned}
\mathcal{D}_1 =& R_{(12)} \left(V''_{R_{(12)}} - \bar{B}_{(12)} V''_{A_{(12)}} \right) + \left(R_{(13)} - R_{(12)} \right) \left(\frac{a_o \delta}{2} V'_{A_{(12)}} B^{1+\frac{1}{\delta}}_{(12)} f'_{(13)} \right) \\
&+ R_{(13)} \left(\frac{\delta}{2}(\delta + 1) V_{A_{(12)}} B^{1+\frac{2}{\delta}}_{(12)} \left(a_o f'_{(13)} \right)^2 + \frac{a_o \delta}{2} V_{A_{(12)}} B^{1+\frac{1}{\delta}}_{(12)} f''_{(13)} \right) \\
&- R_{(13)} \left(V''_{R_{(13)}} - \bar{B}_{(13)} V''_{A_{(13)}} \right) - \left(R_{(12)} - R_{(13)} \right) \left(\frac{a_o \delta}{2} V'_{A_{(13)}} B^{1+\frac{1}{\delta}}_{(13)} f'_{(12)} \right) \\
&- R_{(12)} \left(\frac{\delta}{2}(\delta + 1) V_{A_{(13)}} B^{1+\frac{2}{\delta}}_{(13)} \left(a_o f'_{(12)} \right)^2 + \frac{a_o \delta}{2} V_{A_{(13)}} B^{1+\frac{1}{\delta}}_{(13)} f''_{(12)} \right).
\end{aligned}
\tag{200}
$$

where $R_{(12)} = r_o - L$ and $R_{(13)} = r_o + L$. Then, solving equation (159) under periodic boundary conditions gives

$$
v_1^{[1]} = \frac{\mathcal{D}_1}{\mathcal{K}_1} \nabla_0 \mathbf{v}^{[0]}, \quad v_2^{[1]} = v_3^{[1]} = 0.
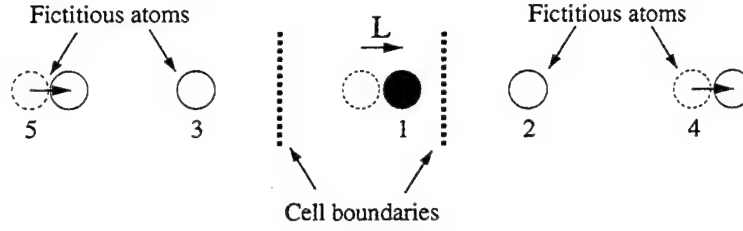\tag{201}
$$

Figure 29. Unit cell of 1-D carbon chain with periodic defect.

The $v^{[1]}/\nabla_0 v^{[0]}$ solution as a function of L/r_o is shown in Figure 30. As expected, the solution has symmetry about the origin and grows asymptotically larger as the size of the defect (L) grows closer to the cut-off radii. Larger defects are avoided presently due to the non-convex structure of the energy well associated with the Tersoff-Brenner potential. This generally leads to unphysical discontinuities in the perturbation velocity ($v^{[1]}$) due to discontinuous second derivatives of the atomistic energy with respect to the defect size. This is attributable to the construction of the empirical potential in equations (151)–(157) which is intrinsically suited for systems where nearest neighbor atoms, even in defect regions, are within the cut-off radius $R^{(2)}$.

It is also noteworthy that arbitrary defect densities can be treated by appropriate modification of the unit cell. In most cases, one can tailor the desired density by increasing the size of the unit cell and performing the summations and the assembly of the atomistic discrete equations over more atoms. Figure 31 illustrates this idea for the 1-D carbon chain.

Numerical experiments show that as the size of the unit cell increases, the perturbative displacement has a sharp discontinuity at the defect. Figure 32 shows this non-local behavior as the number of atoms increases. The problem is of a single defect in chains of increasing size. The defect magnitude is held fixed at $L/r_o = 0.01$. The non-local discontinuity of the perturbative velocity qualitatively agrees with traditional displacement jumps that occur at dislocation cores. The discontinuity indicates that the material property at the defect ($\frac{\partial^2 W}{\partial \mathbf{F} \partial \mathbf{F}}$)

111
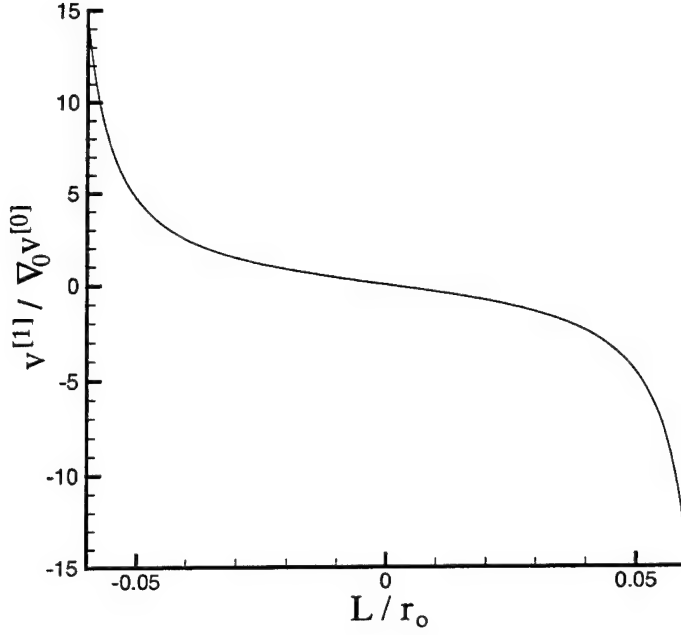
Figure 30. Distribution of $v^{[1]}/\nabla_0 v^{[0]}$ solution as a function of the defect size.
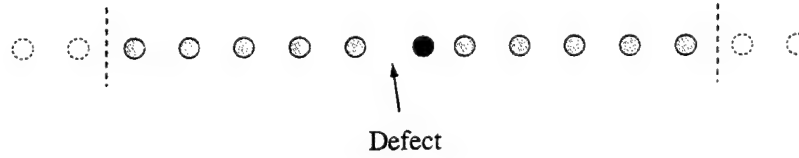
Defect

Figure 31. Larger chain of atoms in perfect arrangement around the defect

region decreases the defect density.

is modified by the last term in equation (163), an amount proportional to $v^{[1]}$ that serves as a correcting force for the non-locality.

Although the primary details of the method have been demonstrated in these two examples, the method can be extended to consider the multiscale problem shown in equation (163) for more general cases involving self-consistent solutions with equation (159). We presently restrict ourselves to analytical 1-D examples where the results, as in the previous examples,
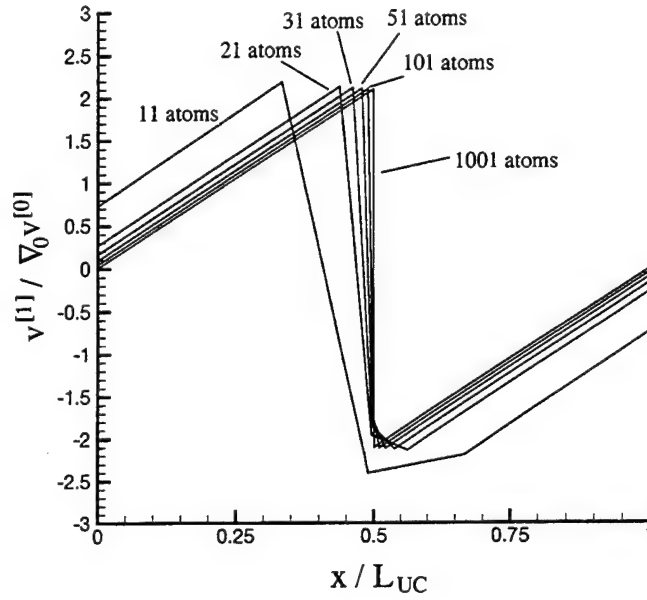
Figure 32. Distribution of $v^{[1]}/\nabla_0 v^{[0]}$ along unit cell length for varying number of atoms ($L/r_o = 0.01$).

can be reported independent of the macroscale solution $v^{[0]}$, and reserve more complex cases in higher dimensions for a separate numerical investigation.

3.8 Closing Remarks

Linking atomic scale physics with continuum scale phenomena is of keen interest in the study of failure, fracture, and reliability of engineering structures. The effects that dominate the failure at the continuum scale typically initiate and evolve from the atomic scale. Despite numerous promising methods in the literature that are capable of linking scales up to the micron level, structures at the meter scale and beyond have only begun to be studied. To this end, in this part we have attempted to address this issue by exploiting the weak convergence

properties of homogenization to devise a scheme which passes atomistic information to very large continuum scales.

We have applied the Cauchy Born rule [12] to the atom scale by assuming that the configuration of atoms used to solve for the perturbation displacement is indeed the minimizing configuration of the atomistic energy. We have not considered the method in conjunction with a molecular dynamics routine, i.e., various strategies of minimizing the atomistic energy by quenching through artificial temperature decrease or solving Newton's equations to minimize the interatom forces.

For this work, the specific case of the Tersoff-Brenner type II potential was considered. But the principles and the general equations can be extended to any potential provided the appropriate derivatives can be obtained as in Appendix A. Typically for classical systems, onerous tensor algebra and calculus are required.

The aim of this part was to develop an approach by which atomistic physics can be embedded into a continuum formulation for large scale systems. This goal has been achieved by formulating a consistent set of equations involving a classical atomistic potential at the fine scale and general finite strain and deformation elasticity at the coarse scale. Simple 1-D analytical results were shown to illustrate the approach and its features. More realistic multiaxial problems in two and three dimensions for more detailed validation are the subjects of ongoing work.

4. References

[1] Sinclair, J. "Improved Atomistic Model of a bcc Dislocation Core." *Journal of Applied Physics*, vol. 42, pp. 5321–5329, 1971.

[2] Mullins, M. and M. A. Dokainish. "Simulation of the (001) Plane Crack in α-Iron Employing a New Boundary Scheme." *Philosophical Magazine A*, vol. 46, pp. 771–787, 1982.

[3] Cleri, F., S. R. Phillpot, D. Wolf, and S. Yip. "Atomistic Simulations of Materials Fracture and the Link Between Atomic and Continuum Length Scales." *Journal of the American Ceramic Society*, vol. 81, pp. 501–516, 1998.

[4] Tadmor, E. B., M. Ortiz, and R. Phillips. "Quasicontinuum Analysis of Defects in Solids." *Philosophical Magazine A*, vol. 73, pp. 1529–1563, 1996.

[5] Broughton, J. Q., F. F. Abraham, N. Bernstein, and E. Kaxiras. "Concurrent Coupling of Length Scales: Methodology and Application." *Physical Review B*, vol. 60, pp. 2391–2403, 1999-II.

[6] Rudd, R. E. and J. Q. Broughton. "Concurrent Coupling of Length Scales In Solid State Systems." *Physica Status Solidi B Basic Research*, vol. 217, pp. 251–291, 2000.

[7] Shenoy, V. B. "Quasicontinuum Models of Atomic-Scale Mechanics." Ph.D. Thesis, Brown University, Providence, RI, 1999.

[8] Friesecke, G. and R. D. James. "A Scheme for the Passage from Atomic to Continuum Theory for Thin Films, Nanotubes and Nanorods." *Journal of the Mechanics and Physics of Solids*, vol. 48, pp. 1519–1540, 2000.

[9] Stillinger, F. H. and T. A. Weber. "Computer Simulation of Local Order in Condensed Phases of Silicon." *Physical Review B*, vol. 31, pp. 5262–5271, 1985.

[10] Abraham, F. F. and I. P. Batra. "Theoretical Interpretation of Atomic-Force-Microscope Images of Graphite." *Surface Science*, vol. 209, pp. L125–L132, 1989.

[11] Ciarlet, P. G. *The Finite Element Method For Elliptic Problems*. Amsterdam: North-Holland Publishing Company, 1978.

[12] Ericksen, J. L. "Cauchy and Born Hypotheses for Crystals." *Phase Transformations and Material Instabilities in Solids*, edited by M. E. Gurtin, pp. 61–77. Orlando, FL: Academic Press, Inc., 1984.

[13] Hashin, Z. "The Elastic Moduli of Heterogeneous Materials." *Transactions of the ASME Journal of Applied Mechanics*, vol. 29, pp. 143–150, March 1962.

[14] Hashin, Z. and S. Shtrikman. "A Variational Approach to the Theory of the Elastic Behaviour of Multiphase Materials." *Journal of the Mechanics and Physics of Solids*, vol. 11, pp. 127–140, 1963.

[15] Hashin, Z. and B. W. Rosen. "The Elastic Moduli of Fiber Reinforced Materials." *Journal of Applied Mechanics Transactions of the ASME*, vol. 31, pp. 223–232, June 1964.

[16] Hill, R. "Elastic Properties of Reinforced Solids: Some Theoretical Principles." *Journal of the Mechanics and Physics of Solids*, vol. 11, pp. 357–372, 1963.

[17] Walpole, L. J. "On Bounds for the Overall Elastic Moduli of Inhomogeneous Systems I." *Journal of Mechanics and Physics of Solids*, vol. 14, pp. 151–162, 1966.

[18] Ishikawa, T. and T. W. Chou. "Thermoelastic Analysis of Hybrid Fabric Composites." *Journal of Materials Science*, vol. 18, pp. 2260–2268, 1983.

[19] Ishikawa, T., M. Matsushima, Y. Hayashi, and T. W. Chou. "Experimental Confirmation of the Theory of Elastic Moduli of Fabric Composites." *Journal of Composite Materials*, vol. 19, pp. 443–458, 1985.

[20] Raju, I. S. and J. T. Wang. "Classical Laminate Theory Models for Woven Fabric Composites." *Journal of Composites Technology and Research*, vol. 16, no. 4, pp. 289–303, October 1994.

[21] Naik, N. K. and P. S. Shembekar. "Elastic Behavior of Woven Fabric Composites: I Lamina Analysis." *Journal of Composite Materials*, vol. 26, no. 15, pp. 2196–2225, 1992.

[22] Naik, N. K. and V. K. Ganesh. "An Analytical Method for Plain Weave Fabric Composites." *Composites*, vol. 26, pp. 281–289, 1995.

[23] Sankar, B. V. and R. V. Marrey. "Analytical Method for Micromechanics of Textile Composites." *Composite Science and Technology*, vol. 57, pp. 703–713, 1997.

[24] Foye, R. L. "The Mechanics of Fabric Reinforced Composites." *Proceedings of the Fiber-Tex Conference*, NASA Conference Publication 3038, pp. 237–247, NASA Langley Research Center, Hampton, VA, September 1988.

[25] Foye, R. L. "Finite Element Analysis of the Stiffness of Fabric Reinforced Composites." NASA Contractor Report 189587, NASA Langley Research Center, Hampton, VA, February 1992.

[26] Whitcomb, J. D. "Three-Dimensional Stress Analysis of Plain Weave Composites." *Composite Materials: Fatigue and Fracture*, edited by T. K. O'Brien, vol. 3, ASTM STP 1110, pp. 417–438, American Society for Testing and Materials, Philadelphia, PA, 1991.

[27] Gowayed, Y. and L. Yi. "Mechanical Behavior of Textile Composite Materials Using a Hybrid Finite Element Approach." *Polymer Composites*, vol. 18, no. 3, pp. 313–319, June 1997.

[28] Sankar, B. V. and R. V. Marrey. "A Unit-Cell Model of Textile Composite Beams for Predicting Stiffness Properties." *Composites Science and Technology*, vol. 49, pp. 61–69, 1993.

[29] Bensoussan, A., J. L. Lions, and G. Papanicolaou. *Asymptotic Analysis for Periodic Structures*. Amsterdam: North-Holland Publishing Company, 1978.

[30] Chang, W. and N. Kikuchi. "Analysis of Residual Stresses Developed in the Curing of Liquid Molding." *Advanced Computational Methods for Material Modeling*, vol. 180, pp. 99–113, 1993.

[31] Terada, K. and N. Kikuchi. "Nonlinear Homogenization Method for Practical Applications." *Computational Methods in Micromechanics American Society of Mechanical Engineers, Applied Mechanics Division*, vol. 212, pp. 1–16, 1995.

[32] Fish, J., K. Shek, M. Pandheeradi, and M. Shepard. "Computational Plasticity for Composite Structures Based on Mathematical Homogenization: Theory and Practice." *Computer Methods in Applied Mechanics and Engineering*, vol. 148, no. 1–2, pp. 53–73, August 1997.

[33] Ghosh, S. and S. Moorthy. "Elastic-Plastic Analysis of Arbitrary Heterogeneous Materials with the Voronoi Cell Finite Element Method." *Computer Methods in Applied Mechanics and Engineering*, vol. 121, pp. 373–409, 1995.

[34] Ghosh, S., K. Lee, and S. Moorthy. "Two Scale Analysis of Heterogeneous Elastic-Plastic Materials with Asymptotic Homogenization and Voronoi Cell Finite Element Model." *Computer Methods in Applied Mechanics and Engineering*, vol. 132, pp. 63–116, 1996.

[35] Walker, K. P., E. H. Jordan, and A. D. Freed. *Nonlinear Mesomechanics of Composites with Periodic Microstructure: First Report*. NASA Technical Memorandum 102051, NASA Lewis Research Center, Cleveland, OH, June 1989.

[36] Moulinec, H. and P. Suquet. "Numerical Method for Computing the Overall Response of Nonlinear Composites with Complex Microstructure." *Computer Methods in Applied Mechanics and Engineering*, vol. 157, no. 1–2, pp. 69–94, April 1998.

[37] Hou, T. Y. and X.-H. Wu. "A Multiscale Finite Element Method For Elliptic Problems In Composite Materials and Porous Media." *Journal of Computational Physics*, vol. 134, no. 1, pp. 169–189, 1997.

[38] Woo, K. and J. Whitcomb. "Global/Local Finite Element Analysis for Textile Composites." *Journal of Composite Materials*, vol. 28, no. 14, pp. 1305–1321, 1994.

[39] Sanchez-Palencia, E. *Non-homogeneous Media and Vibration Theory: Lecture Notes in Physics*. vol. 127. Berlin: Springer-Verlag, 1980.

[40] Lions, J. L. *Some Methods in the Mathematical Analyses of Systems and Their Control*. New York: Gordon and Breach, 1981.

[41] Duvaut, G. "Homogeneisation et Materiaux Composites." *Trends and Applications of Pure Mathematics to Mechanics: Lecture Notes in Physics*, edited by P. Ciarlet and M. Roseau, vol. 195, pp. 35–62, Berlin: Springer-Verlag, 1983.

[42] Oleinik, O. A. "On Homogenization Problems." *Trends and Applications of Pure Mathematics to Mechanics: Lecture Notes in Physics*, edited by P. Ciarlet and M. Roseau, vol. 195, pp. 248–272, Berlin: Springer-Verlag, 1983.

[43] Tartar, L. "Etude des Oscillations dans les Equations aux Derivees Partielles Non-Lineaires." *Trends and Applications of Pure Mathematics to Mechanics. Lecture Notes in Physics. vol. 195*, edited by P. Ciarlet and M. Roseau, pp. 384–412, Berlin: Springer-Verlag, 1983.

[44] Jikov, V. V., S. M. Kozlov, and O. A. Oleinik. *Homogenization of Differential Operators and Integral Functionals*. Berlin: Springer-Verlag, 1994.

[45] Cioranescu, D. and J. S. J. Paulin. *Homogenization of Reticulated Structures*. New York: Springer, 1999.

[46] Bakhvalov, N. S. and G. P. Panasenko. *Homogenisation: Averaging Processes in Periodic Media Mathematical Problems in the Mechanics of Composite Materials*. Dordrecht, The Netherlands: Kluwer Academic, 1989.

[47] Keller, J. B. "Darcy's Law for Flow in Porous Media and the Two-Space Method." *Non-Linear Partial Differential Equations in Engineering and Applied Science*, edited by R. Sternberg, A. Kalinowski, and J. Papadakis, pp. 429–443, New York: Marcel Dekker, 1980.

[48] Ene, H. I. "Application of the Homogenization Method to Transport in Porous Media." *Dynamics of Fluids in Hierarchical Porous Media*, edited by J. Cushman, pp. 223–241, San Diego, CA: Academic Press Ltd., 1990.

[49] Chang, W. and W. Kikuchi. "Analysis of Non-Isothermal Mold Filling Process in Resin Transfer Molding (RTM) and Structural Reaction Injection Molding (SRIM)." *Computational Mechanics*, vol. 16, pp. 22–35, 1995.

[50] Chung, P. W., K. K. Tamma, and R. R. Namburu. "Homogenization of Temperature-Dependent Conductivity in Composite Materials." *Journal of Thermophysics and Heat Transfer*, vol. 15, no. 1, pp. 10–17, January–March 2001.

[51] Dasgupta, A. and R. K. Agarwal. "Orthotropic Thermal Conductivity of Plain-Weave Fabric Composites Using a Homogenization Technique." *Journal of Composite Materials*, vol. 26, no. 18, pp. 2736–2758, 1992.

[52] Ngo, N., R. V. Mohan, P. W. Chung, K. K. Tamma, and D. R. Shires. "Developments Encompassing Non-Isothermal/Isothermal Liquid Composite Molding Process Modeling/Analysis: Computationally Effective and Affordable Simulations and Validations." *Journal of Thermoplastic Composite Materials*, vol. 11, no. 6, pp. 493–532, November 1998.

[53] Lene, F. "Damage Constitutive Relations for Composite Materials." *Engineering Fracture Mechanics*, vol. 25, no. 5–6, pp. 713–728, 1986.

[54] Bendsöe, M. P. and N. Kikuchi. "Generating Optimal Topologies in Structural Design Using a Homogenization Method." *Computer Methods in Applied Mechanics and Engineering*, vol. 71, pp. 197–224, 1988.

[55] Guedes, J. M. and N. Kikuchi. "Preprocessing and Postprocessing for Materials Based on the Homogenization Method With Adaptive Finite Element Methods." *Computer Methods in Applied Mechanics and Engineering*, vol. 83, no. 2, pp. 143–198, October 1990.

[56] Hollister, S. J., D. P. Fyhrie, K. J. Jepsen, and S. A. Goldstein. "Application of Homogenization Theory to the Study of Trabecular Bone Mechanics." *Journal of Biomechanics*, vol. 24, no. 9, pp. 825–839, 1991.

[57] Lene, F. and P. Paumelle. "Micromechanisms of Damage in Woven Composite." *Composite Material Technology*, vol. 45, pp. 97–105, 1992.

[58] Hollister, S. J. and N. Kikuchi. "A Comparison of Homogenization and Standard Mechanics Analyses for Periodic Porous Composites." *Computational Mechanics*, vol. 10, pp. 73–95, 1992.

[59] Chung, P. W. and K. K. Tamma. "Woven Fabric Composites Developments In Engineering Bounds, Homogenization and Applications." *International Journal for Numerical Methods in Engineering*, vol. 45, no. 12, pp. 1757–1790, 1999.

[60] Kawamoto, T. and T. Kyoya. "Some Applications of Homogenization Method in Rock Mechanics." *Impact of Computational Mechanics on Engineering Problems*, edited by V. Pulmano and V. Murti, pp. 63–70, Rotterdam: A. A. Balkema, 1993.

[61] Lefik, M. and B. A. Schrefler. "3-D Finite Element Analysis of Composite Beams With Parallel Fibres, Based on Homogenization Theory." *Computational Mechanics*, vol. 14, pp. 2–15, 1994.

[62] Papa, E. "A Unilateral Damage Model for Masonry Based on a Homogenization Procedure." *Mechanics of Cohesive-Frictional Materials*, vol. 1, pp. 349–366, 1996.

[63] Golanski, D., K. Terada, and N. Kikuchi. "Micro and Macro Scale Modeling of Thermal Residual Stresses in Metal Matrix Composite Surface Layers by the Homogenization Method." *Computational Mechanics*, vol. 19, pp. 188–202, 1997.

[64] Chung, P. W., K. K. Tamma, and R. R. Namburu. "Asymptotic Expansion Homogenization for Heterogeneous Media: Computational Issues and Applications." *Composites Part A: Applied Science and Manufacturing*, vol. 32, no. 9, pp. 1291–1301, September 2001.

[65] Sanchez-Hubert, J. and E. Sanchez-Palencia. "Sur Certains Problèmes Physiques D'homogénéisation Donnant Lieu à des Phénomènes de Relaxation." *Comptes Rendus Hebdomadaires des Seances de l'Academie des Sciences Paris, Série A*, vol. 286, pp. 903–906, May 1978.

[66] Francfort, G. A. and P. M. Suquet. "Homogenization and Mechanical Dissipation in Thermoviscoelasticity." *Archive for Rational Mechanics and Analysis*, vol. 96, pp. 265–293, 1986.

[67] Chung, P. W., K. K. Tamma, and R. R. Namburu. "Micro/Macro Homogenization Approach for Viscoelastic Creep Analysis With Dissipative Correctors for Heterogeneous Woven Fabric Layered Media." *Composites Science and Technology*, vol. 60, no. 12–13, pp. 2233–2253, September 2000.

[68] Chung, P. W., K. K. Tamma, and R. R. Namburu. "A Finite Element Thermo-Viscoelastic Creep Approach for Heterogeneous Structures With Dissipative Correc-

tors." *Finite Elements in Analysis and Design*, vol. 36, no. 20, pp. 279–313, November 2000.

[69] Chung, P. W., K. K. Tamma, and R. R. Namburu. "A Finite Element Thermoviscoelastic Creep Approach for Heterogeneous Structures." *Journal of Thermal Stresses*, vol. 23, no. 8, pp. 703–729, 2000.

[70] Koishi, M., M. Shiratori, T. Miyoshi, and K. Kabe. "Homogenization Method for Dynamic Viscoelastic Analysis of Composite Materials." *JSME International Journal Series A*, vol. 40, no. 3, pp. 306–312, 1997.

[71] Shibuya, Y. "Evaluation of Creep Compliance of Carbon-Fiber-Reinforced Composites by Homogenization Theory." *JSME International Journal Series A.*, vol. 40, no. 3, pp. 313–319, 1997.

[72] Guedes, J. M. "Non-Linear Computational Model for Composite Materials Using Homogenization." Ph.D. Thesis, University of Michigan, Ann Arbor, MI, 1990.

[73] Suquet, P. "Local and Global Aspects in the Mathematical Theory of Plasticity." *Plasticity Today Modeling Methods and Applications*, edited by A. Sawczuk and G. Bianchi, London: Elsevier, 1985.

[74] Galvanetto, U., F. Ohmenhauser, and B. A. Schrefler. "Homogenized Constitutive Law for Periodic Composite Materials With Elasto-Plastic Components." *Composite Structures*, vol. 39, pp. 263–271, 1997.

[75] Smit, R. J. M., W. A. M. Brekelmans, and H. E. H. Meijer. "Prediction of the Mechanical Behavior of Nonlinear Heterogeneous Systems by Multi-Level Finite Element Modeling." *Computer Methods in Applied Mechanics and Engineering*, vol. 155, pp. 181–192, 1998.

[76] Takano, N., Y. Ohnishi, M. Zako, and K. Nishiyabu. "The Formulation of Homogenization Method Applied to Large Deformation Problem for Composite Materials." *International Journal of Solids and Structures*, vol. 37, pp. 6517–6535, 2000.

[77] Wu, X. and N. Ohno. "A Homogenization Theory for Time-Dependent Nonlinear Composites With Periodic Internal Structures." *International Journal of Solids and Structures*, vol. 36, pp. 4991–5012, 1999.

[78] Chung, P. W., R. R. Namburu, and K. K. Tamma. "Three-Dimensional Elasto-Plastic Heterogeneous Media Subjected to Short Transient Loads." *AIAA/ASME/ASCE/AHS Structures, Structural Dynamics and Materials Conference Collection of Technical Papers*, vol. 1, pp. 411–421, St. Louis, MO, 1999.

[79] Brenner, S. C. and L. R. Scott. *The Mathematical Theory of Finite Element Methods*. New York: Springer-Verlag, 1994.

[80] Zienkiewicz, O. C. and R. L. Taylor. *The Finite Element Method*. London: McGraw-Hill, 1989.

[81] Huebner, K. H., E. A. Thornton, and T. G. Byrom. *The Finite Element Method for Engineers*. New York: John Wiley and Sons, 1994.

[82] Reddy, J. N. *An Introduction to the Finite Element Method*. New York: McGraw-Hill, Inc., 1993.

[83] Hinton, E., T. Rock, and O. C. Zienkiewics. "A Note on Mass Lumping and Related Processes in the Finite Element Method." *Earthquake Engineering and Structural Dynamics*, vol. 4, pp. 245–249, 1976.

[84] Chung, P. W. "Methods for Determining Structural Constitution of Woven Fabric Composites." Master's Thesis, University of Minnesota, Minneapolis, MN, 1996.

[85] Mura, T. *Micromechanics of Defects in Solids*. Dordrecht, The Netherlands: Martinus Nijhoff Publishers, 1987.

[86] Christensen, R. M. *Mechanics of Composite Materials*. New York: John Wiley and Sons, 1979.

[87] Rayleigh, L. "On the Influence of Obstacles Arranged in Rectangular Order Upon the Properties of a Medium." *Philosophical Magazine*, vol. 34, pp. 481–502, 1882.

[88] Darcy, H. *Les Fontaines Publiques de la Ville de Dijon*. Libraire des Corps Imperiaux des Ponts et Chaussées et des Mines, Dalmont, Paris: Victor Dalmont, 1856.

[89] Hashin, Z. "Theory of Mechanical Behavior of Heterogeneous Media." *Applied Mechanics Review*, vol. 17, no. 1, pp. 1–9, January 1964.

[90] Eshelby, J. D. "The Continuum Theory of Lattice Defects." *Progress in Solid State Physics*, edited by F. Seitz and D. Turnbull, vol. 3, p. 79, New York: Academic Press, 1956.

[91] Ishikawa, T. and T. W. Chou. "Stiffness and Strength Behavior of Woven Fabric Composites." *Journal of Materials Science*, vol. 17, pp. 3211–3220, 1982.

[92] Chou, T. W. *Microstructural Design of Fiber Composites*. New York: Cambridge University Press, 1992.

[93] Bakhvalov, N. and G. Panasenko. *Homogenization: Averaging Processes in Periodic Media*. Dordrecht, The Netherlands: Kluwer, 1989.

[94] Tersoff, J. "Empirical Interatomic Potential for Carbon, With Applications to Amorphous Carbon." *Physical Review Letters*, vol. 61, no. 25, pp. 2879–2882, 19 December 1988.

[95] Brenner, D. W. "Empirical Potential for Hydrocarbons for Use in Simulating the Chemical Vapor Deposition of Diamond Films." *Physical Review B*, vol. 42, no. 15, pp. 9458–9471, 15 November 1990.

INTENTIONALLY LEFT BLANK.

Appendix A. Derivatives of the Tersoff-Brenner Potential

The derivatives needed to form the Euler-Lagrange equations and the Hessian are shown here in detail. To simplify the notation, we define the following expressions,

$$r_{(ij)} = \left| \mathbf{r}_{(ij)} \right|, \tag{A-1}$$

$$f'_{(ij)}(r) = \frac{\partial f_{(ij)}}{\partial r_{(ij)}} \qquad f''_{(ij)}(r) = \frac{\partial^2 f_{(ij)}}{\partial r^2_{(ij)}}. \tag{A-2}$$

Note that although the equations are written in component form with respect to atoms, it is still in dyadic notation due to the multi-axial components of $\mathbf{r}_{(ij)}$. That is $\mathbf{r}_{(ij)} \cdot \mathbf{e}_1$ is the component of the vector originating at atom i and terminating at atom j in the direction of $\mathbf{e}_1$, $\mathbf{r}_{(ij)} \cdot \mathbf{e}_2$ is the component in the direction of $\mathbf{e}_2$, etc. Referring to equations in this report, (151)–(157), the derivatives in equation (165) are defined by

$$\frac{\partial E_b}{\partial \mathbf{r}_{(ij)}} = \sum_i \sum_{j(>i)} \left[V'_R \frac{\partial r_{(ij)}}{\partial \mathbf{r}_{(ij)}} - V_A \frac{\partial \bar{B}}{\partial \mathbf{r}_{(ij)}} - \bar{B} V'_A \frac{\partial r_{(ij)}}{\partial \mathbf{r}_{(ij)}} \right], \tag{A-3}$$

$$\frac{\partial E_b}{\partial \mathbf{r}_{(ik)}} = \sum_i \sum_{j(>i)} \left[-V_A \frac{\partial \bar{B}}{\partial \mathbf{r}_{(ik)}} \right], \tag{A-4}$$

$$\frac{\partial E_b}{\partial \mathbf{r}_{(jk)}} = \sum_i \sum_{j(>i)} \left[-V_A \frac{\partial \bar{B}}{\partial \mathbf{r}_{(jk)}} \right], \tag{A-5}$$

$$\frac{\partial V_R}{\partial r_{(ij)}} = V'_R = f'_{(ij)} \frac{D^{(e)}}{(S-1)} e^{-\alpha_1 (r_{(ij)} - R^{(e)})} - \alpha_1 \frac{f_{(ij)} D^{(e)}}{(S-1)} e^{-\alpha_1 (r_{(ij)} - R^{(e)})}, \tag{A-6}$$

$$\frac{\partial V_A}{\partial r_{(ij)}} = V'_A = f'_{(ij)} \frac{D^{(e)} S}{(S-1)} e^{-\alpha_2 (r_{(ij)} - R^{(e)})} - \alpha_2 \frac{f_{(ij)} D^{(e)} S}{(S-1)} e^{-\alpha_2 (r_{(ij)} - R^{(e)})}, \tag{A-7}$$

$$\frac{\partial \bar{B}}{\partial \mathbf{r}_{(ij)}} = \frac{1}{2} \left\{ -\delta B_{(ij)}^{1+\frac{1}{\delta}} \sum_{k \neq (i,j)} \left[\frac{\partial G(\theta_{(ijk)})}{\partial \mathbf{r}_{(ij)}} f_{(ik)} \right] - \delta B_{(ji)}^{1+\frac{1}{\delta}} \sum_{k \neq (i,j)} \left[\frac{\partial G(\theta_{(jik)})}{\partial \mathbf{r}_{(ij)}} f_{(ik)} \right] \right\}, \quad \text{(A-8)}$$

$$\frac{\partial \bar{B}}{\partial \mathbf{r}_{(ik)}} = -\frac{\delta}{2} B_{(ij)}^{1+\frac{1}{\delta}} \sum_{k \neq (i,j)} \left[\frac{\partial G(\theta_{(ijk)})}{\partial \mathbf{r}_{(ik)}} f_{(ik)} + G(\theta_{(ijk)}) f'_{(ik)} \frac{\partial r_{(ik)}}{\partial \mathbf{r}_{(ik)}} \right], \quad \text{(A-9)}$$

$$\frac{\partial \bar{B}}{\partial \mathbf{r}_{(jk)}} = -\frac{\delta}{2} B_{(ji)}^{1+\frac{1}{\delta}} \sum_{k \neq (i,j)} \left[\frac{\partial G(\theta_{(jik)})}{\partial \mathbf{r}_{(jk)}} f_{jk} + G(\theta_{(jik)}) f'_{jk} \frac{\partial r_{(jk)}}{\partial \mathbf{r}_{(jk)}} \right], \quad \text{(A-10)}$$

$$\frac{\partial G(\theta_\gamma)}{\partial \mathbf{r}_{(mn)}} = \frac{2a_o c_o^2 (1 + \cos \theta_\gamma)}{[d_o^2 + (1 + \cos \theta_\gamma)^2]^2} \frac{\partial \cos \theta_\gamma}{\partial \mathbf{r}_{(mn)}}, \quad \text{(A-11)}$$

for $(mn) = (ij), (ik)$ when $\gamma = (ijk)$ and $(mn) = (ij), (jk)$ when $\gamma = (jik)$. The angles $\theta_{(ijk)}$ and $\theta_{(jik)}$, shown in Figure A-1, are the angles subtending the connecting lines at the atoms i and j, respectively. Note that $\mathbf{r}_{(ij)} = -\mathbf{r}_{(ji)}$. The following identities can also be shown:

$$\begin{aligned} \frac{\partial r_{(ij)}}{\partial \mathbf{r}_{(ij)}} &= \frac{\partial (\mathbf{r}_{(ij)} \cdot \mathbf{r}_{(ij)})^{1/2}}{\partial \mathbf{r}_{(ij)}} \\ &= \frac{1}{2} \frac{1}{r_{(ij)}} 2\mathbf{r}_{(ij)} \\ &= \frac{\mathbf{r}_{(ij)}}{r_{(ij)}}, \end{aligned} \quad \text{(A-12)}$$

$$\begin{aligned} \frac{\partial \cos \theta_{(ijk)}}{\partial \mathbf{r}_{(ij)}} &= \frac{\partial}{\partial \mathbf{r}_{(ij)}} \left(\frac{\mathbf{r}_{(ij)} \cdot \mathbf{r}_{(ik)}}{r_{(ij)} r_{(ik)}} \right) \\ &= \frac{\mathbf{r}_{(ik)}}{r_{(ij)} r_{(ik)}} - \frac{\mathbf{r}_{(ij)}}{r_{(ij)}^2} \cos \theta_{(ijk)}, \end{aligned} \quad \text{(A-13)}$$

$$\frac{\partial \cos \theta_{(ijk)}}{\partial \mathbf{r}_{(ik)}} = \frac{\mathbf{r}_{(ij)}}{r_{(ij)} r_{(ik)}} - \frac{\mathbf{r}_{(ik)}}{r_{(ik)}^2} \cos \theta_{(ijk)}, \quad \text{(A-14)}$$

$$\frac{\partial \cos \theta_{(jik)}}{\partial \mathbf{r}_{(ij)}} = -\frac{\mathbf{r}_{(jk)}}{r_{(ji)} r_{(jk)}} + \frac{\mathbf{r}_{(ji)}}{r_{(ji)}^2} \cos \theta_{(jik)}, \quad \text{(A-15)}$$

$$\frac{\partial \cos \theta_{(jik)}}{\partial \mathbf{r}_{(jk)}} = \frac{\mathbf{r}_{(ji)}}{r_{(ji)} r_{(jk)}} - \frac{\mathbf{r}_{(jk)}}{r_{(jk)}^2} \cos \theta_{(jik)}. \quad \text{(A-16)}$$

It is important to note that

$$\frac{\partial \mathbf{r}_{(ij)}}{\partial \mathbf{q}_{(m)}} = \begin{cases} -\mathbf{I} & m = i \\ \mathbf{I} & m = j \\ \mathbf{0} & m \neq (i, j) \end{cases}, \quad \text{(A-17)}$$
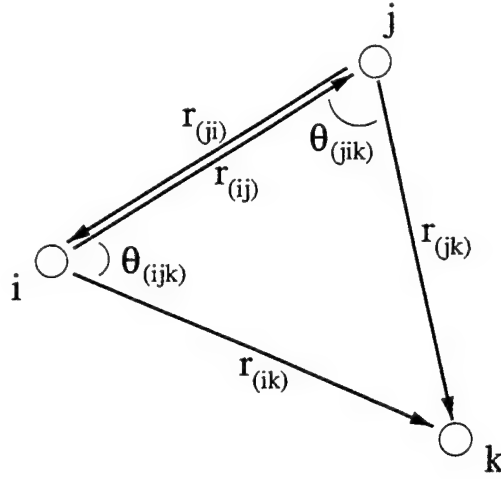
128

Figure A-1. Angles and interatom vectors.

where $\mathbf{I}$ is the 3×3 identity tensor for a system in a 3-D domain. The derivative with respect to $\mathbf{r}_{(ik)}$ can be obtained likewise. This indicates that the summations in equations (A-3), (A-4), (A-8), and (A-9), when multiplied by equation (A-17) in equation (165) are nontrivial if and only if m is equal to i, j, or k.

For the Hessian in equation (166), the differential terms are defined by,

$$\frac{\partial^2 E_b}{\partial \mathbf{r}_{(ij)} \partial \mathbf{r}_{(ij)}} = \sum_i \sum_{j(>i)} \left[\left(V_R'' - \bar{B} V_A'' \right) \left(\frac{\partial r_{(ij)}}{\partial \mathbf{r}_{(ij)}} \otimes \frac{\partial r_{(ij)}}{\partial \mathbf{r}_{(ij)}} \right) + V_A' \frac{\partial^2 r_{(ij)}}{\partial \mathbf{r}_{(ij)} \partial \mathbf{r}_{(ij)}} - V_A' \left(\frac{\partial \bar{B}}{\partial \mathbf{r}_{(ij)}} \otimes \frac{\partial r_{(ij)}}{\partial \mathbf{r}_{(ij)}} \right) \right.$$
$$\left. - V_A \frac{\partial^2 \bar{B}}{\partial \mathbf{r}_{(ij)} \partial \mathbf{r}_{(ij)}} - V_A' \left(\frac{\partial r_{(ij)}}{\partial \mathbf{r}_{(ij)}} \otimes \frac{\partial \bar{B}}{\partial \mathbf{r}_{(ij)}} \right) \right], \tag{A-18}$$

$$\frac{\partial^2 E_b}{\partial \mathbf{r}_{(ij)} \partial \mathbf{r}_{(ik)}} = \sum_i \sum_{j(>i)} \left[-V_A' \left(\frac{\partial \bar{B}}{\partial \mathbf{r}_{(ik)}} \otimes \frac{\partial r_{(ij)}}{\partial \mathbf{r}_{(ij)}} \right) - V_A \frac{\partial^2 \bar{B}}{\partial \mathbf{r}_{(ij)} \partial \mathbf{r}_{(ik)}} \right], \tag{A-19}$$

$$\frac{\partial^2 E_b}{\partial \mathbf{r}_{(ik)} \partial \mathbf{r}_{(ij)}} = \sum_i \sum_{j(>i)} \left[-V_A' \left(\frac{\partial r_{(ij)}}{\partial \mathbf{r}_{(ij)}} \otimes \frac{\partial \bar{B}}{\partial \mathbf{r}_{(ik)}} \right) - V_A \frac{\partial^2 \bar{B}}{\partial \mathbf{r}_{(ik)} \partial \mathbf{r}_{(ij)}} \right], \tag{A-20}$$

$$\frac{\partial^2 E_b}{\partial \mathbf{r}_{(ik)} \partial \mathbf{r}_{(ik)}} = \sum_i \sum_{j(>i)} \left[-V_A \frac{\partial^2 \bar{B}}{\partial \mathbf{r}_{(ik)} \partial \mathbf{r}_{(ik)}} \right], \tag{A-21}$$

129

$$\frac{\partial^2 E_b}{\partial \mathbf{r}_{(jk)} \partial \mathbf{r}_{(jk)}} = \sum_i \sum_{j(>i)} \left[-V_A \frac{\partial^2 \bar{B}}{\partial \mathbf{r}_{(jk)} \partial \mathbf{r}_{(jk)}} \right], \tag{A-22}$$

$$\frac{\partial^2 E_b}{\partial \mathbf{r}_{(ij)} \partial \mathbf{r}_{(jk)}} = \sum_i \sum_{j(>i)} \left[-V_A' \left(\frac{\partial r_{(ij)}}{\partial \mathbf{r}_{(ij)}} \otimes \frac{\partial \bar{B}}{\partial \mathbf{r}_{(jk)}} \right) - V_A \frac{\partial^2 \bar{B}}{\partial \mathbf{r}_{(ij)} \partial \mathbf{r}_{(jk)}} \right], \tag{A-23}$$

$$\frac{\partial^2 E_b}{\partial \mathbf{r}_{(jk)} \partial \mathbf{r}_{(ij)}} = \sum_i \sum_{j(>i)} \left[-V_A' \left(\frac{\partial \bar{B}}{\partial \mathbf{r}_{(jk)}} \otimes \frac{\partial r_{(ij)}}{\partial \mathbf{r}_{(ij)}} \right) - V_A \frac{\partial^2 \bar{B}}{\partial \mathbf{r}_{(jk)} \partial \mathbf{r}_{(ij)}} \right], \tag{A-24}$$

$$\frac{\partial^2 E_b}{\partial \mathbf{r}_{(ik)} \partial \mathbf{r}_{(jk)}} = \sum_i \sum_{j(>i)} \left[-V_A \frac{\partial^2 \bar{B}}{\partial \mathbf{r}_{(ik)} \partial \mathbf{r}_{(jk)}} \right], \tag{A-25}$$

$$\frac{\partial^2 E_b}{\partial \mathbf{r}_{(jk)} \partial \mathbf{r}_{(ik)}} = \sum_i \sum_{j(>i)} \left[-V_A \frac{\partial^2 \bar{B}}{\partial \mathbf{r}_{(jk)} \partial \mathbf{r}_{(ik)}} \right], \tag{A-26}$$

and additional algebra yields,

$$V_R'' = \frac{\partial^2 V_R}{\partial r_{(ij)} \partial r_{(ij)}} = \left[\frac{f_{(ij)}'' D^{(e)}}{(S-1)} - \frac{2\alpha_1 f_{(ij)}' D^{(e)}}{(S-1)} + \frac{\alpha_1^2 f_{(ij)} D^{(e)}}{(S-1)} \right] e^{-\alpha_1 (r_{(ij)} - R^{(e)})}, \tag{A-27}$$

$$V_A'' = \frac{\partial^2 V_A}{\partial r_{(ij)} \partial r_{(ij)}} = \left[\frac{f_{(ij)}'' D^{(e)} S}{(S-1)} - \frac{2\alpha_2 f_{(ij)}' D^{(e)} S}{(S-1)} + \frac{\alpha_2^2 f_{(ij)} D^{(e)} S}{(S-1)} \right] e^{-\alpha_2 (r_{(ij)} - R^{(e)})}, \tag{A-28}$$

$$\frac{\partial^2 \bar{B}}{\partial \mathbf{r}_{(ij)} \partial \mathbf{r}_{(ij)}} = -\frac{(\delta+1)}{2} B_{(ij)}^{\frac{1}{\delta}} \sum_{k \neq (i,j)} f_{(ik)} \left(\frac{\partial G(\theta_{(ijk)})}{\partial \mathbf{r}_{(ij)}} \otimes \frac{\partial B_{(ij)}}{\partial \mathbf{r}_{(ij)}} \right) - \frac{\delta}{2} B_{(ij)}^{1+\frac{1}{\delta}} \sum_{k \neq (i,j)} \left(f_{(ik)} \frac{\partial^2 G(\theta_{(ijk)})}{\partial \mathbf{r}_{(ij)} \partial \mathbf{r}_{(ij)}} \right)$$
$$-\frac{(\delta+1)}{2} B_{(ji)}^{\frac{1}{\delta}} \sum_{k \neq (i,j)} f_{jk} \left(\frac{\partial G(\theta_{(jik)})}{\partial \mathbf{r}_{(ij)}} \otimes \frac{\partial B_{(ji)}}{\partial \mathbf{r}_{(ij)}} \right) - \frac{\delta}{2} B_{(ji)}^{1+\frac{1}{\delta}} \sum_{k \neq (i,j)} \left(f_{jk} \frac{\partial^2 G(\theta_{(jik)})}{\partial \mathbf{r}_{(ij)} \partial \mathbf{r}_{(ij)}} \right) \tag{A-29}$$

$$\frac{\partial^2 \bar{B}}{\partial \mathbf{r}_{(ij)} \partial \mathbf{r}_{(ik)}} = -\frac{(\delta+1)}{2} B_{(ij)}^{\frac{1}{\delta}} \sum_{k \neq (i,j)} \left[f_{(ik)} \left(\frac{\partial G(\theta_{(ijk)})}{\partial \mathbf{r}_{(ik)}} \otimes \frac{\partial B_{(ij)}}{\partial \mathbf{r}_{(ij)}} \right) + G(\theta_{(ijk)}) f_{(ik)}' \left(\frac{\partial r_{(ik)}}{\partial \mathbf{r}_{(ik)}} \otimes \frac{\partial B_{(ij)}}{\partial \mathbf{r}_{(ij)}} \right) \right]$$
$$-\frac{\delta}{2} B_{(ij)}^{1+\frac{1}{\delta}} \sum_{k \neq (i,j)} \left[f_{(ik)} \frac{\partial^2 G(\theta_{(ijk)})}{\partial \mathbf{r}_{(ij)} \partial \mathbf{r}_{(ik)}} + f_{(ik)}' \left(\frac{\partial r_{(ik)}}{\partial \mathbf{r}_{(ik)}} \otimes \frac{\partial G(\theta_{(ijk)})}{\partial \mathbf{r}_{(ij)}} \right) \right], \tag{A-30}$$

$$\frac{\partial^2 \bar{B}}{\partial \mathbf{r}_{(ik)} \partial \mathbf{r}_{(ij)}} = -\frac{(\delta+1)}{2} B_{(ij)}^{\frac{1}{\delta}} \sum_{k \neq (i,j)} \left[f_{(ik)} \left(\frac{\partial G(\theta_{(ijk)})}{\partial \mathbf{r}_{(ij)}} \otimes \frac{\partial B_{(ij)}}{\partial \mathbf{r}_{(ik)}} \right) \right]$$
$$-\frac{\delta}{2} B_{(ij)}^{1+\frac{1}{\delta}} \sum_{k \neq (i,j)} \left[f_{(ik)} \frac{\partial^2 G(\theta_{(ijk)})}{\partial \mathbf{r}_{(ik)} \partial \mathbf{r}_{(ij)}} + f_{(ik)}' \left(\frac{\partial G(\theta_{(ijk)})}{\partial \mathbf{r}_{(ij)}} \otimes \frac{\partial r_{(ik)}}{\partial \mathbf{r}_{(ik)}} \right) \right], \tag{A-31}$$

130

$$\frac{\partial^2 \bar{B}}{\partial \mathbf{r}_{(ik)} \partial \mathbf{r}_{(ik)}} = -\frac{(\delta+1)}{2} B_{(ij)}^{\frac{1}{\delta}} \sum_{k \neq (i,j)} \left[f_{(ik)} \left(\frac{\partial G(\theta_{(ijk)})}{\partial \mathbf{r}_{(ik)}} \otimes \frac{\partial B_{(ij)}}{\partial \mathbf{r}_{(ik)}} \right) + G(\theta_{(ijk)}) f'_{(ik)} \left(\frac{\partial r_{(ik)}}{\partial \mathbf{r}_{(ik)}} \otimes \frac{\partial B_{(ij)}}{\partial \mathbf{r}_{(ik)}} \right) \right]$$

$$- \frac{\delta}{2} B_{(ij)}^{1+\frac{1}{\delta}} \sum_{k \neq (i,j)} \left[f_{(ik)} \frac{\partial^2 G(\theta_{(ijk)})}{\partial \mathbf{r}_{(ik)} \partial \mathbf{r}_{(ik)}} + 2 f'_{(ik)} \left(\frac{\partial r_{(ik)}}{\partial \mathbf{r}_{(ik)}} \otimes \frac{\partial G(\theta_{(ijk)})}{\partial \mathbf{r}_{(ik)}} \right) \right. \tag{A-32}$$

$$\left. + G(\theta_{(ijk)}) f''_{(ik)} \left(\frac{\partial r_{(ik)}}{\partial \mathbf{r}_{(ik)}} \otimes \frac{\partial r_{(ik)}}{\partial \mathbf{r}_{(ik)}} \right) + G(\theta_{(ijk)}) f'_{(ik)} \frac{\partial^2 r_{(ik)}}{\partial \mathbf{r}_{(ik)} \partial \mathbf{r}_{(ik)}} \right].$$

$$\frac{\partial^2 \bar{B}}{\partial \mathbf{r}_{(ij)} \partial \mathbf{r}_{(jk)}} = -\frac{(\delta+1)}{2} B_{(ji)}^{\frac{1}{\delta}} \sum_{k \neq (i,j)} \left[f_{jk} \left(\frac{\partial G(\theta_{(jik)})}{\partial \mathbf{r}_{(jk)}} \otimes \frac{\partial B_{(ji)}}{\partial \mathbf{r}_{(ij)}} \right) + G(\theta_{(jik)}) f'_{jk} \left(\frac{\partial r_{(jk)}}{\partial \mathbf{r}_{(jk)}} \otimes \frac{\partial B_{(ji)}}{\partial \mathbf{r}_{(ij)}} \right) \right]$$

$$- \frac{\delta}{2} B_{(ji)}^{1+\frac{1}{\delta}} \sum_{k \neq (i,j)} \left[f_{jk} \frac{\partial^2 G(\theta_{(jik)})}{\partial \mathbf{r}_{(ij)} \partial \mathbf{r}_{(jk)}} + f'_{jk} \left(\frac{\partial r_{(jk)}}{\partial \mathbf{r}_{(jk)}} \otimes \frac{\partial G(\theta_{(jik)})}{\partial \mathbf{r}_{(ij)}} \right) \right], \tag{A-33}$$

$$\frac{\partial^2 \bar{B}}{\partial \mathbf{r}_{(jk)} \partial \mathbf{r}_{(ij)}} = -\frac{(\delta+1)}{2} B_{(ji)}^{\frac{1}{\delta}} \sum_{k \neq (i,j)} \left[f_{jk} \left(\frac{\partial G(\theta_{(jik)})}{\partial \mathbf{r}_{(ij)}} \otimes \frac{\partial B_{(ji)}}{\partial \mathbf{r}_{(jk)}} \right) \right]$$

$$- \frac{\delta}{2} B_{(ji)}^{1+\frac{1}{\delta}} \sum_{k \neq (i,j)} \left[f_{jk} \frac{\partial^2 G(\theta_{(jik)})}{\partial \mathbf{r}_{(jk)} \partial \mathbf{r}_{(ij)}} + f'_{jk} \left(\frac{\partial G(\theta_{(jik)})}{\partial \mathbf{r}_{(ij)}} \otimes \frac{\partial r_{(jk)}}{\partial \mathbf{r}_{(jk)}} \right) \right], \tag{A-34}$$

$$\frac{\partial^2 \bar{B}}{\partial \mathbf{r}_{(jk)} \partial \mathbf{r}_{(jk)}} = -\frac{(\delta+1)}{2} B_{(ji)}^{\frac{1}{\delta}} \sum_{k \neq (i,j)} \left[f_{jk} \left(\frac{\partial G(\theta_{(jik)})}{\partial \mathbf{r}_{(jk)}} \otimes \frac{\partial B_{(ji)}}{\partial \mathbf{r}_{(jk)}} \right) + G(\theta_{(jik)}) f'_{jk} \left(\frac{\partial r_{(jk)}}{\partial \mathbf{r}_{(jk)}} \otimes \frac{\partial B_{(ji)}}{\partial \mathbf{r}_{(jk)}} \right) \right]$$

$$- \frac{\delta}{2} B_{(ji)}^{1+\frac{1}{\delta}} \sum_{k \neq (i,j)} \left[f_{jk} \frac{\partial^2 G(\theta_{(jik)})}{\partial \mathbf{r}_{(jk)} \partial \mathbf{r}_{(jk)}} + 2 f'_{jk} \left(\frac{\partial r_{(jk)}}{\partial \mathbf{r}_{(jk)}} \otimes \frac{\partial G(\theta_{(jik)})}{\partial \mathbf{r}_{(jk)}} \right) \right. \tag{A-35}$$

$$\left. + G(\theta_{(jik)}) f''_{jk} \left(\frac{\partial r_{(jk)}}{\partial \mathbf{r}_{(jk)}} \otimes \frac{\partial r_{(jk)}}{\partial \mathbf{r}_{(jk)}} \right) + G(\theta_{(jik)}) f'_{jk} \frac{\partial^2 r_{(jk)}}{\partial \mathbf{r}_{(jk)} \partial \mathbf{r}_{(jk)}} \right],$$

$$\frac{\partial^2 \bar{B}}{\partial \mathbf{r}_{(ik)} \partial \mathbf{r}_{(jk)}} = \frac{\partial^2 \bar{B}}{\partial \mathbf{r}_{(jk)} \partial \mathbf{r}_{(ik)}} = \mathbf{0}, \tag{A-36}$$

$$\frac{\partial^2 r_{(ij)}}{\partial \mathbf{r}_{(ij)} \partial \mathbf{r}_{(ij)}} = \frac{\mathbf{I}}{r_{(ij)}} - \frac{\mathbf{r}_{(ij)} \otimes \mathbf{r}_{(ij)}}{r_{(ij)}^3}. \tag{A-37}$$

To complete the derivation, the following identities are needed,

$$\frac{\partial^2 G}{\partial \mathbf{r}_{(mn)} \partial \mathbf{r}_{(pq)}} = \left(\frac{-8 a_o c_o^2 (1 + \cos \theta_\gamma)^2}{(d_o^2 + (1 + \cos \theta_\gamma)^2)^3} + \frac{2 a_o c_o^2}{(d_o^2 + (1 + \cos \theta_\gamma)^2)^2} \right) \left(\frac{\partial \cos \theta_\gamma}{\partial \mathbf{r}_{(pq)}} \otimes \frac{\partial \cos \theta_\gamma}{\partial \mathbf{r}_{(mn)}} \right)$$

$$+ \frac{2 a_o c_o^2 (1 + \cos \theta_\gamma)}{(d_o^2 + (1 + \cos \theta_\gamma)^2)^2} \frac{\partial^2 \cos \theta_\gamma}{\partial \mathbf{r}_{(mn)} \partial \mathbf{r}_{(pq)}}, \tag{A-38}$$

with the appropriate combinations of $(mn, pq) = (ij, ij), (ij, ik), (ik, ij), (ik, ik)$ for $\gamma = ijk$

and $(mn, pq) = (ij, jk), (jk, ij), (jk, jk)$ for $\gamma = jik$, and,

$$\frac{\partial^2 \cos\theta_{(ijk)}}{\partial \mathbf{r}_{(ij)} \partial \mathbf{r}_{(ij)}} = -\frac{1}{r_{(ij)}^3 r_{(ik)}} \left(\mathbf{r}_{(ij)} \otimes \mathbf{r}_{(ik)} \right) - \frac{\cos\theta_{(ijk)}\mathbf{I}}{r_{(ij)}^2} + \frac{3\cos\theta_{(ijk)}}{r_{(ij)}^4} \left(\mathbf{r}_{(ij)} \otimes \mathbf{r}_{(ij)} \right)$$
$$- \frac{1}{r_{(ij)}^3 r_{(ik)}} \left(\mathbf{r}_{(ik)} \otimes \mathbf{r}_{(ij)} \right), \tag{A-39}$$

$$\frac{\partial^2 \cos\theta_{(ijk)}}{\partial \mathbf{r}_{(ij)} \partial \mathbf{r}_{(ik)}} = -\frac{1}{r_{(ij)}^3 r_{(ik)}} \left(\mathbf{r}_{(ij)} \otimes \mathbf{r}_{(ij)} \right) - \frac{1}{r_{(ij)} r_{(ik)}^3} \left(\mathbf{r}_{(ik)} \otimes \mathbf{r}_{(ik)} \right)$$
$$+ \frac{\cos\theta_{(ijk)}}{r_{(ij)}^2 r_{(ik)}^2} \left(\mathbf{r}_{(ik)} \otimes \mathbf{r}_{(ij)} \right) + \frac{\mathbf{I}}{r_{(ij)} r_{(ik)}}, \tag{A-40}$$

$$\frac{\partial^2 \cos\theta_{(ijk)}}{\partial \mathbf{r}_{(ik)} \partial \mathbf{r}_{(ij)}} = -\frac{1}{r_{(ij)}^3 r_{(ik)}} \left(\mathbf{r}_{(ij)} \otimes \mathbf{r}_{(ij)} \right) - \frac{1}{r_{(ij)} r_{(ik)}^3} \left(\mathbf{r}_{(ik)} \otimes \mathbf{r}_{(ik)} \right)$$
$$+ \frac{\cos\theta_{(ijk)}}{r_{(ij)}^2 r_{(ik)}^2} \left(\mathbf{r}_{(ij)} \otimes \mathbf{r}_{(ik)} \right) + \frac{\mathbf{I}}{r_{(ij)} r_{(ik)}}, \tag{A-41}$$

$$\frac{\partial^2 \cos\theta_{(ijk)}}{\partial \mathbf{r}_{(ik)} \partial \mathbf{r}_{(ik)}} = -\frac{1}{r_{(ij)} r_{(ik)}^3} \left(\mathbf{r}_{(ik)} \otimes \mathbf{r}_{(ij)} \right) - \frac{\cos\theta_{(ijk)}\mathbf{I}}{r_{(ik)}^2} + \frac{3\cos\theta_{(ijk)}}{r_{(ik)}^4} \left(\mathbf{r}_{(ik)} \otimes \mathbf{r}_{(ik)} \right)$$
$$- \frac{1}{r_{(ij)} r_{(ik)}^3} \left(\mathbf{r}_{(ij)} \otimes \mathbf{r}_{(ik)} \right), \tag{A-42}$$

$$\frac{\partial^2 \cos\theta_{(jik)}}{\partial \mathbf{r}_{(ij)} \partial \mathbf{r}_{(ij)}} = -\frac{1}{r_{(ji)}^3 r_{(jk)}} \left(\mathbf{r}_{(jk)} \otimes \mathbf{r}_{(ji)} \right) + \frac{\cos\theta_{(jik)}\mathbf{I}}{r_{(ji)}^2} + \frac{3\cos\theta_{(jik)}}{r_{(ji)}^4} \left(\mathbf{r}_{(ji)} \otimes \mathbf{r}_{(ji)} \right)$$
$$- \frac{1}{r_{(ji)}^3 r_{(jk)}} \left(\mathbf{r}_{(ji)} \otimes \mathbf{r}_{(jk)} \right), \tag{A-43}$$

$$\frac{\partial^2 \cos\theta_{(jik)}}{\partial \mathbf{r}_{(ij)} \partial \mathbf{r}_{(jk)}} = \frac{1}{r_{(ji)}^3 r_{(jk)}} \left(\mathbf{r}_{(ji)} \otimes \mathbf{r}_{(ji)} \right) + \frac{1}{r_{(ji)} r_{(jk)}^3} \left(\mathbf{r}_{(jk)} \otimes \mathbf{r}_{(jk)} \right)$$
$$- \frac{\cos\theta_{(jik)}}{r_{(ji)}^2 r_{(jk)}^2} \left(\mathbf{r}_{(jk)} \otimes \mathbf{r}_{(ji)} \right) - \frac{\mathbf{I}}{r_{(ji)} r_{(jk)}}, \tag{A-44}$$

$$\frac{\partial^2 \cos\theta_{(jik)}}{\partial \mathbf{r}_{(jk)} \partial \mathbf{r}_{(ji)}} = \frac{1}{r_{(ji)}^3 r_{(jk)}} \left(\mathbf{r}_{(ji)} \otimes \mathbf{r}_{(ji)} \right) + \frac{1}{r_{(ji)} r_{(jk)}^3} \left(\mathbf{r}_{(jk)} \otimes \mathbf{r}_{(jk)} \right)$$
$$- \frac{\cos\theta_{(jik)}}{r_{(ji)}^2 r_{(jk)}^2} \left(\mathbf{r}_{(ji)} \otimes \mathbf{r}_{(jk)} \right) - \frac{\mathbf{I}}{r_{(ji)} r_{(jk)}}, \tag{A-45}$$

$$\frac{\partial^2 \cos\theta_{(jik)}}{\partial \mathbf{r}_{(jk)} \partial \mathbf{r}_{(jk)}} = -\frac{1}{r_{(ji)} r_{(jk)}^3} \left(\mathbf{r}_{(ji)} \otimes \mathbf{r}_{(jk)} \right) - \frac{\cos\theta_{(jik)}\mathbf{I}}{r_{(jk)}^2} + \frac{3\cos\theta_{(jik)}}{r_{(jk)}^4} \left(\mathbf{r}_{(jk)} \otimes \mathbf{r}_{(jk)} \right)$$
$$- \frac{1}{r_{(ji)} r_{(jk)}^3} \left(\mathbf{r}_{(jk)} \otimes \mathbf{r}_{(ji)} \right). \tag{A-46}$$

This completes the closed-form derivation of the Hessian for the Tersoff-Brenner[1,2] potential.

Despite the relative algebraic complexity of the expressions, the calculations can be performed readily using computers. The algorithm is based on an additive assembly process by casting the equations in their equivalent matrix forms and then summing over all unique pairs and triples of atoms, which translates well to an iterative computational methodology.

[1]Tersoff, J. "Empirical Interatomic Potential for Carbon, With Applications to Amorphous Carbon." *Physical Review Letters*, vol. 61, no. 25, pp. 2879–2882, 19 December 1988.

[2]Brenner, D. W. "Empirical Potential for Hydrocarbons for Use in Simulating Chemical Vapor Deposition of Diamond Films." *Physical Review B*, vol. 42, no. 15, pp. 9458–9471, 15 November 1990.

INTENTIONALLY LEFT BLANK.

NO. OF COPIES	ORGANIZATION	NO. OF COPIES	ORGANIZATION
2	DEFENSE TECHNICAL INFORMATION CENTER DTIC OCA 8725 JOHN J KINGMAN RD STE 0944 FT BELVOIR VA 22060-6218	3	DIRECTOR US ARMY RESEARCH LAB AMSRL CI LL 2800 POWDER MILL RD ADELPHI MD 20783-1197
1	HQDA DAMO FDT 400 ARMY PENTAGON WASHINGTON DC 20310-0460	3	DIRECTOR US ARMY RESEARCH LAB AMSRL CI IS T 2800 POWDER MILL RD ADELPHI MD 20783-1197

2   DEFENSE TECHNICAL
     INFORMATION CENTER
     DTIC OCA
     8725 JOHN J KINGMAN RD
     STE 0944
     FT BELVOIR VA 22060-6218

1   HQDA
     DAMO FDT
     400 ARMY PENTAGON
     WASHINGTON DC 20310-0460

1   OSD
     OUSD (A&T) /ODDR&E(R)
     DR R J TREW
     3800 DEFENSE PENTAGON
     WASHINGTON DC 20301-3800

1   COMMANDING GENERAL
     US ARMY MATERIEL CMD
     AMCRDA TF
     5001 EISENHOWER AVE
     ALEXANDRIA VA 22333-0001

1   INST FOR ADVNCD TCHNLGY
     THE UNIV OF TEXAS AT AUSTIN
     3925 W BRAKER LN STE 400
     AUSTIN TX 78759-5316

1   US MILITARY ACADEMY
     MATH SCI CTR EXCELLENCE
     MADN MATH
     THAYER HALL
     WEST POINT NY 10996-1786

1   DIRECTOR
     US ARMY RESEARCH LAB
     AMSRL D
     DR D SMITH
     2800 POWDER MILL RD
     ADELPHI MD 20783-1197

1   DIRECTOR
     US ARMY RESEARCH LAB
     AMSRL CI AI R
     2800 POWDER MILL RD
     ADELPHI MD 20783-1197

3   DIRECTOR
     US ARMY RESEARCH LAB
     AMSRL CI LL
     2800 POWDER MILL RD
     ADELPHI MD 20783-1197

3   DIRECTOR
     US ARMY RESEARCH LAB
     AMSRL CI IS T
     2800 POWDER MILL RD
     ADELPHI MD 20783-1197

ABERDEEN PROVING GROUND

2   DIR USARL
     AMSRL CI LP

NO. OF COPIES	ORGANIZATION	NO. OF COPIES	ORGANIZATION

NO. OF
COPIES   ORGANIZATION

1   DIRECTOR
US ARMY RESEARCH LAB
AMSRL CP CA D SNIDER
2800 POWDER MILL RD
ADELPHI MD 20783-1145

1   DIRECTOR
US ARMY RESEARCH LAB
AMSRL CI IS R
2800 POWDER MILL RD
ADELPH MD 20783-1145

1   DEPUTY ASST SCY FOR R&T
SARD TT
RM 3EA79 THE PENTAGON
WASHINGTON DC 20301-7100

1   COMMANDER
US ARMY TACOM
PM TACTICAL VEHICLES
PM RDT&E
6501 ELEVEN MILE ROAD
WARREN MI 48397-5000

1   COMMANDER
US ARMY TACOM
PM TACTICAL SURVIVABLE
SYS
SFAE GCSS W GSI H
6501 ELEVEN MILE RD
WARREN MI 48397-5000

7   COMMANDER
US ARMY TACOM
ASMTA TR R
J CHAPIN
R MCCLELLAND
J FLORENCE
J THOMSON
K BISHNOI
6501 ELEVEN MILE RD
WARREN MI 48397-5000

3   DIRECTOR
US ARMY RESEARCH LAB
AMSRL OP SD TL
2800 POWDER MILL ROAD
ADELPHI MD 20783-1145

ABERDEEN PROVING GROUND

54   DIR USARL
AMSRL CI
D CUOZZO
P EMMERMAN
B FORNOFF
J GANTT
W INGRAM
N RADHAKRISHNAN
AMSRL CI H
C NIETUBICZ
AMSRL CI HC
R ANGELINI
P CHUNG
J CLARKE
D GROVE
B HENZ
D HISLEY
M HURLEY
A MARK
R NAMBURU
P PAPADOS
D PRESSEL
D SHIRES
R VALISETTY
S WILKERSON
C ZOLTANI
AMSRL WM
K BOYD
G HAGNAUER
G HAMMELL
J MCCAULEY
M PETTERSON
J SMITH
D STRAND
B VAIL
T VONG
T WRIGHT

REPORT DOCUMENTATION PAGE

Form Approved OMB No. 0704-0188

1. AGENCY USE ONLY *(Leave blank)*	2. REPORT DATE	3. REPORT TYPE AND DATES COVERED
	January 2002	Final, October 2000–September 2001

4. TITLE AND SUBTITLE
Multiscale Methodology: From Atoms to Continuum

5. FUNDING NUMBERS
DRIFY01-CIS-27

6. AUTHOR(S)
Peter W. Chung and Raju R. Namburu

7. PERFORMING ORGANIZATION NAME(S) AND ADDRESS(ES)
U.S. Army Research Laboratory
ATTN: AMSRL-CI-HC
Aberdeen Proving Ground, MD 21005-5067

8. PERFORMING ORGANIZATION REPORT NUMBER
ARL-TR-2645

9. SPONSORING/MONITORING AGENCY NAMES(S) AND ADDRESS(ES)

10. SPONSORING/MONITORING AGENCY REPORT NUMBER

11. SUPPLEMENTARY NOTES

12a. DISTRIBUTION/AVAILABILITY STATEMENT
Approved for public release; distribution is unlimited.

12b. DISTRIBUTION CODE

13. ABSTRACT*(Maximum 200 words)*

Research in multiscale methods has recently flourished with the help of ever-improving computer technology. These developments enable computational physics methods to challenge many of the fundamental limitations of continuum mechanics with larger atomistic simulations and sophisticated hybrid atomistic-continnuum methods. The foundation of most hybrid methods presently lies in the judicious application of kinematic constraints between regions of atoms and regions of continuum finite elements. This juxtaposes atomic and continuum force fields and introduces an interface along which atoms and nodes are unnaturally constrained. This report is divided into three sections. Section 1 reports on an investigation of finding sources of numerical eror due to this unphysical constraint. A heuristic upper bound is derived for a specific example of graphene. In section 2, a literature review of a technique that can potentially eliminate this error is presented. The review covers efforts in engineering for composite materials rooted in a firm mathematical basis for the so-called asymptotic expansion homogenziation method (AEH). In section 3, AEH is used as a framework for developing analytical multiscale formulations for frozen atoms at the small scale and continuum mechanics at the large scale. Analytical solutions for simple systems are used to illustrate the method and its features.

14. SUBJECT TERMS
multiscale methods, continuum mechanics, atomic physics, finite element methods, computational methods, error analysis, numerical analysis

15. NUMBER OF PAGES
146

16. PRICE CODE

17. SECURITY CLASSIFICATION OF REPORT	18. SECURITY CLASSIFICATION OF THIS PAGE	19. SECURITY CLASSIFICATION OF ABSTRACT	20. LIMITATION OF ABSTRACT
UNCLASSIFIED	UNCLASSIFIED	UNCLASSIFIED	UL

INTENTIONALLY LEFT BLANK.